

AN ABSTRACT OF THE THESIS OF

Eilleen M. Hebert for the degree of Master of Science in Chemical Engineering presented on August 17, 2007.

Title: Oxidative Desulfurization of Dibenzothiophene with Tert-Butyl Hydro Peroxide in a Photochemical Micro-Reactor.

Abstract approved:

Goran N. Jovanovic

Alexandre F. Yokochi

Sulfur content in fuels is an increasingly critical environmental issue. Hydrodesulfurization removes sulfur from hydrocarbons; however, further desulfurization is necessary in fuels. New methods are required. In this study, micro-scaled single phase oxidative desulfurization is explored. An ultraviolet light-assisted micro-reactor is introduced for desulfurization of dibenzothiophene.

Dibenzothiophene is mixed with decane and oxidant, tert-butyl hydro peroxide. The mixture forms a thin layer inside the micro-reactor which has a rectangular window to facilitate ultraviolet light irradiation. Thin spacers, 100 μm and 50 μm , establish fluid thickness within the micro-channel. Ultraviolet light reacts with oxidant to create hydroxyl radicals and convert dibenzothiophene to sulfoxides and sulfones. These products are easily extracted. The overall desulfurization process is a pseudo first-order reaction.

Experiments using the 100 micron spacer are conducted at steady state conditions and three temperatures; 22 $^{\circ}\text{C}$, 40 $^{\circ}\text{C}$, and 60 $^{\circ}\text{C}$. For the 50 micron spacer,

temperature conditions were 22 °C and 40 °C. Micro-reactor residence times range from 2 to 30 seconds. The desulfurization study includes a comparison between theoretical model and experimental results, significance of spacer thickness, significance of temperature, and comparison between outcomes of this study to those obtained from other researchers.

A mathematical model of the micro-reaction system is developed to predict dibenzothiophene conversion. The model includes convection, diffusion, and pseudo first order reaction kinetics in the presence of ultraviolet light. The model is solved numerically using COMSOL software. Experimental data is fitted to the model equations to determine the pseudo first order reaction rate constant. The dibenzothiophene reaction rate constants are $7.76 \times 10^{-4} \text{ s}^{-1}$ and $1.47 \times 10^{-3} \text{ s}^{-1}$ at temperatures of 22 °C and 40 °C, respectively. The mathematical model fit the experimental data well and therefore, may be used to predict concentrations within the micro-reactor for various operating conditions.

Overall, desulfurization of dibenzothiophene using tert-butyl hydro peroxide and ultraviolet light-assisted micro-reactor was more efficient compared to other processes. The micro-reactor was capable of achieving 79 % conversion in about 30 seconds, thus reducing the sulfur content from 125 ppm to about 30 ppm.

©Copyright by Eilleen M. Hebert

August 17, 2007

All Rights Reserved

Oxidative Desulfurization of Dibenzothiophene with Tert-Butyl Hydro Peroxide in
a Photochemical Micro-Reactor

by
Eilleen M. Hebert

A THESIS

submitted to

Oregon State University

in partial fulfillment of
the requirements for the
degree of

Master of Science

Presented August 17, 2007

Commencement June 2008

Master of Science thesis of Eilleen M. Hebert presented on August 17, 2007.

APPROVED:

Co-Major Professor, representing Chemical Engineering

Co-Major Professor, representing Chemical Engineering

Head of the Department of Chemical, Biological, and Environmental Engineering

Dean of the Graduate School

I understand that my thesis will become part of the permanent collection of Oregon State University libraries. My signature below authorizes release of my thesis to any reader upon request.

Eilleen M. Hebert, Author

ACKNOWLEDGEMENTS

My heartfelt thanks go to my parents, Annamaria and George Hebert, and Micah Leis for their continuous emotional support and stern patience over the last six years of treacherous schooling. I also would like to thank my baby brother and roommate, Shawn Hebert, for feeding me on occasion when I could only stare blankly at the stove. I attribute my sanity and sheer determination to those that I love.

A special thank you goes to Carmen Velasco for being a springboard for ideas, validating my work, and essentially being my second brain over the course of the project. I could not have finished without my dear friend.

I thank my major professors, Dr. Goran Jovanovic and Dr. Alexandre Yokochi, for their guidance and professional support that has helped me complete this degree.

I would like to also thank Dr. Kenneth Funk and Dr. Todd Palmer for participating as committee members.

I thank Steven Kunert for kindly reading and editing the thesis when even my own mother would not do so.

I want thank Christopher Jensen for his dedication and help conducting experiments; essentially being my second set of hands in lab.

I wish to thank Jim Parker for his great support in computer modeling and optimization which were crucial for the completing of my thesis.

Thanks also go to Tactical Energy Systems for funding most of the project.

TABLE OF CONTENTS

	<u>Page</u>
INTRODUCTION.....	1
1.1 Sulfur Content Regulations.....	1
1.2 State of Micro-Technology.....	2
1.2.1 Characterization of Micro-Reactors.....	2
1.2.2 Fundamental Advantages of Micro-Reactors.....	3
1.2.3 Benefits of Micro-Processing.....	4
1.3 Goals and Objectives.....	5
BACKGROUND.....	6
2.1 Hydrodesulfurization.....	6
2.1.1 Overview.....	6
2.1.2 Advancements in Hydrodesulfurization.....	7
2.2 Oxidative Desulfurization.....	8
2.2.1 Initial Efforts.....	10
2.2.2 Recent Progress.....	10
MICRO-REACTOR SELECTION.....	14
3.1 Ultrasound-Assisted Micro-Reactor.....	14
3.1.1 Design Version 1.....	15
3.1.2 Design Version 2.....	18
3.2 Ultraviolet Light-Assisted Micro-Reactor.....	21
3.2.1 Preliminary Batch System.....	21
3.2.2 Preliminary Micro-Reactor System.....	22
3.3 Micro-Reactor Comparison.....	24
FUNDAMENTALS.....	26
4.1 Chemistry.....	26
4.2 Velocity Profile.....	33
4.3 Mathematical Model.....	37
4.3.1 Scalar Analysis.....	41
4.3.2 Final COMSOL Model Equations.....	47
EXPERIMENTAL APPARATUS AND METHODS.....	48
5.1 Materials.....	48
5.2 Equipment.....	48
5.3 Desulfurization Experimental Method.....	51

TABLE OF CONTENTS (Continued)

	<u>Page</u>
5.4 Desulfurization Analytical Method.....	54
EXPERIMENTAL MEASUREMENTS	57
6.1 Absent Light Source.....	57
6.2 Desulfurization with 100 Micron Spacer	58
6.3 Desulfurization with 50 Micron Spacer	60
6.4 Material Balance on Sulfur	62
6.4.1 100 Micron System	62
6.4.2 50 Micron System	64
RESULTS AND DISCUSSION.....	68
7.1 Effect of Spacer Thickness.....	68
7.2 Effect of Temperature	69
7.3 Mathematical Model	70
CONCLUSIONS AND RECOMMENDATIONS	74
8.1 Conclusions from Experimental Data	74
8.2 Conclusions from Model.....	75
8.3 Recommendations	76
BIBLIOGRAPHY	79
APPENDICES.....	84

LIST OF FIGURES

<u>Figure</u>	<u>Page</u>
2.1. Hydrogenolysis Reaction	6
2.2. Hydrodesulfurization Process	7
2.3. Dibenzothiophene Oxidation	9
2.4. Diels-Alder Reaction.....	9
3.1. Digital Sonifier with Disruptor Horn	14
3.2. Expanded Ultrasound Reactor Design 1 Sketch	15
3.3. Micro-Reactor Design 1 Inner Plate	16
3.4. DBT Concentrations Before and After 5 Minutes of Sonication in Micro-Reactor Design 1 with TBHP as the Oxidant.....	17
3.5. DBT Concentrations Before and After 15 Minutes of Sonication in Micro-Reactor Design 1 with H ₂ O ₂ as the Oxidant	17
3.6. Expanded Ultrasound Reactor Design 2 Sketch	18
3.7. Micro-Reactor Design 2 Inner Plate	19
3.8. DBT Concentrations Before and After 10 Minutes of Sonication in Micro-Reactor Design 2 with TBHP as the Oxidant.....	20
3.9. DBT Concentrations Before and After 10 Minutes of Sonication in Micro-Reactor Design 2 with H ₂ O ₂ as the Oxidant	20
3.10. DBT Concentrations Before and After 10 Minutes of UV Exposure at Various Distances from Light Source in Batch System with TBHP as Oxidant ...	22
3.11. DBT Concentrations Before and After Short Times at 15 cm Distance from Light Source in Micro-Reactor System with TBHP as Oxidant.....	23
3.12. DBT Concentrations Before and After Long Time at 15 cm Distance from Light Source in Micro-Reactor System with TBHP as Oxidant.....	23
4.1. Generation of Hydroxyl Radicals.....	28

LIST OF FIGURES (Continued)

<u>Figure</u>	<u>Page</u>
4.2. Spectrophotogram of Mercury Lamp.....	30
4.3. Spectrum of 0.129 M Tert-butyl Hydro Peroxide in Decane Solution. Dashed Vertical Line is Operating Condition. Horizontal Line Gives Absorbance.	30
4.4. Sketch of Light Distribution Within Micro-Reactor	31
4.5. Intensity, I_0 , at Various Distances from Mercury Lamp (254 nm) with Horizontal Line to Indicate Operating Condition for This Work	32
4.6. Sketch of Velocity Profile.....	33
4.7. Sketch of Differential System	37
4.8. Absorbance Spectrum of Tert-Butyl Hydro Peroxide and Dibenzothiophene Solution Exposed to Ultraviolet Light Over Time	44
4.9. Absorbance Spectrum of Tert-Butyl Hydro Peroxide and Dibenzothiophene Solution Shielded From Ultraviolet Light Over Time	44
4.10. Absorbance Spectrum of Tert-Butyl Hydro Peroxide and Dibenzothiophene Solution Shielded From Ultraviolet Light Over Time	45
5.1. Expanded UV Light Reactor Sketch	49
5.2. Exploded Micro-Reactor	50
5.3. Micro-Reactor Side View	50
5.4. HPLC Analytical System	51
5.5. Desulfurization Experimental Setup	53
5.6. Experimental Setup With Emphasis on Reactor Inlet and Outlet Ports.....	53
5.7. Sample Dibenzothiophene Chromatogram	54
5.8. Sample Sulfone Chromatogram	55
5.9. Sample Tert-butyl Hydro Peroxide Chromatogram.....	55

LIST OF FIGURES (Continued)

<u>Figure</u>	<u>Page</u>
6.1. DBT and TBHP Concentrations at Multiple Residence Times Without the Presence of UV Light Using a 50 μm Spacer at a System Temperature of 22 $^{\circ}\text{C}$.	58
6.2. Normalized Concentration of DBT at Various Residence Times for Three Temperatures in Micro-Reactor with 100 μm Thick Spacer	59
6.3. Normalized Concentration of TBHP at Various Residence Times for Three Temperatures in Micro-Reactor with 100 μm Thickness	59
6.4. Normalized Concentration of DBT at Various Residence Times for Two Temperatures in Micro-Reactor with 50 μm Thick Spacer	61
6.5 Normalized Concentration of TBHP at Various Residence Times for Two Temperatures in Micro-Reactor with 50 μm Thickness	61
6.6. Material Balance on Sulfur Containing Species in Micro-Reactor System with 100 μm Spacer Operated at 22 $^{\circ}\text{C}$	63
6.7. Total Sulfur Concentration of Micro-Reactor System Outlet Operated with 100 μm Spacer and Temperature of 22 $^{\circ}\text{C}$	63
6.8. Material Balance on Sulfur Containing Species in Micro-Reactor System with 50 μm Spacer Operated at 22 $^{\circ}\text{C}$	65
6.9. Total Sulfur Concentration of Micro-Reactor System Outlet Operated with 50 μm Spacer and Temperature of 22 $^{\circ}\text{C}$	65
6.10. Material Balance on Sulfur Containing Species in Micro-Reactor System with 50 μm Spacer Operated at 40 $^{\circ}\text{C}$	66
6.11. Total Sulfur Concentration of Micro-Reactor System Outlet Operated with 50 μm Spacer and Temperature of 40 $^{\circ}\text{C}$	66
7.1. Normalized Concentration of DBT at Various Residence Times for Micro-Reactor Spacers of 50 μm and 100 μm at 40 $^{\circ}\text{C}$ Temperature.....	68
7.2. Normalized Concentration of DBT at Various Residence Times for Micro-Reactor 100 μm Spacer at Temperatures of 22 $^{\circ}\text{C}$ and 60 $^{\circ}\text{C}$	69

LIST OF FIGURES (Continued)

<u>Figure</u>	<u>Page</u>
7.3. Surface Plot of Optimized COMSOL Model with Extinction Coefficient and Reaction Rate Constant as Adjustable Parameters.....	71
7.4. COMSOL Model Solutions for Various Initial Rate Constant Values.....	71
7.5. 100 Micron Spacer Experimental Data Fitted With Optimized COMSOL Model	72
7.6. 50 Micron Spacer Experimental Data Fitted With Optimized COMSOL Model	72

LIST OF TABLES

<u>Table</u>	<u>Page</u>
3.1 Results from Micro-Scaled Experiments	24
8.1. Comparison of This Study's Conditions and Results to Open Literature	76

LIST OF APPENDICIES

<u>Appendix</u>	<u>Page</u>
A. Literature Review Summary	85
B. Micro-Reactor Flow Rates and Velocities	86
C. Diffusion Coefficient Calculations.....	87
D. Dibenzothiophene Calibration Curves	88
E. Sulfone Calibration Curves	89
F. Tert-Butyl Hydro Peroxide Calibration Curves.....	90
G. HPCL Measurements for NO LIGHT Experiments.....	91
H. HPCL Measurements for 100 Micron Experiments.....	92
I. HPCL Measurements for 50 Micron Experiments	94
J. Material Balance for 100 Micron Experiments	95
K. Material Balance for 50 Micron Experiments.....	97
L. Paired T-Test Statistics	100
M. COMSOL Model Report	102

LIST OF APPENDIX FIGURES

<u>Figure</u>	<u>Page</u>
D.1. Dibenzothiophene Calibration Curve.....	88
D.2. Sulfur Calibration Curve for Dibenzothiophene	88
E.1. Sulfone Calibration Curve	89
E.2. Sulfur Calibration Curve for Sulfone	89
F.1. Tert-Butyl Hydro Peroxide Calibration Curve	90

LIST OF APPENDIX TABLES

<u>Table</u>	<u>Page</u>
A.1. Summary of Two Phase Liquid Systems Using H ₂ O ₂ Oxidation	85
A.2. Summary of Single Phase Liquid Oxidation Systems	85
B.1. Volumetric Flow Rates and Fluid Velocities for Given Residence Times in Micro-Reactor with a Spacer Thickness of 100 Microns.....	86
B.2. Volumetric Flow Rates and Fluid Velocities for Given Residence Times in Micro-Reactor with a Spacer Thickness of 50 Microns.....	86
C.1. Diffusion Coefficients at Various Temperatures.....	87
G.1. HPLC Measurements of Tert-Butyl Hydro Peroxide and Dibenzothiophene for Experiments Conducted Without Ultraviolet Light at 22 °C and 50 Micron Spacer.....	91
H.1. HPLC Measurements of Tert-Butyl Hydro Peroxide and Dibenzothiophene for Experiments Conducted at 22 °C and 100 Micron Spacer	92
H.2. HPLC Measurements of Tert-Butyl Hydro Peroxide and Dibenzothiophene for Experiments Conducted at 40 °C and 100 Micron Spacer	92
H.3. HPLC Measurements of Tert-Butyl Hydro Peroxide and Dibenzothiophene for Experiments Conducted at 60 °C and 100 Micron Spacer	93
I.1. HPLC Measurements of Tert-Butyl Hydro Peroxide and Dibenzothiophene for Experiments Conducted at 22 °C and 50 Micron Spacer.....	94
I.2. HPLC Measurements of Tert-Butyl Hydro Peroxide and Dibenzothiophene for Experiments Conducted at 40 °C and 50 Micron Spacer.....	94
J.1. HPLC Measurements of Tert-Butyl Hydro Peroxide, Sulfone, and Dibenzothiophene for Experiments Conducted at 22 °C and Micro-Reactor Spacer of 100 Micron Thickness	96
J.2. Sulfur Material Balance on Sulfone and Dibenzothiophene for 100 Micron and 22 °C Experiment. Lists Amount of Sulfur Present and Absent at Various Residence Times.	96

LIST OF APPENDIX TABLES (Continued)

<u>Table</u>	<u>Page</u>
K.1. HPLC Measurements of Tert-Butyl Hydro Peroxide, Sulfone, and Dibenzothiophene for Experiments Conducted at 22 °C and Micro-Reactor Spacer of 50 Micron Thickness	98
K.2. Sulfur Material Balance on Sulfone and Dibenzothiophene for 50 Micron and 22 °C Experiment. Lists Amount of Sulfur Present and Absent at Various Residence Times	98
K.3. HPLC Measurements of Tert-Butyl Hydro Peroxide, Sulfone, and Dibenzothiophene for Experiments Conducted at 40 °C and Micro-Reactor Spacer of 50 Micron Thickness	99
K.4. Sulfur Material Balance on Sulfone and Dibenzothiophene for 50 Micron and 40 °C Experiment. Lists Amount of Sulfur Present and Absent at Various Residence Times	99
L.1. <i>T</i> -Test Results from Three Dibenzothiophene Data Pairs from Experiments Conducted with 100 μm Thick Spacer.....	101
L.2. <i>T</i> -Test Results from Dibenzothiophene Data Pair from Experiment Conducted with 50 μm Thick Spacer	101

Oxidative Desulfurization of Dibenzothiophene with Tert-Butyl Hydro Peroxide in a Photochemical Micro-Reactor

CHAPTER 1 INTRODUCTION

1.1 Sulfur Content Regulations

SO₂ gases, the main source of acid rain and air pollution, result from the conversion of fuels containing sulfur compounds in combustion engines. As a result of environmental impact, strict requirements on low sulfur content in fuels are becoming prominent throughout the world. During the next 3-5 years, diesel sulfur content is expected to reach sub-15 ppm (parts per million) in the United States, Canada and the European Union.

Diesel engines emit particulate matter composed of carbon soot, soluble organic fractions, and sulfates in the sub-micron size range. These elements have been shown to cause respiratory ailments with potentially cancer causing consequences. Soluble organic fractions are made up of condensed aromatic compounds originating from partial combustion of diesel fuel. Indigenous sulfur oxidizes in combustion environments form sulfur dioxide and sulfur trioxide. However, some sulfur forms hydrated sulfates and become part of the total particulate matter that is emitted into the atmosphere (Brown and Espenson, 1996). The extent of sulfated particulate matter is directly related to the sulfur content of diesel fuel. Therefore, reducing sulfur in fuel helps to reduce total particulate matter emissions.

Effective June 2007, EPA is mandating a 500 ppm sulfur cap on all off-road diesel, with a 2010 deadline for all highway and some off-road diesel to be at the 15 ppm ultra-low sulfur diesel level. In June 2010, the sulfur cap will be lowered to 15 ppm for all non-road diesels other with the exception of locomotive and

marine fuels, but small refiners are exempted from that rule. In June 2012, the ultra-low sulfur diesel requirement will apply to locomotive and marine diesel, and by June 2014 the ultra-low sulfur diesel cap will extend to small refiners that make non-road diesel (Fletcher, 2007).

From 1 January 2009, all diesel fuel marketed in the European Union will have an ultra-low sulfur content of no more than 10 ppm (Report, 2007). Abu Dhabi, of the United Arab Emirates, has enacted an action plan calling for the replacement of the currently used diesel with diesel of 50 ppm sulfur content by 2010. By the year 2012, diesel with a sulfur content of 10 ppm will be introduced (UPI, 2007). Federal regulations in Canada, effective October 2006, mandate fuel companies reduce sulfur content of on-road diesel fuel from 500 ppm to 15 ppm (Pedro Arrais, 2006).

Currently, hydrodesulfurization is used to remove sulfur from hydrocarbons in petroleum refineries. However, further desulfurization is necessary so new methods of desulfurization are required.

1.2 State of Micro-Technology

1.2.1 Characterization of Micro-Reactors

By nature of the term “Micro-Technology,” micro-reactors are miniaturized reaction systems fabricated using precision engineering. Internal structures of micro-reactors are characterized by dimensions in the sub-millimeter range. Micro-reactors have diameters in the 100 to 1000 micron range and lengths in the 1 to 10 mm range. The construction of micro-reactors is performed in a hierarchic manner; consisting of an assembly of units composed of many smaller subunits.

With very small internal volumes, micro-reactors intensify mass transfer and heat transfer. These advantages to the chemical engineering field are the main drivers for micro-reactor investigation.

1.2.2 Fundamental Advantages of Micro-Reactors

Originating from chemical engineering first principles, there are inherent benefits associated with miniaturized reaction vessels that make micro-reactors more favorable than traditional systems.

Decreasing Linear Dimensions

Important chemical reactor processing properties, such as temperature, concentration, or pressure (and their gradients), increase with the reduction of linear micro-reactor dimensions. Therefore, the driving forces for heat transfer, mass transfer, and diffusion flux per unit area also increase when using micro-reactors. Diffusion times are shorter and the limitation of mass transfer on rate of reaction can be dramatically lowered. For example, mixing time in micro-mixers can be as fast as milliseconds. Such times are not attainable using macro stirring equipment or other conventional mixers.

High surface to volume ratios deliver efficient mass and heat transfer. The average laboratory and production vessel has a ratio of $1,000 \text{ m}^2/\text{m}^3$ and $100 \text{ m}^2/\text{m}^3$, respectively. Specific surfaces available in micro-reactors are on the order of $10,000 \text{ m}^2/\text{m}^3$ (Sugimoto, et al., 2006). Heat transfer coefficients in micro-exchangers exceed those of conventional heat exchangers by an order of magnitude. Therefore, micro-scaled reactors are often used for fast, highly exothermic or endothermic chemical reactions. The high heat transfer results yield fast heating and cooling of reaction mixtures. Also, more favorable operating conditions are attainable compared to larger-scale reactors. Reactions can be performed under isothermal conditions for well-defined residence times and decomposition of unstable products can be avoided generating higher selectivity and product quality. Improved heat transfer makes higher reaction temperatures achievable, reducing reaction volumes and catalysts quantity.

Numbering Up

Increasing throughput is possible with repetition of basic micro-reactor units; called the numbering-up approach. The functional unit is simply applied again and again. Connection between units can be realized using distribution lines and fractal structures. Flexibility is apparent in that any specific units can be deactivated or added for plant advancement, whereas, increasing reactor dimensions or scaling-up is necessary for conventional reactors. Numbering-up assures desired features of the unit are maintained while total system size escalates (Zhang, et al., 2004).

1.2.3 Benefits of Micro-Processing

Micro-reactors enable fast translation of research results into production due to advantageous operating conditions leading to more precise data. In production, profits are directly correlated with reactor throughput and therefore reaction volume. Micro-reactor volumes yield comparatively high manufacturing costs. According to the economy of scale, production costs increase with decreasing reactor volume. Thus, when similar performance is obtained from conventional reactors and micro-reactors, production using micro-reactors is unprofitable. However, in specific instances having a lower capacity is a benefit.

Continuous Processing

In specialty chemical synthesis, reaction times are often longer than kinetically needed due to slow mass and heat transfer in low surface area systems (Wang, et al., 2005). Due to fast transport in thin layers of fluid, continuous flow micro-reactors can replace current equipment. Pharmaceutical synthesis, and pigments technology are examples of replacing batch process with a continuous process in micro-reactors (Kleemann, 2002). Processes may be completed faster. In addition, selectivity may increase. Hence, micro-reactors yields can exceed that of batch processes.

Safety Concerns

Due to short diffusion paths and enhanced conversion rates, micro-systems can intensify reactive processes. Micro-reactors have demonstrated safe process operations in otherwise explosive regimes. If a reaction did “run away,” then the resulting heat generation would not be a threatening amount. Moreover, the small scale of micro-reactors allows for very fast interruption of a chemical process. Small reactor dimensions also make it easier to use distributed reactants at the place of consumption thus avoiding the transportation and storage of dangerous or hazardous materials (Zhang, et al., 2004). By nature, small reactant and product quantities lead to increased inherent safety of the reactor. Even if a micro-reactor fails, the small quantity of chemicals released accidentally could be easily contained. Processing would have to be achieved by numbering-up identical units, thus keeping the individual reaction units small. These features illustrate that micro-reactors are promising tools for safe operations in manufacturing.

1.3 Goals and Objectives

The primary goal of this thesis is to demonstrate that desulfurization of sulfur containing compounds, specifically dibenzothiophene, is possible via a single phase ultraviolet light-assisted micro-reaction process.

The necessary objectives to achieve this goal are:

- To design the micro-reactor.
- To build the micro-reaction system.
- To perform experiments.
- To design a mathematical model of the process.
- To analyze data using an appropriate mathematical model.

CHAPTER 2 BACKGROUND

2.1 Hydrodesulfurization

2.1.1 Overview

Hydrodesulfurization is a catalytic hydrogenation process that removes contaminants such as nitrogen, metals, oxygen, and sulfur from liquid petroleum fractions. If not contained, these contaminants travel through the refinery processing units having harmful effects on equipment, catalysts, and product quality. Hydrogenolysis is a type of hydrogenation and results in the cleavage of the carbon-X chemical bond, where X is a sulfur, nitrogen or oxygen atom. In hydrodesulfurization the net result is formation of C-H and H-S chemical bonds.

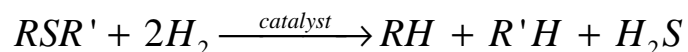


Figure 2.1. Hydrogenolysis Reaction

Using a generic sulfur compound as an example, the hydrodesulfurization reaction above simply decomposes the compound into smaller carbon-containing molecules and hydrogen sulfide gas via a reaction with hydrogen.

In a typical catalytic hydrodesulfurization unit, feedstock is mixed with hydrogen and preheated. Next, the feedstock flows through a pressurized fixed-bed reactor containing Co-Mo or Ni-Mo catalysts. In the reactor, sulfur and nitrogen compounds are converted into H₂S and NH₃. The products are quenched then liquid and gas phases are separated. The hydrogen-rich gas from the separation is recycled, and the gas stream rich in H₂S is sent to a gas treating unit. There, the H₂S is removed and the resulting gas becomes fuel for the refinery furnaces. The

liquid stream is sent to an H₂S stripping column generating the clean final product (Mochida and Choi, 2004).

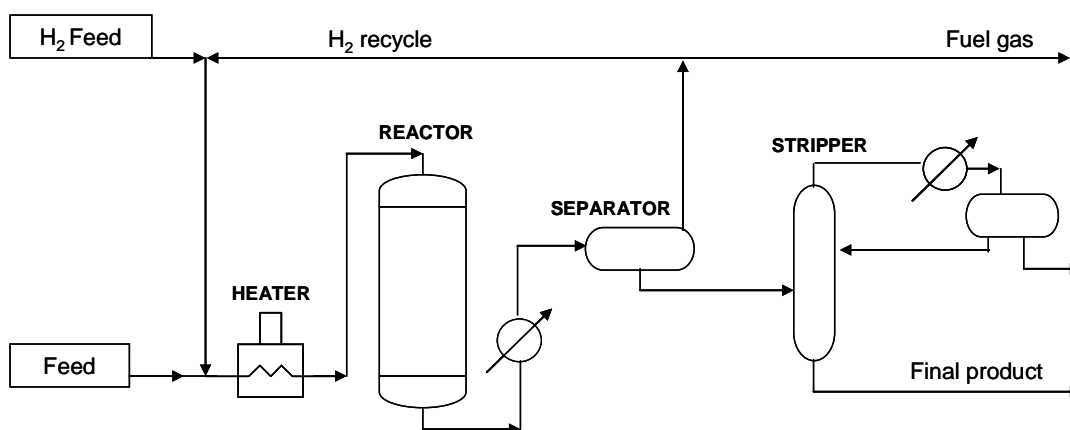


Figure 2.2. Hydrodesulfurization Process

There are disadvantages associated with hydrodesulfurization. Reaction conditions cause safety concerns with such high temperatures and pressures. Operational costs need minimizing through the reduction of hydrogen consumption and expensive catalysts. The largest challenge in the current hydrodesulfurization process is that it does not effectively remove larger sulfur-containing molecules due to low reactivity of highly aromatic sulfur species. The hydrodesulfurization reactivity decreases by about an order of magnitude upon the addition of each aromatic ring (Houalla, et al., 1980). Therefore, the order of reaction rate constants from fastest to slowest is thiophene, benzothiophene and dibenzothiophene. Reactivity further decreases when substituents sterically hinder the reaction such as dibenzothiophene with functional groups in the four- and six-positions (Nag, et al., 1979).

2.1.2 Advancements in Hydrodesulfurization

Recent improvements in catalyst performance maintain hydrodesulfurization as a commercially viable option for diesel. Major hydrodesulfurization-catalyst

suppliers have been modifying catalyst formulations to enhance hydrogenation of aromatic rings by increasing hydrogenating ability of the catalyst and incorporating acidic features in catalysts to induce isomerization of substituents away from sterically hindering positions (Song, 2003). Academic research advances have led to alternative catalyst carriers, such as mixed oxides, through alternative preparative methods, including sol–gels and meso-porous bulk sulfides, and to novel active phases, like thulium phosphides (Bej, et al., 2004), (Kim, et al., 2005).

The hydrodesulfurization process design has also been innovated. “Iso-therming,” a concept developed by Process-Dynamics and Linde, eliminates the need to circulate hydrogen through catalyst (Ackerson and Byars, 2005). Hydrogen and oil are mixed with a solvent such that hydrogen solubility is "high" relative to the oil feed. Reactor conditions and solvent are adjusted so all hydrogen required in hydro-processing reactions is available in solution. A solution containing all feed reactants is then supplied to a plug flow reactor packed with catalyst where the reactions proceed. Therefore, the large trickle bed reactors can be replaced by much smaller tubular reactor because no additional hydrogen is required.

2.2 Oxidative Desulfurization

Oxidative fuel desulfurization converts recalcitrant thiophenes and other sulfur-containing compounds into polar sulfoxides, polar sulfones and other polar oxidation products which can be removed from fuel by extraction using a polar solvent. Dibenzothiophene (DBT) is a large sulfur-containing compound with a stable aromatic ring structure such that it remains in fuels after the hydrodesulfurization process. The oxidation reaction of dibenzothiophene is well known (Adiwidjaja, et al., 1993). Oxidation of sulfur by a hydroxyl radical produces a sulfoxide and further oxidation generates a highly polar sulfone.

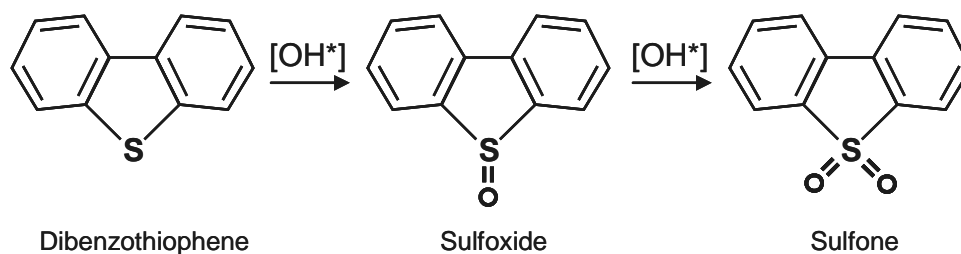


Figure 2.3. Dibenzothiophene Oxidation

A polar aqueous fluid can serve as extracting solvent for all polar sulfur-containing compounds produced by oxidation of dibenzothiophene. Thiophene sulfones can undergo further conversion via well known Diels-Alder reaction (Jackson and Moody, 1990). The reaction forms a cyclic product, via a cyclic transition state, described as a “cyclo-addition.” This polymerization reaction is avoided due to difficult to remove non-polar products. Dibenzothiophene, however, does not undergo the Diels-Alder reaction because it has a very stable molecular structure.

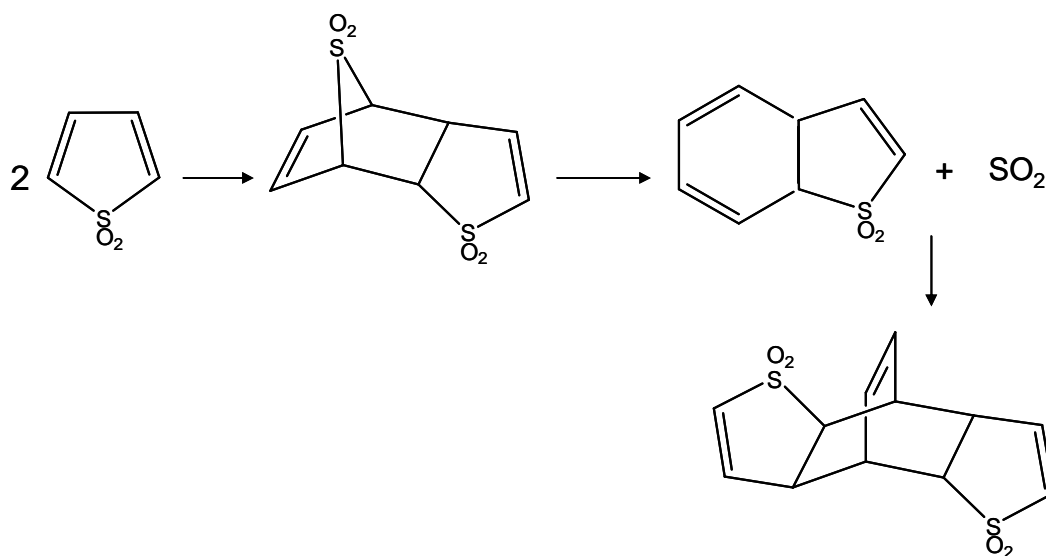


Figure 2.4. Diels-Alder Reaction

Oxidative desulfurization offers several advantages when compared to hydrodesulfurization. The use of mild reaction conditions, such as room temperature and atmospheric pressure, makes the process desirable. Cost savings are incurred with the reduction of expensive materials like catalysts and hydrogen. Additionally, processes are easy to control. Most importantly, highly aromatic sulfur species are more reactive.

2.2.1 Initial Efforts

History on oxidative desulfurization dates back to the 1920's with initial attempts to oxidize sulfur and also to nitrate aromatic molecules. Nitrated aromatics were thought to have a high cetane number. However, nitric acids and nitric oxides, like HNO_3 or NO/NO_2 gases, lead to high amounts of residue formation (Tam, et al., 1990). Afterward in the 1960's, oxidation of more aromatic sulfur species by hydro peroxides and per acids were reported and patents from oil companies emerged on desulfurization of sulfides using of hydro peroxides as oxidants (Ito and van Veen, 2006). In the late 1990's, the main oxidants being employed were hydro peroxides like hydrogen peroxide (H_2O_2) and tert-butyl hydro peroxide (TBHP) in combination with a catalyst or per-acids. For example, H_2O_2 and formic acid was explored (Ito and van Veen, 2006). Those oxidants convert sulfur efficiently to sulfones without forming a residual product.

2.2.2 Recent Progress

Oxidative desulfurization can be classified into five different categories. The first is a two phase liquid system using aqueous hydrogen peroxide as oxidant. Next are single phase liquid systems with organic hydro peroxides as oxidants. Third is a gas-liquid system oxidized by means of ozone, NO_2 , or O_2 . Next are biological oxidation systems via O_2 and bacteria. The final category is a miscellaneous group of unconventional methods that also cause desulfurization.

Two Phase Liquid Oxidation Systems

Two liquid phase systems, usually consisting of aqueous hydrogen peroxide introduced to oil, are very well explored. Literature discusses a variety of catalysts and assisting components, such as phase transfer agents like tertaocylammonium bromide (Collins, et al., 1997) and co-adsorbents like active carbon (Yu, et al., 2005) (Ania and Bandosz, 2006). Also mentioned is acetonitrile as a co-solvent (Campos-Martin, et al., 2004) (Hulea, et al., 2001) and physical methods including ultrasound (Mei, et al., 2003). Catalysts vary from organic acids like formic acid (Otsuki, et al., 2000) (Yu, et al., 2005) to phosphotungstic acids (Collins, et al., 1997) (Mei, et al., 2003) or biperoxotungstate (Campos-Martin, et al., 2004). Heterogeneous catalysts include titanium-silica based catalysts (Hulea, et al., 2001), solid bases like hydrotalcites, and MgLa oxides (Palomeque, et al., 2002). Using activated carbon in a H₂O₂-formic acid oxidation system is suggested to yield deeper desulfurization (Yu, et al., 2005). Further, it seems the presence of an extracting agent like acetonitrile enhances sulfone oxidation substantially (Hulea, et al., 2001). Appendix A summarizes recent literature on two phase liquid oxidation and extraction systems using aqueous hydrogen peroxide as the main oxidizing agent for sulfur containing compounds.

Single Phase Liquid Oxidation Systems

Tert-butyl hydro peroxide is well investigated in single phase liquid systems. An advantage of the single phase technique is simple reactor engineering, exploiting a fixed bed system. Lyondell Chemicals (Han and Leyshon, 2005) and ENI Technology (Zanibelli, et al., 2004) announced tert-butyl hydro peroxide based commercial oxidative desulfurization processes. The processes perform sulfone extraction via adsorption. Lyondell uses silica and titania, while ENI applies amorphous mixed oxides containing silica, alumina, ceria, and magnesia. One group found that titanium-silica based catalysts enhance tert-butyl hydro peroxide oxidation chemistry (Corma Canos, et al., 2002). For selective oxidation of sulfide, an unusual catalyst like silica tethered oxorhenium (V) dithiolate has been used

(Stanger, et al., 2006). Appendix A displays recent work in single phase liquid systems that utilize hydro peroxides for oxidation.

Gas-Liquid Oxidation Systems

In gas-liquid systems, oxygen is a powerful oxidant. Molecular oxygen in the presence of cobalt catalysts and aldehydes oxidizes sulfur species in diesel fuel (Murata, et al., 2004). The cobalt acetate facilitates oxidation of aldehydes, leading to per acid formation which reacts with sulfur to create sulfone. Cobalt and manganese based catalysts for air oxidation of aromatic sulfur compounds are reported (Thirugnanasampanthar, et al., 2005). Air with catalytic FeBr_3 stabilized in cyclodextrin oxidizes sulfides to sulfoxides (Rossi and de Rossi, 2004). Few recent advances have been made in gas-liquid systems.

Biological Oxidation Systems

Conceptually, using a biological system for oxidation of sulfur species is very attractive. The reaction occurs in water and oxygen at ambient temperature and pressure. Bacteria that convert dibenzothiophene and alkyl sulfides are well investigated, whereas fewer bacteria are found for benzothiophene and thiophene (Atlas, et al., 2000). Bio-desulfurization does not show very deep desulfurization due to more bacterial activity at higher sulfur concentrations. Therefore, bio-desulfurization may not have the ability to achieve required low sulfur levels. There is also the potential for competitive bacterial reactions, common in biological systems. However, successful biological processes utilize only one type of bacteria, such as Thiobacilli, that survive in poisonous H_2S environments, converting H_2S to elemental sulfur efficiently (Kleinjan, et al., 2003). Occasional reports appear on newly developed bacteria for desulfurization; for instance, *Nocardia globerulea* R-9 could be a potential bacterium for reducing the sulfur content of petroleum products (Luo Mingfang, 2003).

Miscellaneous Desulfurization Systems

As previously noted, the obstacle in diesel desulfurization is low reactivity of highly aromatic sulfur compounds. Therefore, another desulfurization approach is the application of an energy source to decompose sulfur compounds. Microwaves can aid in hydrotreating. Hydrocarbon streams containing sulfur are mixed with organic catalyst. Applying microwave or radio frequency energy (500-3000 MHz) generates monatomic hydrogen at reaction surfaces of the catalyst which reacts with sulfur compounds (Purta, et al., 2004). High energy radiation beams, or X-rays, can be also applied for desulfurization. Hydrocarbons and an AgNO_3 catalyst, irradiated with X-rays, result in removable metal sulfides. The silver is regenerated for reuse as AgNO_3 (Ayakawa and Ono, 2002). Radiochemical desulfurization reactions can be induced by gamma radiation and result in significant sulfur removal. Cobalt-oxide catalyst impregnated on Al_2O_3 promotes dibenzothiophene removal in gamma irradiated environments (Qu, et al., 2006).

Ultraviolet light induces photo-oxidation of sulfur containing compounds in extraction systems. Hydroxyl radicals are formed from irradiation of hydrogen peroxide. These activated radicals react with present sulfur species to create sulfones (Shiraishi, et al., 2000). However, desulfurization by photochemical electron-transfer oxidation in organic two-phase extraction systems based on visible light with wavelengths greater than 400 nm is also achievable (Shiraishi, et al., 1999). Sulfur-rich diesel oil can be irradiated with a mercury lamp in the presence of dichloroacetic acid and acetonitrile to increase the intensity of photosensitized oxidation (Zhan, et al., 2005). Results from using a titanium(IV) oxide-hectorite nano-film photo-catalyst indicated that photo-oxidation of dibenzothiophene was effective in reducing sulfur levels (Robertson and Bandosz, 2006). Using tungsten containing layered double hydroxide as a catalyst determined that tungsten anions are active catalysts promoting fast oxidation of sulfur containing organic compounds with 30% hydrogen peroxide under mild reaction conditions (Hulea, et al., 2006). Photo-oxidation of sulfur containing compounds is a viable desulfurization method.

CHAPTER 3

MICRO-REACTOR SELECTION

All reactions are not limited to a single method of activation. For oxidation of dibenzothiophene, activation using ultrasound and ultraviolet light were explored to determine the best system on which to perform experiments.

3.1 Ultrasound-Assisted Micro-Reactor

Two different ultrasound-activated reaction systems were investigated. Both ultrasound-assisted micro-reactor designs use a Digital Sonifier manufactured by BRANSON Ultrasonics Corporation, model 450 with a ½” diameter tapped stepped disruptor horn to generate ultrasonic waves, shown in Figure 3.1.



Figure 3.1. Digital Sonifier with Disruptor Horn

3.1.1 Design Version 1

The first ultrasound-assisted micro-reactor consisted of three major components, visible in Figure 3.2. The upper part is made of white Delrin, has two inlet and two outlet Swagelok ports, and has an o-ring lined chamber to house the sonicator horn. The lower piece has barbed ports and an empty space for cooling water to pass through; it is also made of Delrin. The two Delrin constituents encase the inner plate and are screwed together to form a leak-proof seal.

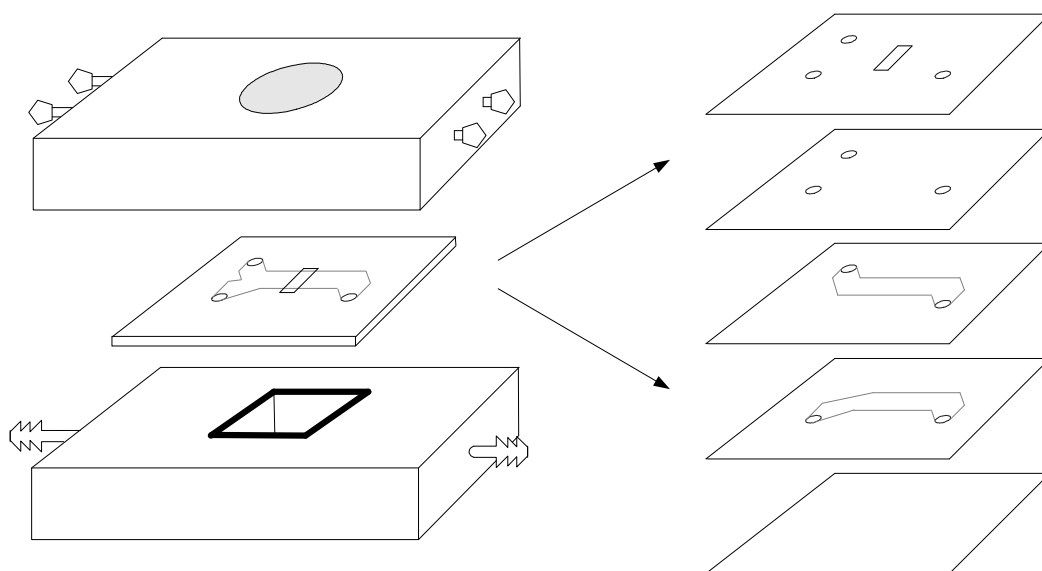


Figure 3.2. Expanded Ultrasound Reactor Design 1 Sketch

The inner plate is made up of five stainless steel sheets that are fused together to create the reaction chamber. The bottom sheet just keeps the cooling fluid and the reacting fluid separate. The next two sheets above it create discrete inlet channels that merge into the reaction chamber and outlet port. Next is an extension of the inlets and outlet. The uppermost sheet has inlet and outlet areas but also a cutout section that creates a “well” for the ultrasound coupling fluid between the sonicator tip and the top of the reaction chamber.

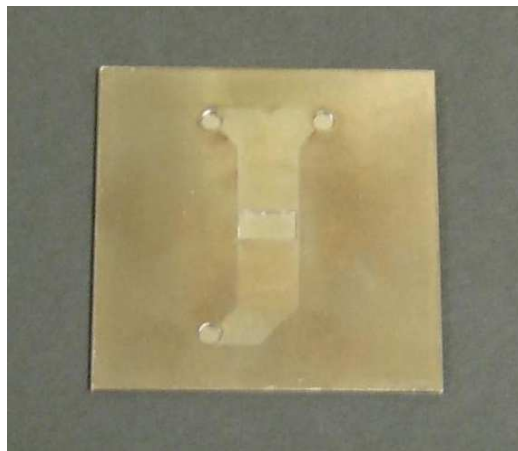


Figure 3.3. Micro-Reactor Design 1 Inner Plate

The sheets are combined together to form the inner reaction plate in Figure 3.3. Clearly visible are the two reactor inlets and outlet, along with the voided area intended for ultrasonic wave coupling and an outline of the internal fluid chamber.

Single Phase TBHP Results

Two feed streams of the same TBHP/DBT/decane reactants are fed into the micro-reactor explained above at a flow rate that yields a residence time of 5 minutes. Heating water set to 70 °C warms the fluid as it passes through the micro-reactor and is indirectly exposed to the coupled energy of the sonicator set to 70 % of total power. The single phase system results depicted in Figure 3.4 demonstrate 3.6 % of dibenzothiophene is removed from the feed solution using TBHP as the oxidizing agent.

Two Phase H₂O₂ Results

Feed streams of aqueous H₂O₂ and dibenzothiophene doped decane are supplied to the micro-reactor at a residence time of 15 minutes. Similarly, the heating water is fixed to 70 °C and the liquids are indirectly sonicated at 70 % of total power. The portrayal of these results in Figure 3.5 demonstrates that 1.1 % of dibenzothiophene is removed from the feed solution with H₂O₂ as the oxidant.

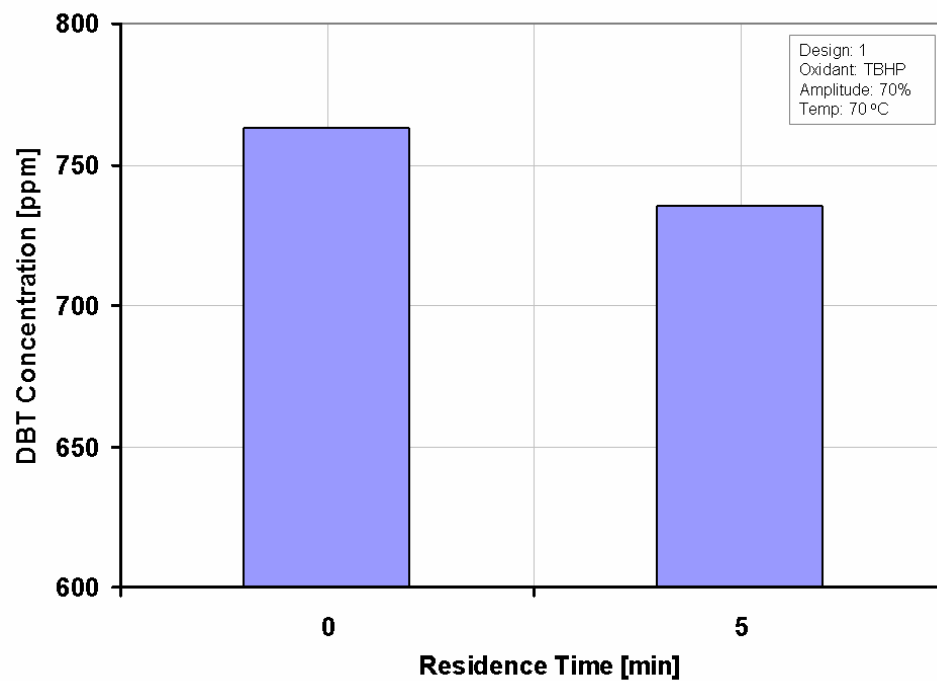


Figure 3.4. DBT Concentrations Before and After 5 Minutes of Sonication in Micro-Reactor Design 1 with TBHP as the Oxidant

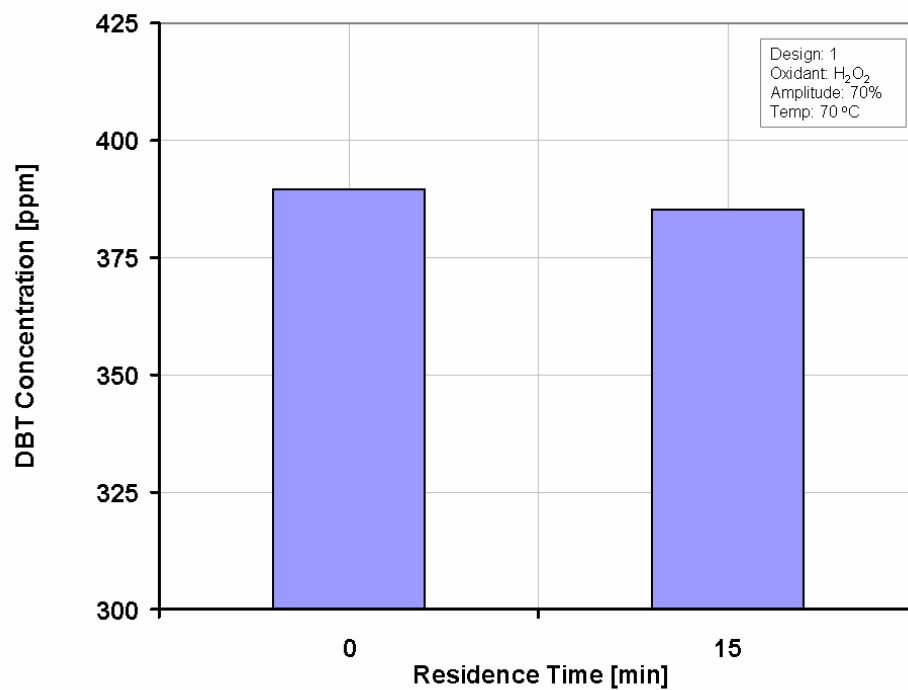


Figure 3.5. DBT Concentrations Before and After 15 Minutes of Sonication in Micro-Reactor Design 1 with H₂O₂ as the Oxidant

3.1.2 Design Version 2

It was determined that ultrasonic waves generated from the sonicator were not traveling through the silicone coupling fluid or the top layer of the micro-reaction chamber to activate the oxidants within the reactant solution. After doing a few large scale tests, direct sonication of feed fluid was found to yield higher dibenzothiophene conversions. Therefore, the micro-reactor was redesigned as to expose liquids to the direct impact of ultrasonic energy waves.

As shown in Figure 3.6, the Delrin casing still comprises upper and lower portions of the micro-reaction system. The lower compartment still allows for reactor cooling and heating, while the upper piece provides reactor inlets, outlets, and sonicator entrance. Both reactor inlet ports were used, however, only one of the reactor outlets was utilized. The second outlet was blocked off. Silicone vacuum grease was used to form a seal between the sonicator horn and the upper Delrin.

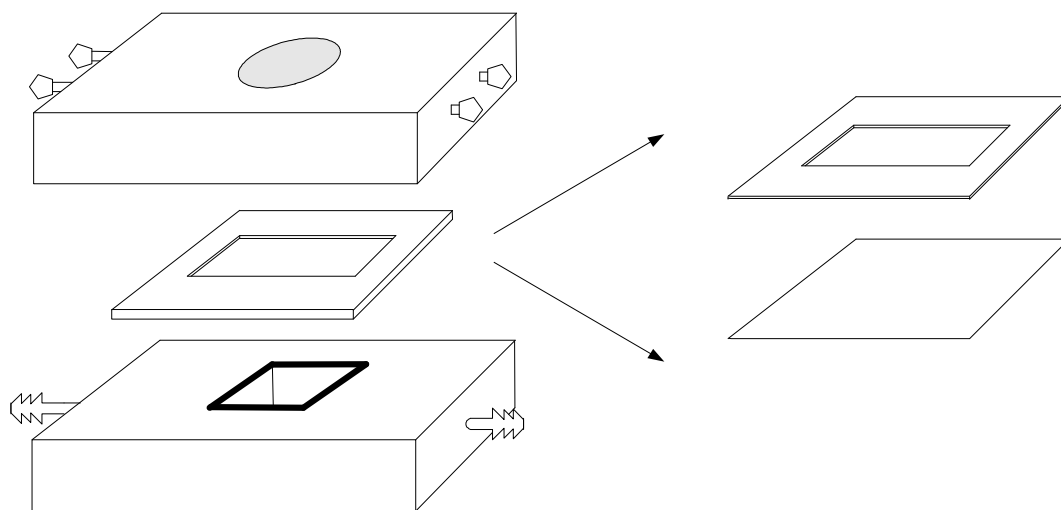


Figure 3.6. Expanded Ultrasound Reactor Design 2 Sketch

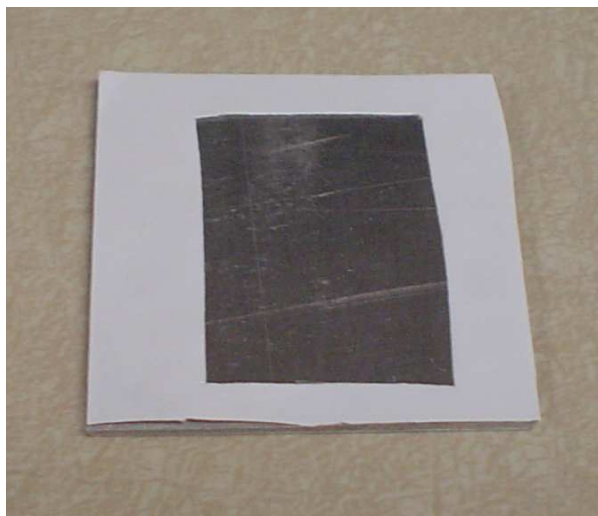


Figure 3.7. Micro-Reactor Design 2 Inner Plate

The inner plate, Figure 3.7, is made up of a 2 mm thick aluminum plate and a sheet of 127 μm thick Teflon. The sonicator tip is immersed in the reactant fluid flowing as a thin film approximately 36.5 mm by 26.7 mm by 0.127 mm defined by the Teflon cut out.

Single Phase TBHP Results

The solitary phase is fed into the micro-reactor with a residence time of 10 minutes. Heating water is adjusted to 90 $^{\circ}\text{C}$ and the solution is directly sonicated at 50 % of total power. Figure 3.8 reveals a dibenzothiophene conversion of 7.9 % by means of TBHP oxidation.

Two Phase H_2O_2 Results

Both feed streams, aqueous and dibenzothiophene-rich decane, are presented to the micro-reactor at a residence time of 10 minutes. Likewise, the heating water is at 90 $^{\circ}\text{C}$ and reactants are directly sonicated at 50 % of total power. The results in Figure 3.9 demonstrate that 4.2 % of dibenzothiophene is removed from feed solution by way of reaction with H_2O_2 .

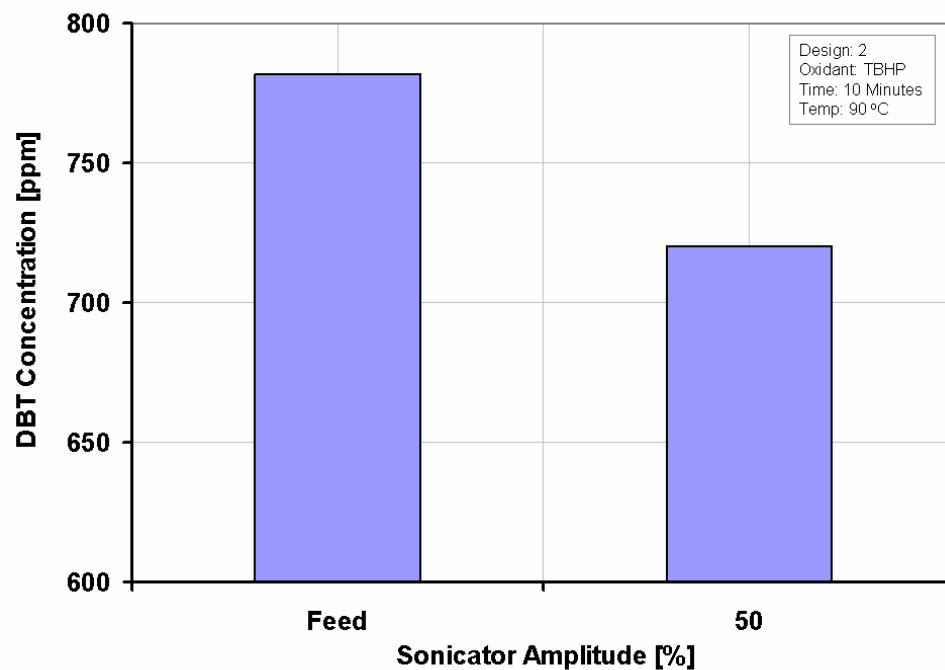


Figure 3.8. DBT Concentrations Before and After 10 Minutes of Sonication in Micro-Reactor Design 2 with TBHP as the Oxidant

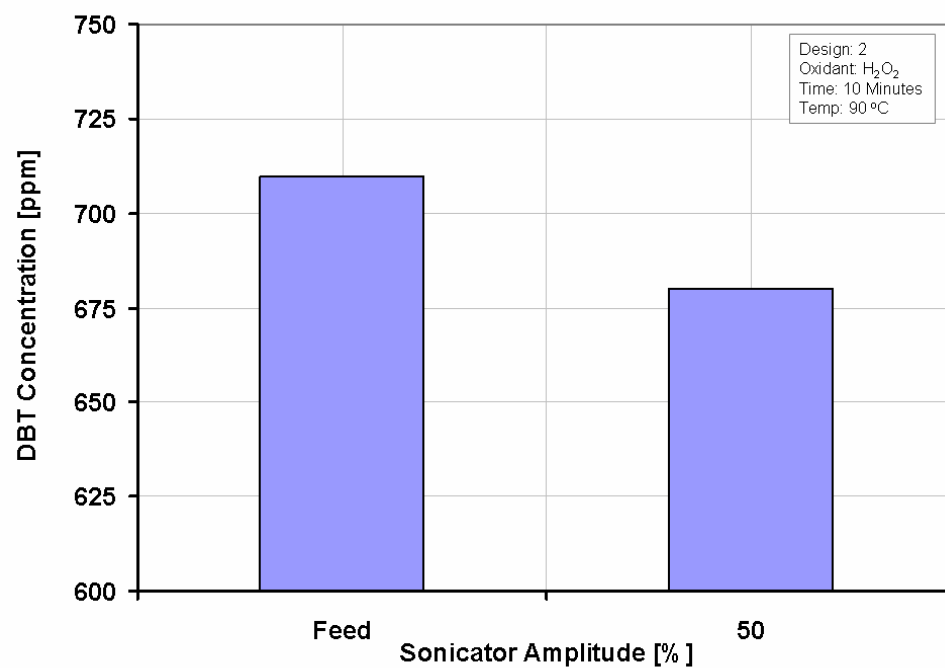


Figure 3.9. DBT Concentrations Before and After 10 Minutes of Sonication in Micro-Reactor Design 2 with H₂O₂ as the Oxidant

3.2 Ultraviolet Light-Assisted Micro-Reactor

The effects of using ultraviolet light for reaction activation and H_2O_2 as an oxidant have been previously documented in the March 2005 Oregon State University chemical engineering master's thesis by Ali H. Al-Raie. Dibenzothiophene is mixed with hexane at a concentration of 300 ppm. The mixture is introduced into a micro-reactor concurrently with hydrogen peroxide in equal volumetric flow rates. The reactants form two thin layers inside the micro-reactor that are irradiated by a ultraviolet light source 1.5 cm above the reactor. He achieves approximately 60% dibenzothiophene conversion in about a 10 minute residence time, bringing the concentration down to approximately 120 ppm dibenzothiophene.

3.2.1 Preliminary Batch System

A meso-scaled batch system was used for preliminary exploration of ultraviolet light on the system containing TBHP as the oxidant. In a glass petrie dish, 5 ml of a TBHP/DBT/decane feed solution is exposed to ultraviolet light for 10 minutes at a distance of 15 cm, 6.5 cm, and 1.5 cm. The feed has a dibenzothiophene concentration of 740 ppm or about 130 ppm sulfur.

Figure 3.10 shows the dibenzothiophene concentration as a function of ultraviolet light intensity or distance. The dibenzothiophene concentration decreases as distance between the micro-reactor and ultraviolet light source decrease. The overall best conversion of dibenzothiophene is 89 % and occurs at 1.5 cm from the light source. The final dibenzothiophene concentration is 84 ppm, which translates into a sulfur concentration of just below 15 ppm. These results are expected to improve when introduced into a micro-scaled continuously flowing system.

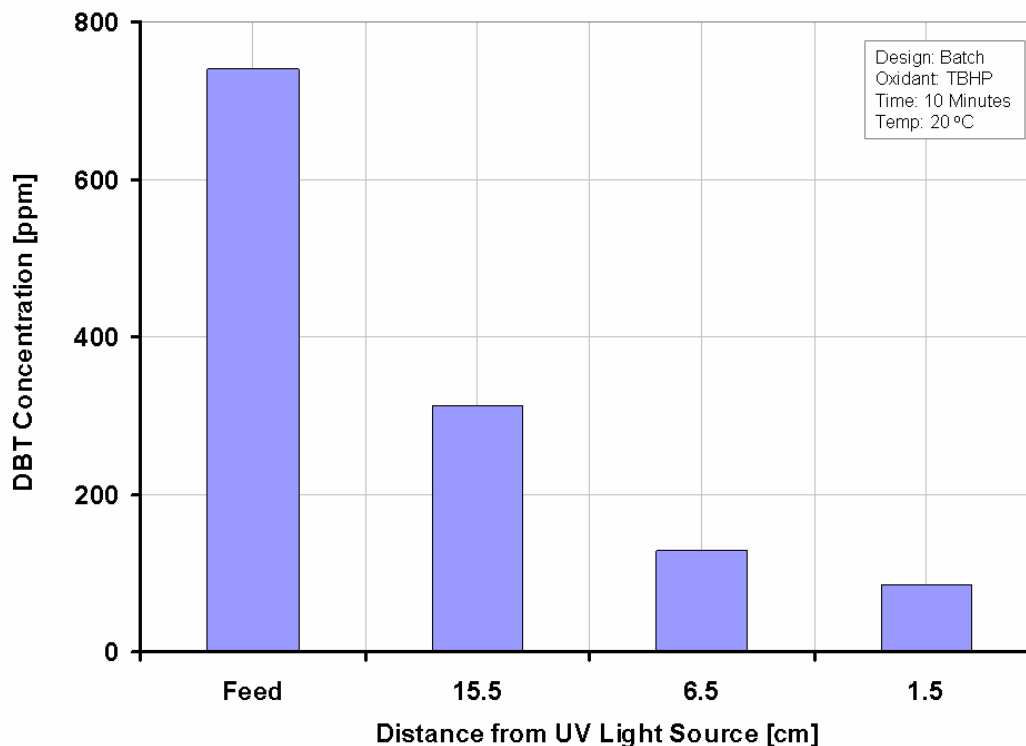


Figure 3.10. DBT Concentrations Before and After 10 Minutes of UV Exposure at Various Distances from Light Source in Batch System with TBHP as Oxidant

3.2.2 Preliminary Micro-Reactor System

A ultraviolet light micro-reactor set from International Crystal Laboratories was used as a reaction vessel and is described in more detail in Chapter 5 Experimental Apparatus and Methods.

Two experiments were conducted using the ultraviolet light micro-reactor. The first explored short residence times. The ultraviolet light source was positioned 15 cm away from the micro-reactor. The results, in Figure 3.11, show a downward trend with a maximum dibenzothiophene conversion of about 16 %. The second experiment investigated the same ultraviolet source distance at a longer residence time of 10 minutes assuming the best possible conversion for dibenzothiophene is reached under these slow flow conditions. Overall dibenzothiophene conversion of 23 % is obtained for these operating conditions shown in Figure 3.12.

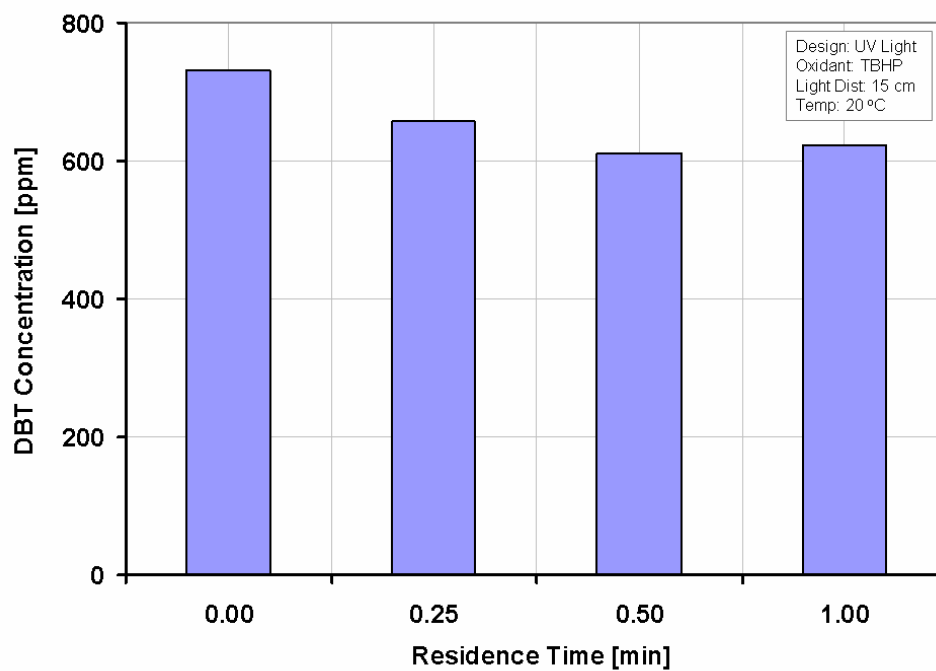


Figure 3.11. DBT Concentrations Before and After Short Times at 15 cm Distance from Light Source in Micro-Reactor System with TBHP as Oxidant

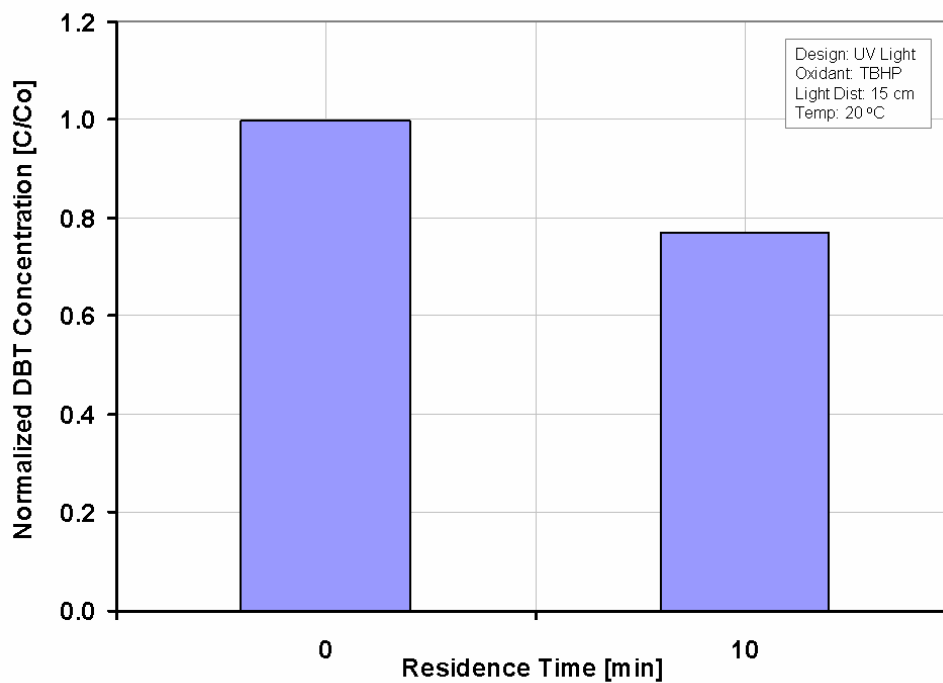


Figure 3.12. DBT Concentrations Before and After Long Time at 15 cm Distance from Light Source in Micro-Reactor System with TBHP as Oxidant

3.3 Micro-Reactor Comparison

The dibenzothiophene conversion results from the previously described ultrasound-assisted and ultraviolet light-assisted experiments are summarized in Table 3.1 below. A number of interesting observations can be made from these results.

Using TBHP as an oxidizing agent yields consistently higher conversion of dibenzothiophene compared to hydrogen peroxide in every system. As far as ultrasound-assisted micro-reactors are concerned, the direct sonication utilized in Design 2, gives consistently higher dibenzothiophene conversion with any oxidizing agent. Finally, limiting the focus to within the realm of ultrasound reaction activation, using TBHP as the oxidant and direct sonication of the fluid generates the best dibenzothiophene conversion.

Table 3.1 Results from Micro-Scaled Experiments

Oxidizing Agent	Activation Method	Maximum DBT Conversion
H ₂ O ₂	Ultrasound- Design 2	4.2%
H ₂ O ₂	Ultrasound- Design 1	1.1%
TBHP	Ultrasound- Design 2	7.9%
TBHP	Ultrasound- Design 1	3.6%
TBHP	UV Light	23.1%

The dibenzothiophene conversion that is achieved via the ultraviolet light-assisted micro-reactor is significantly larger than any of the ultrasound-assisted micro-reactor systems. A conversion of about 23% is attained with the light source about 15 cm above the reactor.

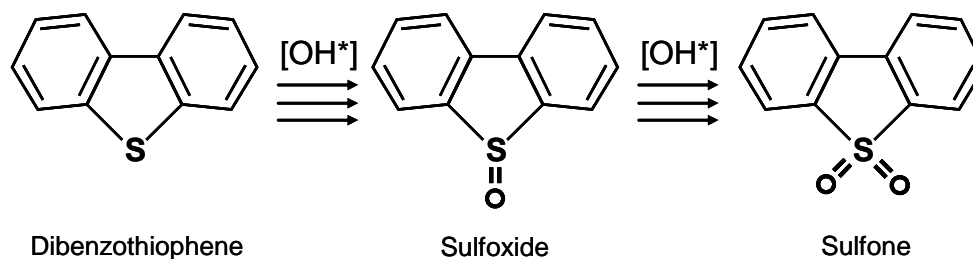
It was decided to discontinue using ultrasound waves to activate the dibenzothiophene desulfurization reaction based on the low conversion rates that were attained.

With as high as 90 % dibenzothiophene conversion on the batch scale and positive results from the micro-reactor, it was determined to further explore the use of TBHP for desulfurization of dibenzothiophene within an ultraviolet light-assisted micro-reactor.

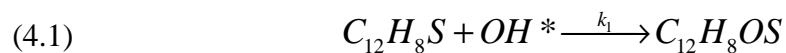
CHAPTER 4
FUNDAMENTALS

4.1 Chemistry

The oxidation reaction achieved in this research uses tert-butyl hydro peroxide and dibenzothiophene as reactants.



As mentioned previously, dibenzothiophene is oxidized by hydroxyl radicals to ultimately form the dibenzothiophene sulfone.



A homogeneous reaction occurs within the micro-reactor wherever hydroxyl radicals and dibenzothiophene are present together. The reaction of dibenzothiophene is a function of the dibenzothiophene concentration, hydroxyl radical concentration, and ultraviolet light intensity. However, in the second reaction, the sulfoxide concentration also plays a role in reaction kinetics.

The rate equations for dibenzothiophene and sulfoxide are illustrated below in equations (4.3) and (4.4).

$$(4.3) \quad -r_{DBT} = k_1 C_{DBT} C_{OH^*}$$

$$(4.4) \quad -r_{SO} = k_2 C_{SO} C_{OH^*} - k_1 C_{DBT} C_{OH^*}$$

To determine the overall reaction kinetics, the sum of the resistances of each reaction rate constant is explored in equations (4.5) through (4.9).

It is proposed that the first reaction, converting dibenzothiophene to sulfoxide, is a much slower reaction than the second reaction that produces sulfone. Therefore, the first reaction rate constant, k_1 , is smaller than the second rate constant, k_2 .

$$(4.5) \quad \frac{1}{K} = \frac{1}{k_1} + \frac{1}{k_2}$$

$$(4.6) \quad \frac{1}{K} = \frac{k_2}{k_1 k_2} + \frac{k_1}{k_1 k_2}$$

The second term on the right hand side of equation (4.6) is essentially zero because the reaction rate constant, k_1 , is comparatively very small.

$$(4.7) \quad \frac{1}{K} = \frac{k_2}{k_1 k_2} + (0)$$

In the term that remains, the reaction rate constant, k_2 , cancels out of the numerator and denominator.

$$(4.8) \quad \frac{1}{K} = \frac{\cancel{k_2}}{k_1 \cancel{k_2}}$$

Thus, the inverse overall reaction rate constant is equal to the inverse of reaction rate constant, k_1 .

$$(4.9) \quad \frac{1}{K} = \frac{1}{k_1}$$

Finally, overall reaction kinetics are found to approximate the slow step in the series and the final reaction rate equation is given in equation (4.10).

$$(4.10) \quad -r_{DBT} = k_1 C_{DBT} C_{OH^*}$$

Hydroxyl radicals are generated from tert-butyl hydro peroxide as depicted in Figure 4.1.

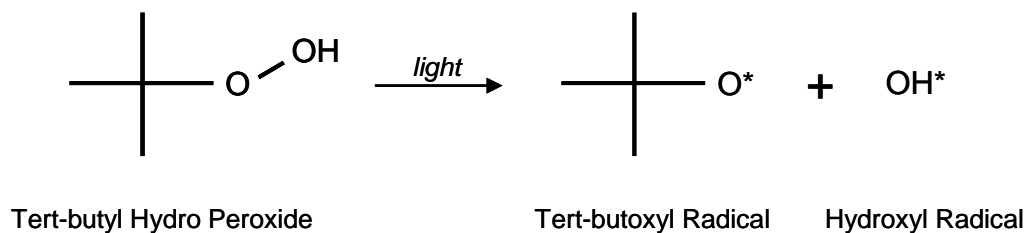


Figure 4.1. Generation of Hydroxyl Radicals

Tert-butyl hydro peroxide decomposes into a tert-butoxyl radical and a hydroxyl radical in the presence of light, given in equation (4.11). The hydroxyl radical is highly reactive and will readily react with other molecules that are present in the surrounding environment. The reaction rate constant, k_4 , incorporates these radical quenching reactions into the kinetics.



Formation of hydroxyl radical occurs when tert-butyl hydro peroxide is exposed to an ultraviolet light source. A mercury lamp emits light at a wavelength of 254 nm indicated in Figure 4.2 by the large light intensity at that wavelength. Notice that intensity is measured as the photon count per instrument integration time and instrument surface area. In this case, photon counts are given for a 1.1 millisecond integration time. The spectrophotometer surface is a 400 μm diameter circle with an area of about $1.26 \cdot 10^{-7} \text{ m}^2$.

Hydroxyl radicals can be created via a mercury lamp that emits ultraviolet light at 254 nm. Ultraviolet light penetrates the quartz window and prompts the formation of hydroxyl radicals. As seen in Figure 4.3, a solution of tert-butyl hydro peroxide with a concentration of 0.129 M has an absorbance of 1.1 at 254 nm.

The concentration of hydroxyl radicals cannot be measured directly. Therefore, it is determined as a function of the tert-butyl hydro peroxide concentration and light intensity vertically through the micro-reactor.

$$(4.12) \quad r_{OH^*} = k_3 C_{TBHP} I - k_4 C_{OH^*}$$

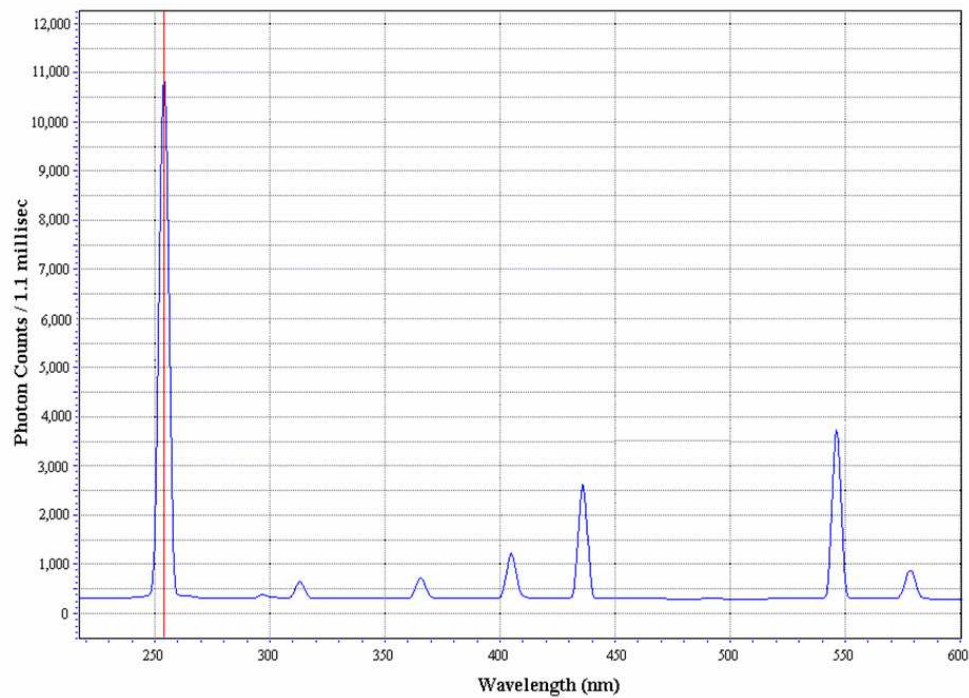


Figure 4.2. Spectrophotogram of Mercury Lamp

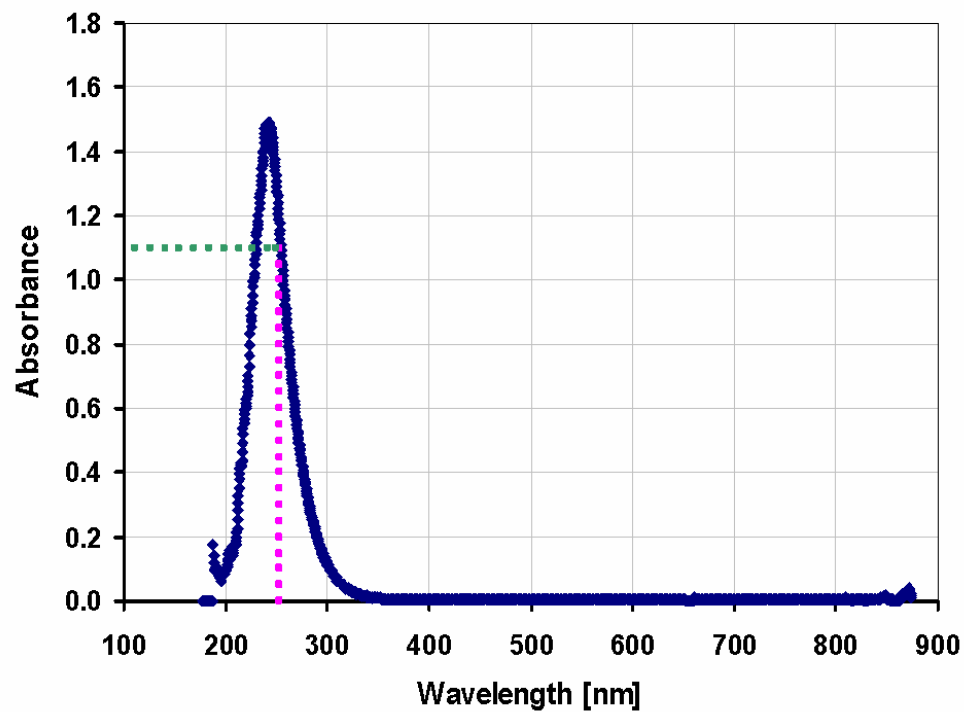


Figure 4.3. Spectrum of 0.129 M Tert-butyl Hydro Peroxide in Decane Solution. Dashed Vertical Line is Operating Condition. Horizontal Line Gives Absorbance.

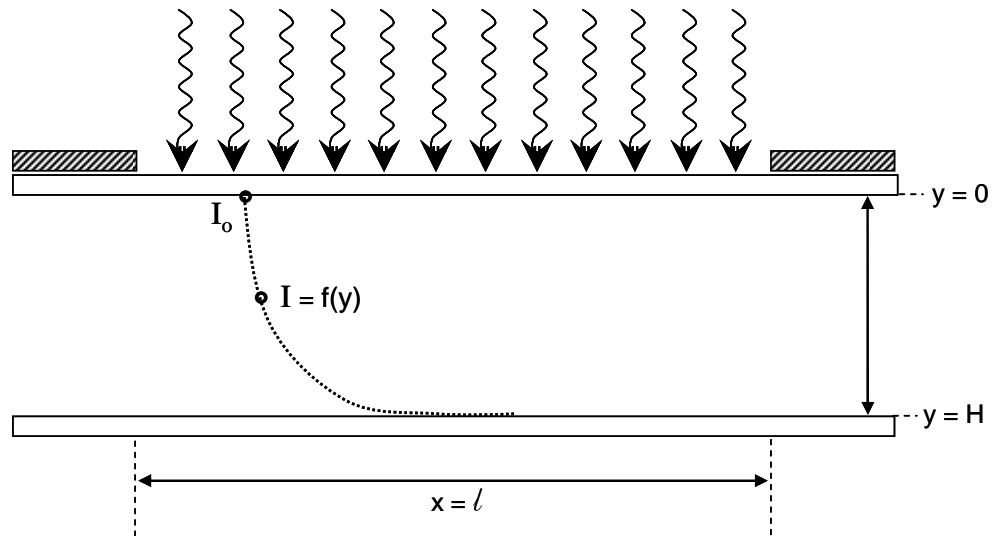


Figure 4.4. Sketch of Light Distribution Within Micro-Reactor

Light intensity, I , is the distribution of ultraviolet light within the micro-reactor fluid. Figure 4.4 is a sketch of the light attenuation.

The ultraviolet light distribution through the fluid within the micro-reactor is given by the following exponential equation.

$$(4.13) \quad I = I_0 \cdot 10^{(-[\varepsilon_{TBHP} C_{TBHP} + \varepsilon_{DBT} C_{DBT}]y)}$$

The intensity of ultraviolet light before penetration into the fluid, I_0 , can be measured experimentally at the back of the quartz window. The I_0 value changes with distance from the light source as seen in Figure 4.5.

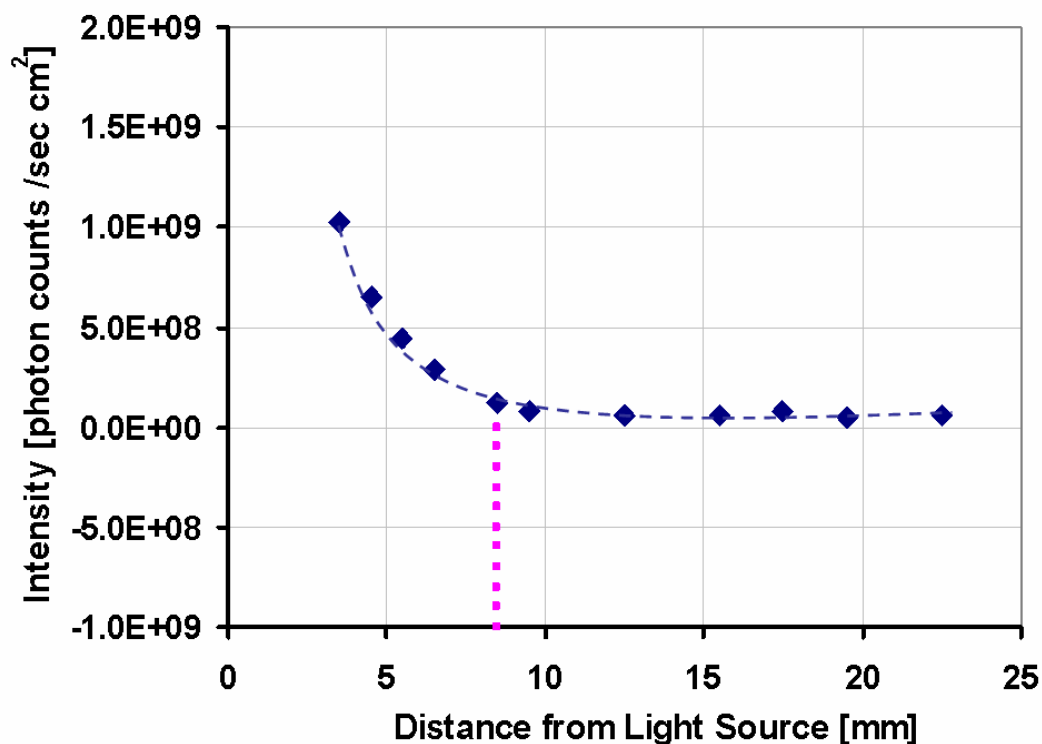


Figure 4.5. Intensity, I_0 , at Various Distances from Mercury Lamp (254 nm) with Horizontal Line to Indicate Operating Condition for This Work

With the micro-reactor positioned 8.5 mm below the mercury lamp, Figure 4.5 yields an I_0 of 10566 photon counts over a 1.1 millisecond integration time and a $1.26 \times 10^{-7} \text{ m}^2$ surface area or simply $7.64 \times 10^{13} \text{ counts sec}^{-1} \text{ m}^{-2}$.

The extinction coefficient, ϵ for a known concentration of tert-butyl hydro peroxide in decane can be determined using the absorbance measured in Figure 4.3 and Beer's Law.

$$(4.14) \quad \epsilon = \frac{A}{CL}$$

Path length, L , is given by the dimensions of the 1 cm square quartz cuvette. The value of the tert-butyl hydro peroxide extinction coefficient is $8.53 \text{ M}^{-1} \text{ cm}^{-1}$ at a concentration of 0.129 M and an absorbance of 1.1 at 254 nm. For

dibenzothiophene at a concentration of 0.000078 M and absorbance of 1.1, the extinction coefficient is $14061 \text{ M}^{-1}\text{cm}^{-1}$. The sulfone extinction coefficient is $1728 \text{ M}^{-1}\text{cm}^{-1}$ at a concentration of 0.00027 M and a 0.48 absorbance.

Inserting the extinction coefficient and I_0 light intensity from Figure 4.5 into equation (4.13) then ultraviolet light intensity throughout the micro-reactor fluid can be determined.

4.2 Velocity Profile

The flow of fluid through the micro-reactor effects reaction conversion. Therefore, the velocity profile through the channel must be found. Figure 4.6 gives a sketch of the velocity profile within the micro-reactor.

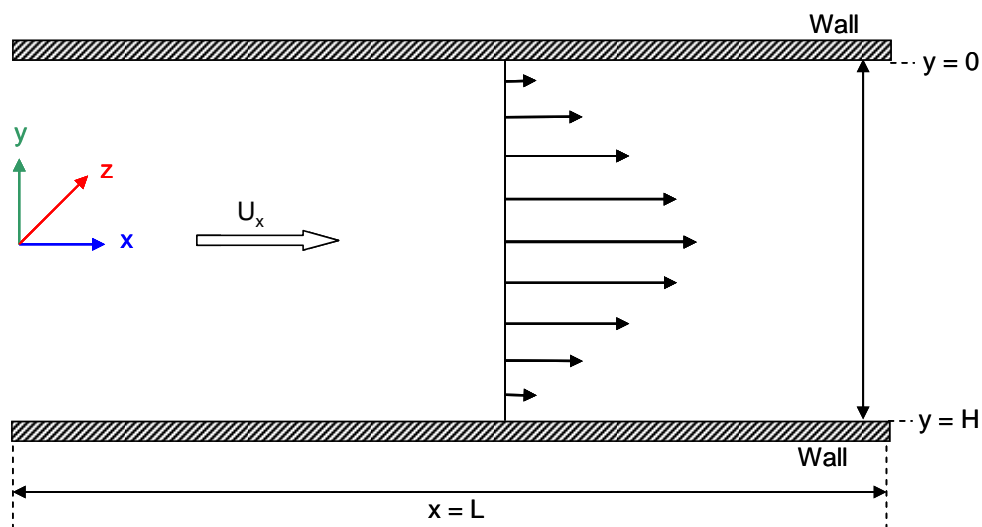


Figure 4.6. Sketch of Velocity Profile

The velocity profile can be simplified using system assumptions.

Assumptions

- The system is at steady state.
- Physical properties are constant.
- Within the reactor, fluid flow is laminar.
- The system has uniform temperature.
- The liquids are Newtonian fluids.
- A rectangular coordinate system is used.
- Gravity is ignored; $g_x = g_y = g_z = 0$.
- Velocities in y and z directions are negligible; $U_y = U_z = 0$.
- Velocity in the x direction is a function of y only; $U_x = U_x(y) \neq 0$.

The velocity profile can be determined by solving the continuity equation and equations of motion for a rectangular coordinate system.

The continuity equation given below can be reduced to equation (4.16) using the above assumptions.

$$(4.15) \quad \frac{\partial \rho}{\partial t} + \frac{\partial}{\partial x}(\rho U_x) + \frac{\partial}{\partial y}(\rho U_y) + \frac{\partial}{\partial z}(\rho U_z) = 0$$

$$(4.16) \quad \frac{\partial U_x}{\partial x} = 0$$

This proves that velocity in the x direction is not a function of x or z but a function of y only.

The fluid dynamics within the micro-reactor are modeled by Navier-Stokes equations. Each directional fluid flow equation is given below.

X-Component:

$$(4.17) \quad \rho\left(\frac{\partial U_x}{\partial t} + U_x \frac{\partial U_x}{\partial x} + U_y \frac{\partial U_x}{\partial y} + U_z \frac{\partial U_x}{\partial z}\right) = -\frac{\partial P}{\partial x} + \rho g_x + \mu\left(\frac{\partial^2 U_x}{\partial x^2} + \frac{\partial^2 U_x}{\partial y^2} + \frac{\partial^2 U_x}{\partial z^2}\right)$$

Y-Component:

$$(4.18) \quad \rho\left(\frac{\partial U_y}{\partial t} + U_x \frac{\partial U_y}{\partial x} + U_y \frac{\partial U_y}{\partial y} + U_z \frac{\partial U_y}{\partial z}\right) = -\frac{\partial P}{\partial y} + \rho g_y + \mu\left(\frac{\partial^2 U_y}{\partial x^2} + \frac{\partial^2 U_y}{\partial y^2} + \frac{\partial^2 U_y}{\partial z^2}\right)$$

Z-Component:

$$(4.19) \quad \rho\left(\frac{\partial U_z}{\partial t} + U_x \frac{\partial U_z}{\partial x} + U_y \frac{\partial U_z}{\partial y} + U_z \frac{\partial U_z}{\partial z}\right) = -\frac{\partial P}{\partial z} + \rho g_z + \mu\left(\frac{\partial^2 U_z}{\partial x^2} + \frac{\partial^2 U_z}{\partial y^2} + \frac{\partial^2 U_z}{\partial z^2}\right)$$

Incorporating the assumptions stated earlier, momentum transfer differential equations are simplified and reduce to the following three equations.

$$(4.20) \quad 0 = -\frac{\partial P}{\partial x} + \mu \frac{\partial^2 U_x}{\partial y^2}$$

$$(4.21) \quad 0 = -\frac{\partial P}{\partial y}$$

$$(4.22) \quad 0 = -\frac{\partial P}{\partial z}$$

From equations (4.21) and (4.22), it is concluded that pressure is only a function of x . Hence, the partial pressure drop in the direction of x can be rewritten as shown in equation (4.23).

$$(4.23) \quad \frac{\partial P}{\partial x} = \frac{-\Delta P}{L}$$

Therefore, equation (4.20) becomes equation (4.24); the simplified x-component of the Navier-Stokes equation.

$$(4.24) \quad \mu \frac{\partial^2 U_x}{\partial y^2} = \frac{-\Delta P}{L} \quad \text{or} \quad \frac{\partial}{\partial y} \left(\frac{\partial U_x}{\partial y} \right) = \frac{-\Delta P}{\mu L}$$

The simplified equation is integrated twice, generating equations (4.25) and (4.26).

$$(4.25) \quad \left(\frac{\partial U_x}{\partial y} \right) = \frac{-\Delta P}{\mu L} y + c_1$$

$$(4.26) \quad U_x = \frac{-\Delta P}{2\mu L} y^2 + c_1 y + c_2$$

The boundary conditions for the system are as follows.

Boundary Conditions

A. No slip at the top wall

$$U_x = 0 \quad \text{where } y = 0$$

B. No slip at the bottom wall

$$U_x = 0 \quad \text{where } y = H$$

Applying boundary condition A to equation (4.25) determines the second integration constant, c_1 , is zero. Applying boundary condition B to equation (4.26) establishes value of the second constant, c_1 .

$$(4.27) \quad c_2 = 0$$

$$(4.28) \quad c_1 = \frac{\Delta P}{2\mu L} H$$

Therefore, the final velocity profile is given in equation (4.29).

$$(4.29) \quad U_x = \frac{\Delta P}{2\mu L} y(H - y)$$

4.3 Mathematical Model

In the following section, a mathematical model is developed that will be used to predict the amount of dibenzothiophene being consumed by the ultraviolet light-assisted, micro-scaled process.

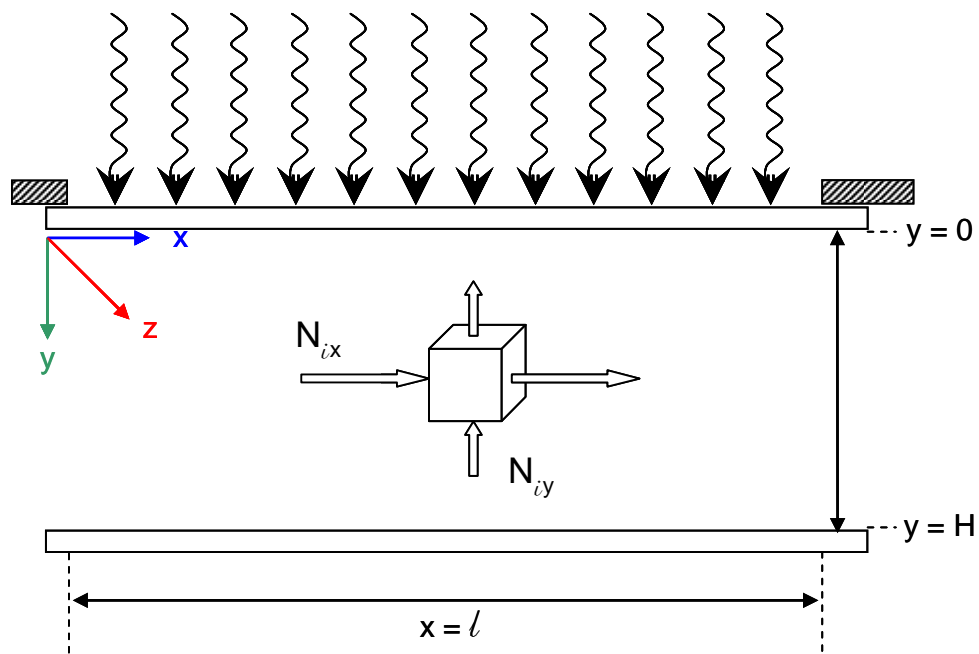


Figure 4.7. Sketch of Differential System

Consider a differential element of fluid within the micro-reactor with dimensions of Δx , Δy , and Δz as depicted in Figure 4.7 above.

Conducting a material balance on dibenzothiophene in the differential element yields the following.

Input:

$$(4.30) \quad N_{i_x} \Big|_{x,t} \Delta y \Delta z + N_{i_y} \Big|_{y,t} \Delta x \Delta z + N_{i_z} \Big|_{z,t} \Delta x \Delta y$$

Output:

$$(4.31) \quad N_{i_x} \Big|_{x+\Delta x,t} \Delta y \Delta z + N_{i_y} \Big|_{y+\Delta y,t} \Delta x \Delta z + N_{i_z} \Big|_{z+\Delta z,t} \Delta x \Delta y$$

Generation:

$$(4.32) \quad r_i \Delta x \Delta y \Delta z$$

Accumulation:

$$(4.33) \quad \frac{[C_i \Big|_{(t+\Delta t)} - C_i \Big|_{(t)}]}{\Delta t} \Delta x \Delta y \Delta z$$

The subscript “i” denotes species i. Ultimately, equations (4.30) through (4.33) combine together to form the mass conservation equation depicted below:

Input – Output + Generation = Accumulation

$$(4.34) \quad \begin{bmatrix} N_{i_x} \Big|_{x,t} \Delta y \Delta z \\ + N_{i_y} \Big|_{y,t} \Delta x \Delta z \\ + N_{i_z} \Big|_{z,t} \Delta x \Delta y \end{bmatrix} - \begin{bmatrix} N_{i_x} \Big|_{x+\Delta x,t} \Delta y \Delta z \\ + N_{i_y} \Big|_{y+\Delta y,t} \Delta x \Delta z \\ + N_{i_z} \Big|_{z+\Delta z,t} \Delta x \Delta y \end{bmatrix} + r_i \Delta x \Delta y \Delta z = \frac{[C_i \Big|_{(t+\Delta t)} - C_i \Big|_{(t)}]}{\Delta t} \Delta x \Delta y \Delta z$$

This equation is then divided by the volume, $\Delta x \Delta y \Delta z$ to yield:

$$(4.35) \quad \frac{[N_{i_x}|_{x,t} - N_{i_x}|_{x+\Delta x,t}]}{\Delta t} + \frac{[N_{i_y}|_{y,t} - N_{i_y}|_{y+\Delta y,t}]}{\Delta t} + \frac{[N_{i_z}|_{z,t} - N_{i_z}|_{z+\Delta z,t}]}{\Delta t} + r_i = \frac{[C_i(t+\Delta t, x) - C_i(t, x)]}{\Delta t}$$

Finally, the limit is taken as Δx , Δy , Δz , and Δt go to zero and the final differential mass conservation equation remains.

$$(4.36) \quad -\frac{\partial}{\partial x} N_{i_x} - \frac{\partial}{\partial y} N_{i_y} - \frac{\partial}{\partial z} N_{i_z} + r_i = \frac{\partial}{\partial t} C_i$$

A general flux equation encompassing both diffusive mass transfer through the solvent, denoted as “species B”, and convective mass transfer of the bulk fluid can be developed for each direction in the coordinate system:

$$(4.37) \quad N_{i_x} = -D_{iB} \frac{\partial}{\partial x} C_i + U_x C_i$$

$$(4.38) \quad N_{i_y} = -D_{iB} \frac{\partial}{\partial y} C_i + U_y C_i$$

$$(4.39) \quad N_{i_z} = -D_{iB} \frac{\partial}{\partial z} C_i + U_z C_i$$

Substituting each flux equation into the appropriate location in equation (4.36) yields:

$$(4.40) \quad -\frac{\partial}{\partial x} \left[-D_{iB} \frac{\partial}{\partial x} C_i + U_x C_i \right] - \frac{\partial}{\partial y} \left[-D_{iB} \frac{\partial}{\partial y} C_i + U_y C_i \right] \\ - \frac{\partial}{\partial z} \left[-D_{iB} \frac{\partial}{\partial z} C_i + U_z C_i \right] + r_i = \frac{\partial}{\partial t} C_i$$

With rearranging, the overall differential equation is determined.

$$(4.41) \quad \left[D_{iB} \frac{\partial^2}{\partial x^2} C_i + D_{iB} \frac{\partial^2}{\partial y^2} C_i + D_{iB} \frac{\partial^2}{\partial z^2} C_i \right] - \left[U_x \frac{\partial}{\partial x} C_i + U_y \frac{\partial}{\partial y} C_i + U_z \frac{\partial}{\partial z} C_i \right] \\ + r_i = \frac{\partial}{\partial t} C_i$$

Assumptions

- The system is at steady state.
- Physical properties are constant.
- The system has uniform temperature.
- The liquid is Newtonian fluids.
- A rectangular coordinate system is used.
- The laminar flow profile given by U_x is fully developed.
- There is a homogeneous reaction given by r_i within the micro-reactor
- Diffusion in the z directions is negligible.

Using the system assumptions stated above, the set of overall mass balance equations is:

Dibenzothiophene:

$$(4.42) \quad \left[D_{\text{DBT/DEC}} \frac{\partial^2}{\partial x^2} C_{\text{DBT}} + D_{\text{DBT/DEC}} \frac{\partial^2}{\partial y^2} C_{\text{DBT}} \right] - U_x \frac{\partial}{\partial x} C_{\text{DBT}} - k_1 C_{\text{DBT}} C_{\text{OH}^*} = 0$$

Hydroxyl Radical:

$$(4.43) \quad \left[D_{\text{OH}^*/\text{DEC}} \frac{\partial^2}{\partial x^2} C_{\text{OH}^*} + D_{\text{OH}^*/\text{DEC}} \frac{\partial^2}{\partial y^2} C_{\text{OH}^*} \right] - \left[U_x \frac{\partial}{\partial x} C_{\text{OH}^*} \right] + \left[\begin{array}{l} -k_1 C_{\text{DBT}} C_{\text{OH}^*} + k_3 C_{\text{TBHP}} I \\ -k_4 C_{\text{OH}^*} \end{array} \right] = 0$$

Tert-Butyl Hydro Peroxide:

$$(4.44) \quad \left[D_{\text{TBHP/DEC}} \frac{\partial^2}{\partial x^2} C_{\text{TBHP}} + D_{\text{TBHP/DEC}} \frac{\partial^2}{\partial y^2} C_{\text{TBHP}} \right] - \left[U_x \frac{\partial}{\partial x} C_{\text{TBHP}} \right] + [k_3 C_{\text{TBHP}} I] = 0$$

Ultraviolet Light:

$$(4.13) \quad I = I_o \cdot 10^{-(\varepsilon_{\text{TBHP}} C_{\text{TBHP}} + \varepsilon_{\text{DBT}} C_{\text{DBT}})y}$$

4.3.1 Scalar Analysis

A comparison is conducted in equation (4.45) to determine which term is more significant in the x direction; diffusive mass transfer or convective mass transfer.

$$(4.45) \quad \frac{D_{iB} \frac{\partial^2}{\partial x^2} C_i}{U_x \frac{\partial}{\partial x} C_i} \sim \frac{D_{iB} \frac{1}{\ell^2} C_i}{U_x \frac{1}{\ell} C_i} \sim \frac{D_{iB} \frac{1}{\ell}}{U_x} \sim \frac{10^{-9} [m^2/\text{sec}] \frac{1}{0.01[m]}}{0.01[m/\text{sec}]} \sim 10^{-9} \ll 1$$

Clearly, diffusion is not as significant as convection in the x direction for any species. Exact fluid velocities and species diffusion coefficients are available in Appendix B and Appendix C. Therefore, the final set of overall mass balance equations consists of the next four equations. The mass transfer system boundary conditions for each species follow.

Dibenzothiophene:

$$(4.46) \quad D_{\text{DBT/DEC}} \frac{\partial^2}{\partial y^2} C_{\text{DBT}} - U_x \frac{\partial}{\partial x} C_{\text{DBT}} - [k_1 C_{\text{DBT}} C_{\text{OH}^*}] = 0$$

Hydroxyl Radical:

$$(4.47) \quad D_{\text{OH}^*/\text{DEC}} \frac{\partial^2}{\partial y^2} C_{\text{OH}^*} - U_x \frac{\partial}{\partial x} C_{\text{OH}^*} + [-k_1 C_{\text{DBT}} C_{\text{OH}^*} + k_3 C_{\text{TBHP}} I - k_4 C_{\text{OH}^*}] = 0$$

Tert-Butyl Hydro Peroxide:

$$(4.48) \quad D_{\text{TBHP/DEC}} \frac{\partial^2}{\partial y^2} C_{\text{TBHP}} - U_x \frac{\partial}{\partial x} C_{\text{TBHP}} + [k_3 C_{\text{TBHP}} I] = 0$$

Ultraviolet Light:

$$(4.13) \quad I = I_o \cdot 10^{(-[\epsilon_{\text{TBHP}} C_{\text{TBHP}} + \epsilon_{\text{DBT}} C_{\text{DBT}}]y)}$$

Boundary Conditions

A. Inlet concentration is constant

$$C_i = C_{i0} \quad \text{where } x = 0$$

B. Impenetrable boundary at the walls

$$\frac{\partial}{\partial y} C_i = 0 \quad \text{where } y = 0$$

$$y = H$$

To ease numerical solving and optimization, the chemistry of the system has been simplified to pseudo first order chemical reaction kinetics.

Figure 4.8 shows multiple absorbance spectrum of solution containing tert-butyl hydro peroxide (left) and dibenzothiophene (center and right) as it is exposed to ultraviolet light. A decrease is visible in the dibenzothiophene absorbance corresponding to a decrease in the dibenzothiophene concentration. As ultraviolet exposure time increases, a sulfone absorbance peak grows in place of the dibenzothiophene peak. Dibenzothiophene is directly converted to sulfone as characterized by the isosbestic point at about 280 nm wavelength. This implies that hydroxyl radicals are very quickly created and readily react with dibenzothiophene.

Consequently, Figure 4.9 demonstrated the absorbance spectrum once the ultraviolet light is turned off. There is no change in the spectrum, indicating that hydroxyl radicals are very short lived and die off so rapidly that dibenzothiophene and sulfone concentrations do not change.

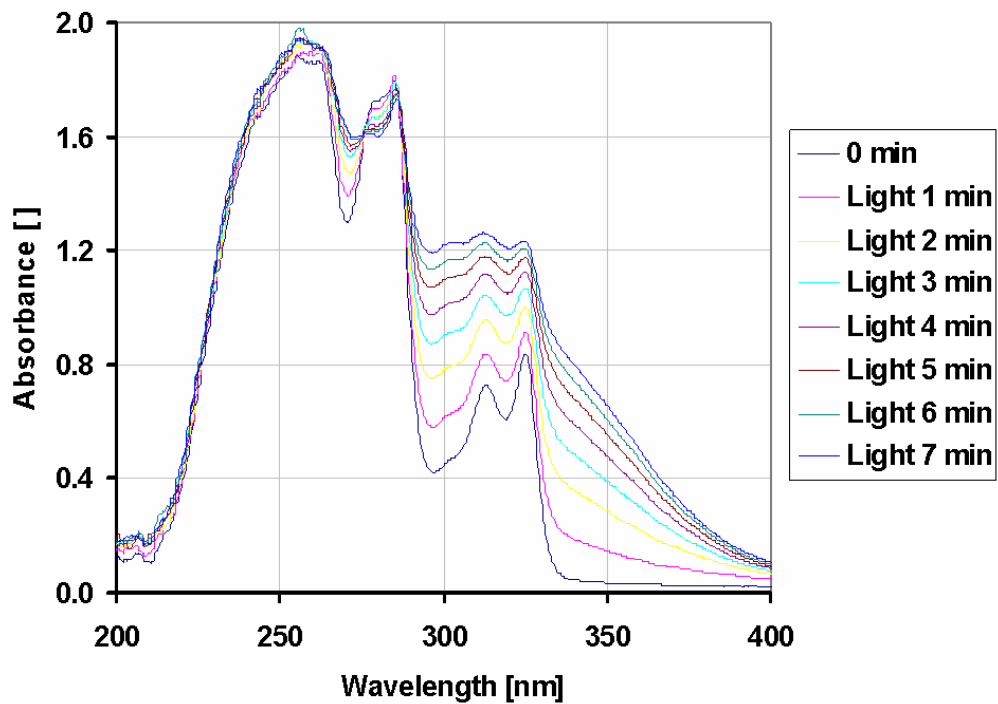


Figure 4.8. Absorbance Spectrum of Tert-Butyl Hydro Peroxide and Dibenzothiophene Solution Exposed to Ultraviolet Light Over Time

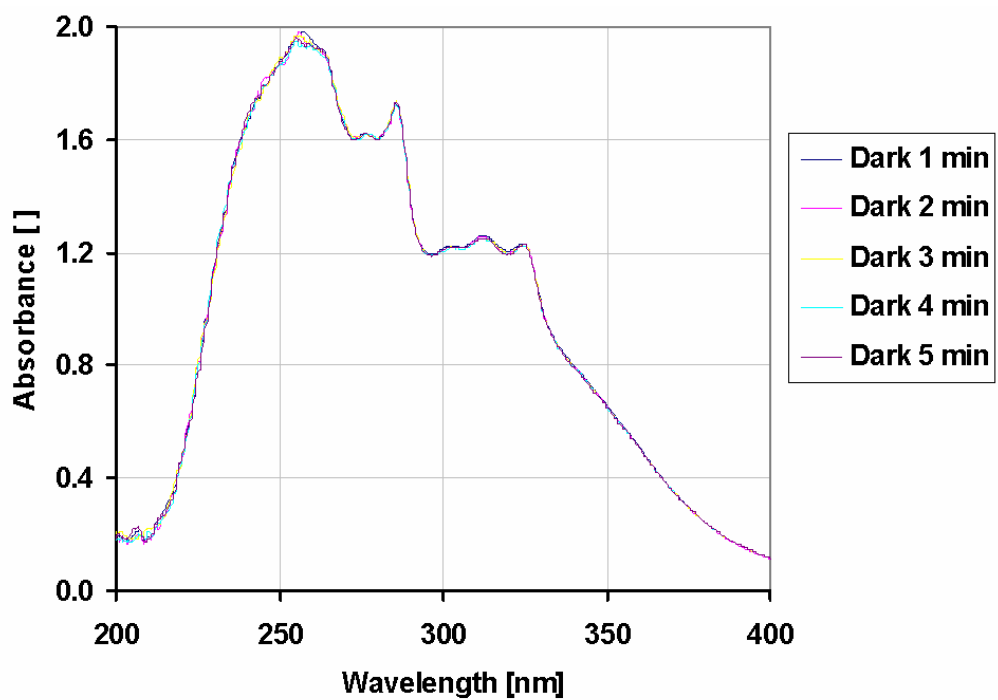


Figure 4.9. Absorbance Spectrum of Tert-Butyl Hydro Peroxide and Dibenzothiophene Solution Shielded From Ultraviolet Light Over Time

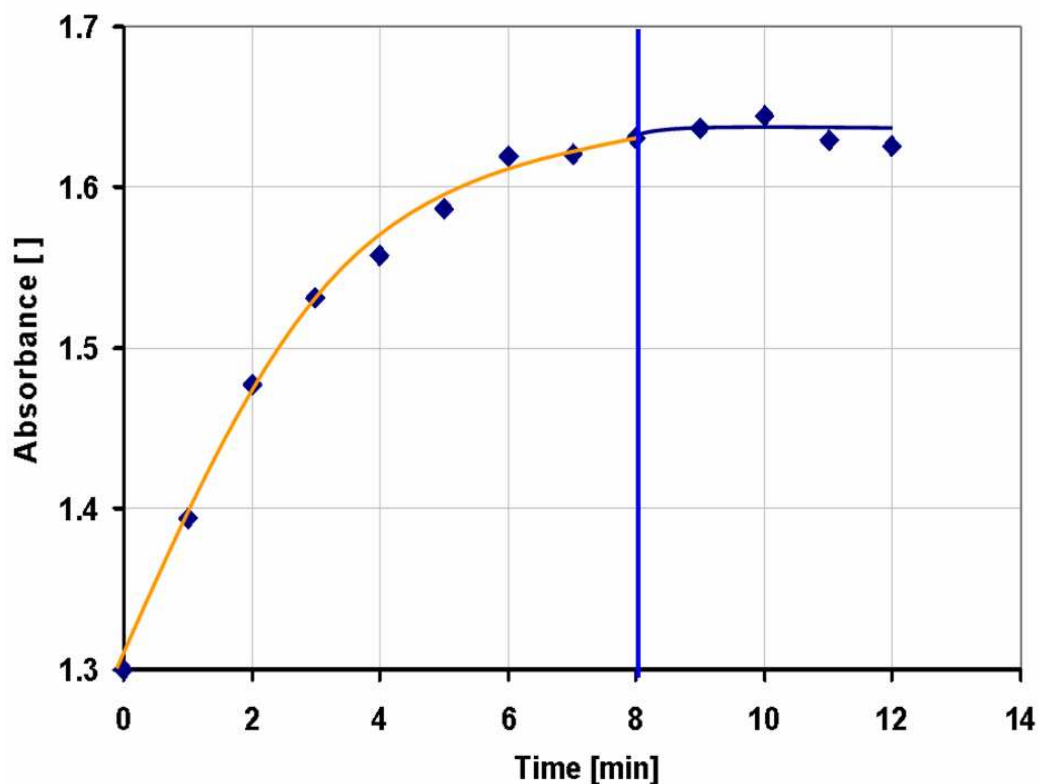


Figure 4.10. Absorbance Spectrum of Tert-Butyl Hydro Peroxide and Dibenzothiophene Solution Shielded From Ultraviolet Light Over Time

Figure 4.10 combines light and dark information from Figure 4.8 and Figure 4.9 to illustrate absorbance as a function of time for a wavelength of 271 nm. Ultraviolet light is removed at 8 minutes, illustrated by the blue line and a flattening in absorbance. The reaction stops when ultraviolet light is eliminated. This further supports that the dibenzothiophene reaction is a function of light intensity as absorbance does not change significantly once light is taken away.

The desulfurization reaction is reduced to a function of dibenzothiophene concentration and light intensity as seen in equation (4.49).

$$(4.49) \quad -r_{DBT} = k_1 C_{DBT} I$$

Equation (4.49) can be rewritten into a pseudo first order reaction, equation (4.50), where the rate constant is a combination of k_1 and light intensity. Thus, the optimized COMSOL model reaction rate constant, k , will have units of surface area per photon count.

$$(4.50) \quad -r_{DBT} = k C_{DBT}$$

$$(4.51) \quad k = \frac{k_1}{I}$$

A constant extinction coefficient is used in the simplified model. Given in equation (4.52), the new extinction coefficient is a combination of each reactant's coefficient and average concentration.

$$(4.52) \quad \varepsilon = \varepsilon_{TBHP} \overline{C_{TBHP}} + \varepsilon_{DBT} \overline{C_{DBT}}$$

The final set of mass balance equations and boundary conditions need to be scaled to facilitate simulation of the system using modeling software; COMSOL Multiphysics Version 3.3.

$$(4.53) \quad \frac{x}{\ell} = \eta$$

$$(4.54) \quad \frac{y}{H} = \xi$$

The x direction will be scaled with respect to ℓ , the length of the micro-reactor window, as shown in (4.53). The y direction will be scaled with respect to H , the spacer and fluid thickness, given by (4.54).

4.3.2 Final COMSOL Model Equations

The final model equations to be put into COMSOL Multiphysics Version 3.3 are given in equations (4.55) through (4.57).

Ultraviolet Light:

$$(4.55) \quad I = I_o \cdot 10^{(-\varepsilon \xi H)}$$

Velocity Profile:

$$(4.56) \quad \frac{U_x}{\ell} = \frac{\Delta P}{2\mu\ell^2} H^2 \xi(1-\xi)$$

Dibenzothiophene:

$$(4.57) \quad \frac{D_{DBT,y}}{H^2} \frac{\partial^2}{\partial \xi^2} C_{DBT} + \frac{D_{DBT,x}}{\ell^2} \frac{\partial^2}{\partial \eta^2} C_{DBT} - \frac{U_x}{\ell} \frac{\partial}{\partial \eta} C_{DBT} - [k C_{DBT}] = 0$$

The new boundary conditions for the scaled mass transfer system are as follows:

Boundary Conditions

A. Inlet concentration is constant

$$C_i = C_{i0} \quad \text{where } \eta = 0$$

B. Impenetrable boundary at the walls

$$\frac{\partial}{\partial y} C_i = 0 \quad \text{where } \xi = 0$$

$$\xi = 1$$

CHAPTER 5

EXPERIMENTAL APPARATUS AND METHODS

5.1 Materials

Dibenzothiophene (purity 98+ % Fluka Chemical Company) is used to model sulfur containing compounds in fuel. Dibenzothiophene sulfone (purity 97 % ALDRICH Chemical Company) is used for calibration of HPLC. Tert-butyl hydroperoxide solution is used as the oxidizing agent (~5.5 M in decane) was obtained from Fluka Chemical Company. Decane (purity 95+ % from Fluka Chemical Company) is used as the simulation fuel. A mixture of acetonitrile (purity 99.8 % from EMD Chemicals, Inc.) and reverse osmosis (RO) water from a Millipore Corporation Milli-Q Academic A10 system is used as the mobile phase in the HPLC. Tetrahydrofuran with a purity of 99.9+ %, obtained from EMD Chemicals, Inc. is used to clean the HPLC and the micro-reactor. All chemicals were used as received.

5.2 Equipment

A programmable syringe pump manufactured by New Era Pump Systems, Inc. model NE-1010 is used to deliver feed reactants to the micro-reactor. A mercury lamp, model STER-L-RAY G12T6L-52431 from Atlantic Ultraviolet Co., with a wave length of 254 nm irradiates reactants inside the micro-reactor.

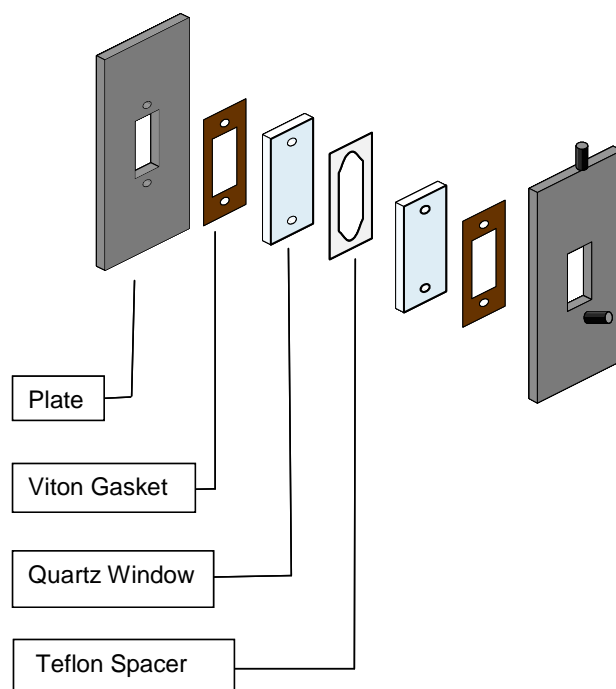


Figure 5.1. Expanded UV Light Reactor Sketch

A set from International Crystal Laboratories was used as a reaction vessel. The micro-reactor is a liquid cell model SL-3 consisting of the following elements assembled with screws as shown in Figure 5.1, Figure 5.2, and Figure 5.3:

- Stainless steel front plate, part # 0005-599.
- Stainless steel back plate, part # 0005-600.
- Two Viton gaskets, part # 0001-2107.
- Two polished quartz windows with dimensions of 38.5 mm x 19.5 mm x 4 mm, part # 0002H-7827.
- Teflon spacer set of various thicknesses (50, 100 and 200 μm), part # 0001-3875.

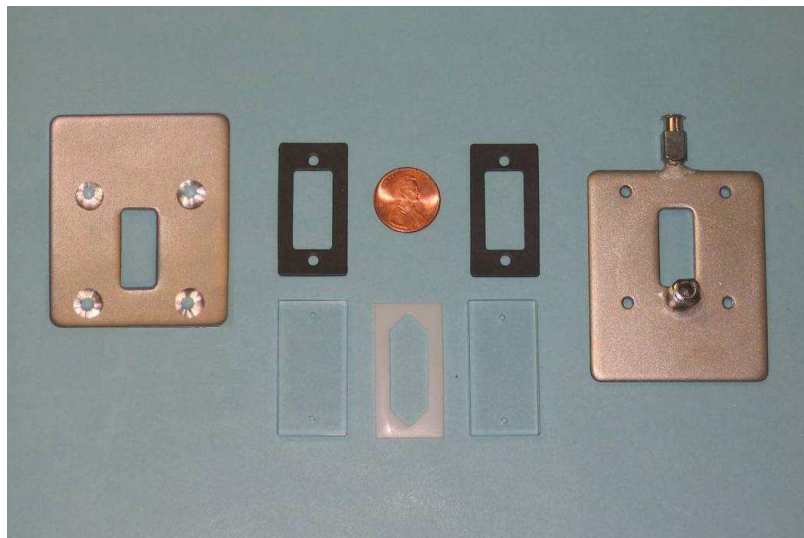


Figure 5.2. Exploded Micro-Reactor

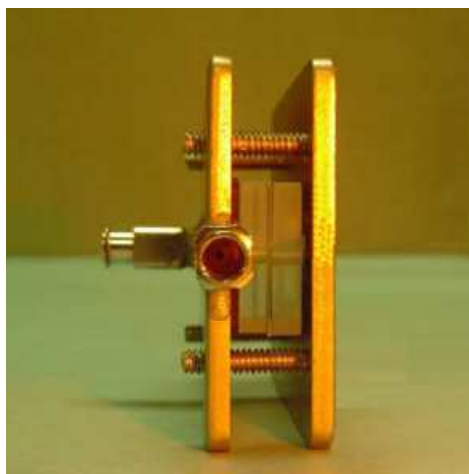


Figure 5.3. Micro-Reactor Side View

High-pressure liquid chromatography instrument (HPLC) shown in Figure 5.4 is used to determine the concentrations of tert-butyl hydro peroxide, dibenzothiophene, and sulfone in the reactor product stream. An HPLC pump delivers mobile phase to the column at the flow rate of 1.0 ml/min and up to 3000

psi. Samples are injected into a sample loop of approximately 20 μl . The column is a Waters XTerra RP18 column with particle size of 3.5 μm , column inner diameter of 4.6 mm, column length of 150 mm, and pore size of 125 \AA with silica gel packing. The column is heated to 30 $^{\circ}\text{C}$. Finally, a Hewlett Packard variable ultraviolet detector set to the wavelength of 275 nm determines the components. The mobile phase used in the HPLC consists of 66 % acetonitrile and 34 % RO water. All chemicals are HPLC grade.

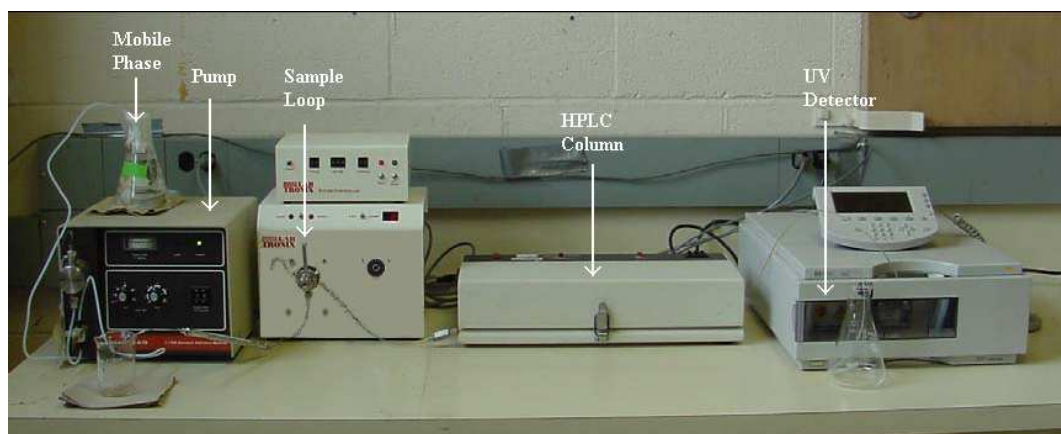


Figure 5.4. HPLC Analytical System

5.3 Desulfurization Experimental Method

The experiment setup is shown in Figure 5.6 and Figure 5.7. A solution of dibenzothiophene in decane enclosed in a 60 ml syringe and mounted on the syringe pump. The syringe pump delivers the solution to the micro-reactor at a constant volumetric flow rate. The feed stream enters the micro-reactor and forms a thin film. The thickness of the layer is determined by the spacer's thickness.

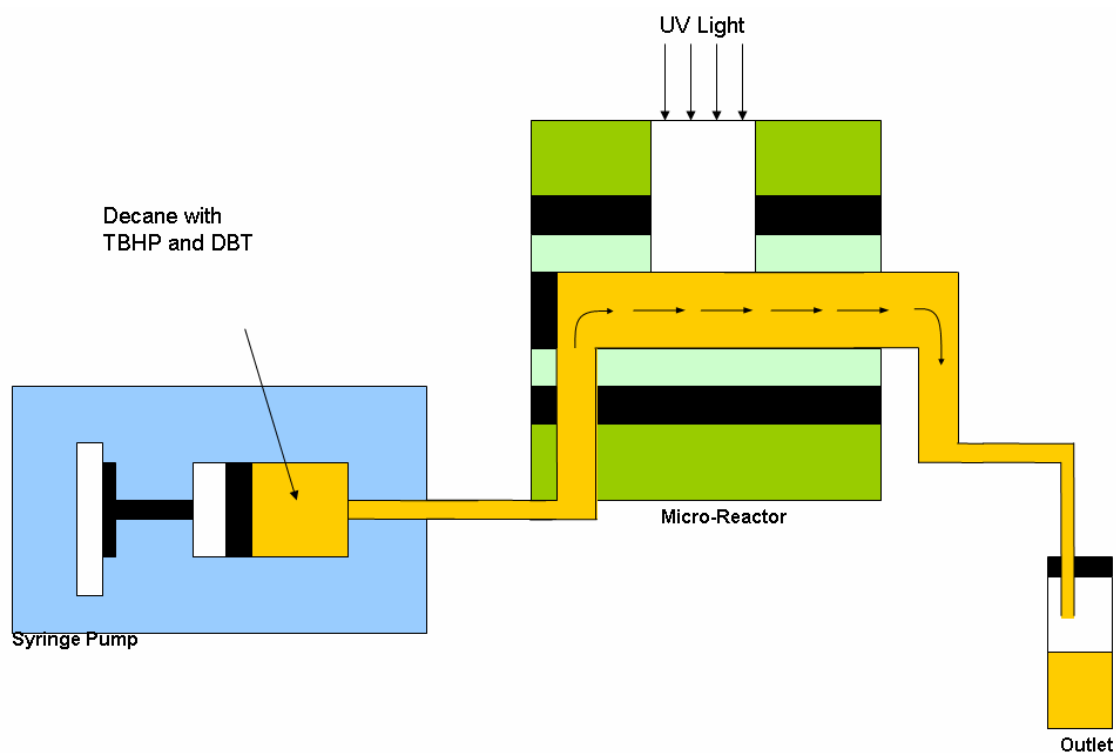


Figure 5.5. Sketch of Experimental Set Up

For the 100 μm thick spacer, volumetric flow rates of 660.0, 330.0, 220.0, 165.0, 132.0, 110.0, 88.0, 73.3, 66.0, 57.4, 52.8, 48.9, and 44.0 $\mu\text{l}/\text{min}$ were used. These rates correspond to residence times of 2, 4, 6, 8, 10, 12, 15, 18, 20, 23, 25, 27, and 30 seconds, respectively.

For the 50 μm thick spacer, volumetric flow rates of 165.0, 132.0, 110.0, 82.5, 66.0, 55.0, 44.0, 36.7, 33.0, 28.7, 26.4, 24.4, and 22.0 $\mu\text{l}/\text{min}$ were used. These rates correspond to residence times of 4, 5, 6, 8, 10, 12, 15, 18, 20, 23, 25, 27, and 30 seconds, respectively.

A mercury lamp is suspended above the micro-reactor window and irradiates the fluid within. The system is allowed to reach steady state. Fluid exiting the micro-reactor is collected in amber-colored vials and samples are injected into the HPLC to determine compositions.

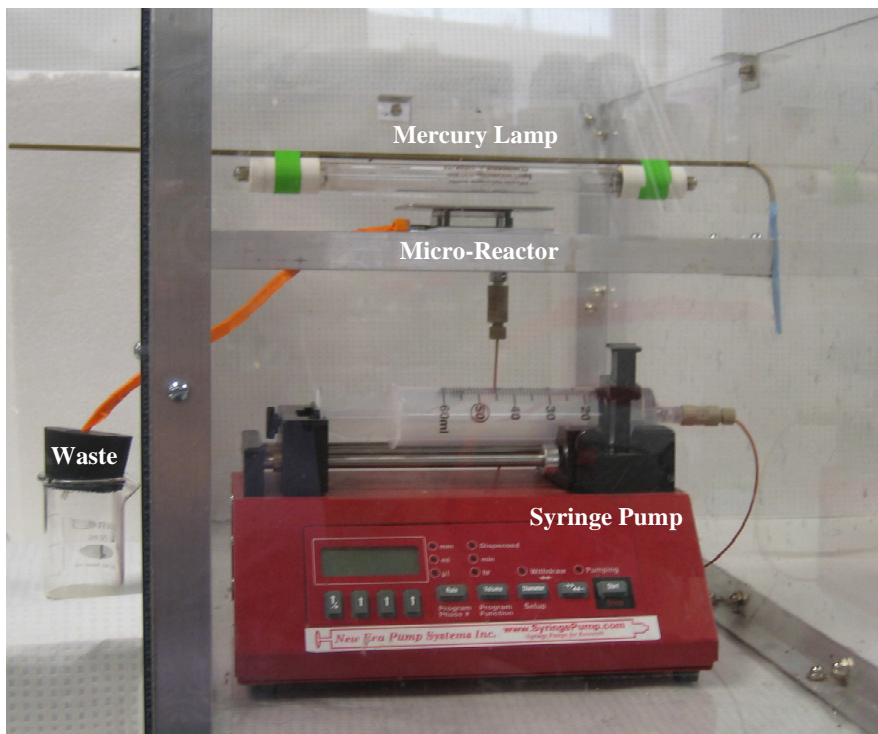


Figure 5.6. Desulfurization Experimental Setup

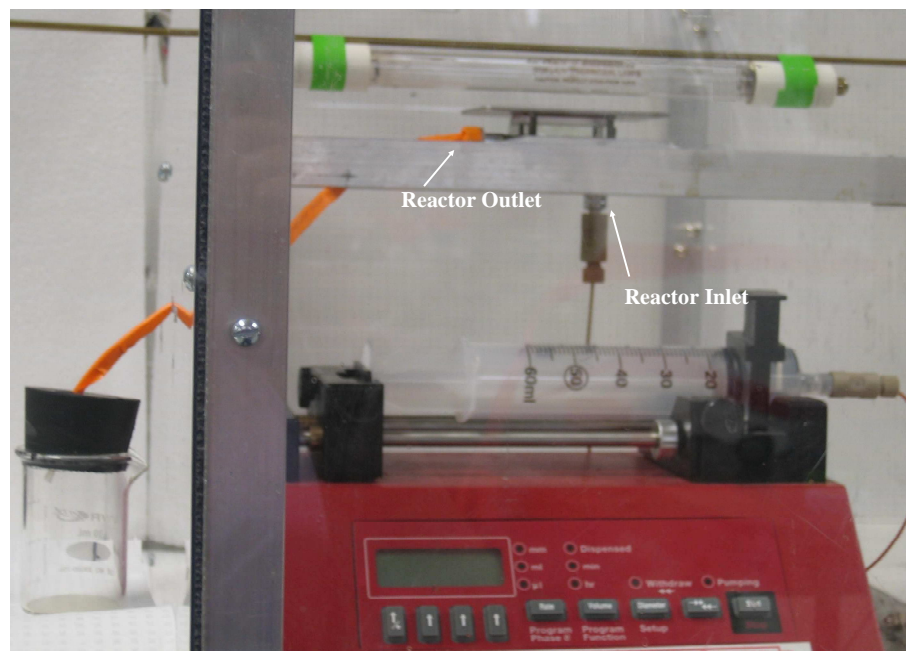


Figure 5.7. Experimental Setup With Emphasis on Reactor Inlet and Outlet Ports

5.4 Desulfurization Analytical Method

An HPLC was used to determine species concentrations. Calibration curves were created using a series of decane solutions at known concentrations. The calibration curves of dibenzothiophene in decane, sulfone in decane, and tert-butyl hydro peroxide in decane, Appendix D - F, yield a species concentration for a given peak area in the reactor product stream.

The dibenzothiophene, dibenzothiophene sulfone, and tert-butyl hydro peroxide peaks eluted from the silica gel column at a specific retention times. Figure 5.8, Figure 5.9, and Figure 5.10 show chromatographs of dibenzothiophene, sulfone and tert-butyl hydro peroxide, respectively.

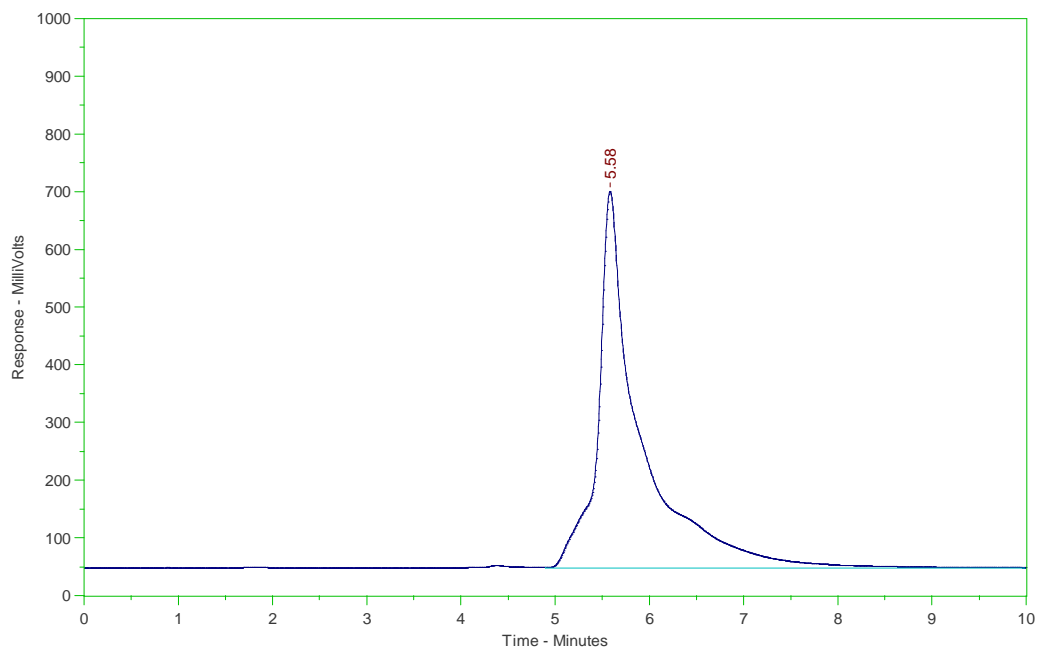


Figure 5.8. Sample Dibenzothiophene Chromatogram

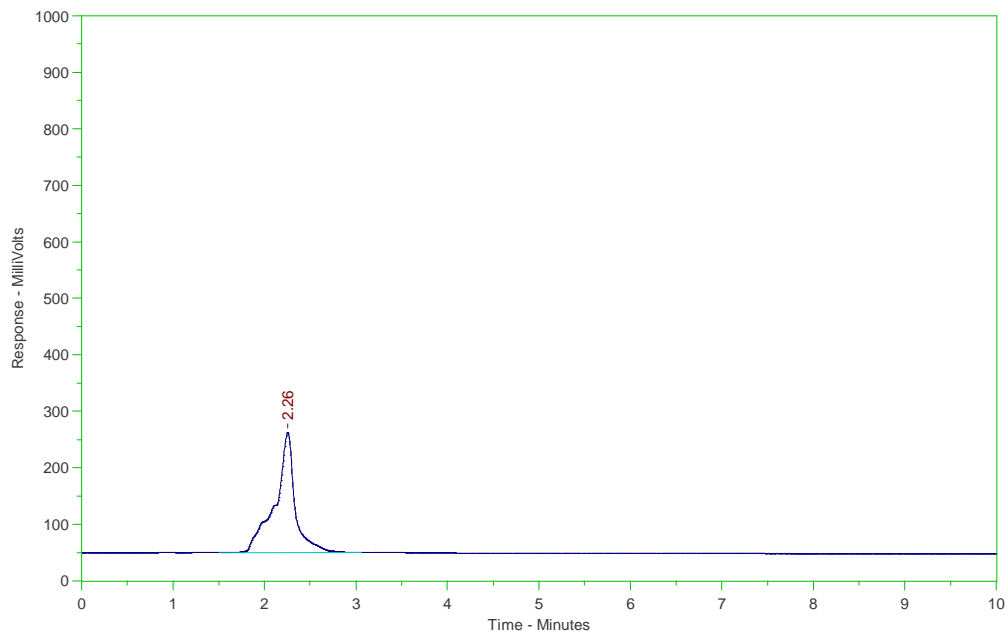


Figure 5.9. Sample Sulfone Chromatogram

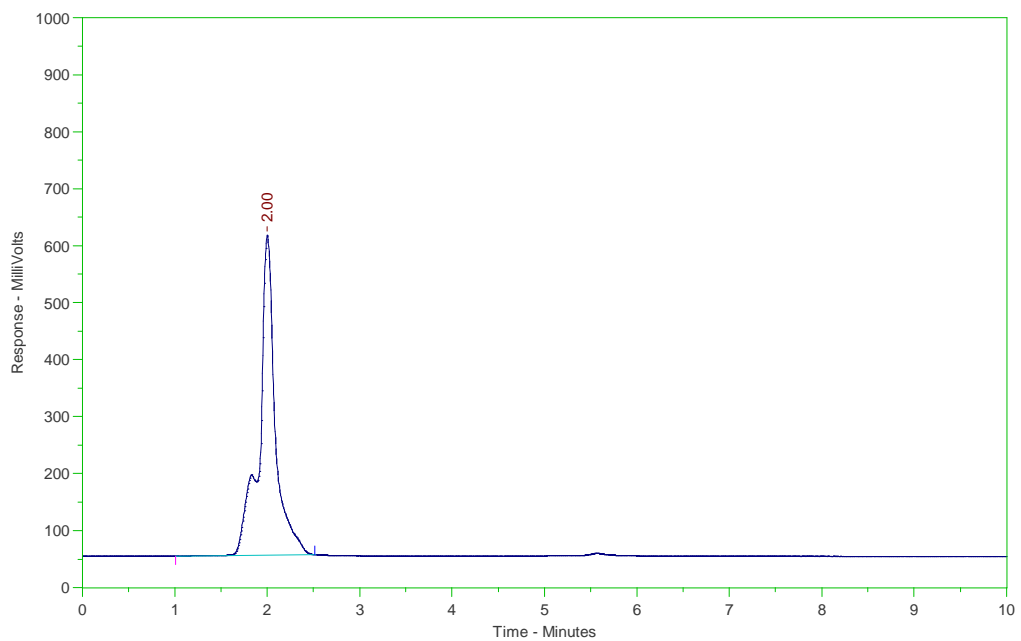


Figure 5.10. Sample Tert-butyl Hydro Peroxide Chromatogram

The obtained peaks for dibenzothiophene, sulfone, and tert-butyl hydro peroxide have retention times of about 5.6 minutes, 2.3 minutes and 2.0 minutes, respectively, at these HPLC conditions. The analog voltage signal from the absorbance cell in the UV detector was recorded by Visual Designer, the data acquisition software.

CHAPTER 6

EXPERIMENTAL MEASUREMENTS

Experiments were conducted following the experimental and analytical methods described in Chapter 5. The desulfurization results of all HPLC analysis are listed in Appendix G - K.

At least one experiment in every data set for a given set of experimental conditions was repeated five times. The variance between the five experiments was never more than 8.6 %. Thus, experiments qualify as reproducible. Instrument error was determined by running the same samples through the HPLC ten times. Variance in HPLC measurements was less than 1%. Hence, subsequent samples were only run once. To determine if the data sets are statistically different from each other, a paired t-test is implemented. Appendix L outlines the method used to test the dibenzothiophene conversion data.

6.1 Absent Light Source

To ensure the oxidation in dibenzothiophene is a direct result from ultraviolet light exposure, a single experiment was conducted in the absence of an ultraviolet light source. A feed solution with a known amount of dibenzothiophene and tert-butyl hydro peroxide in decane ran through the micro-reactor at multiple flow rates yielding different residence times whilst the mercury lamp was not energized.

Figure 6.1 indicates dibenzothiophene and tert-butyl hydro peroxide concentrations as a function of residence time in the dark experiment. Results show concentrations do not change significantly over time when a light source is not present. It can be concluded that the oxidation reaction within the micro-reactor only occurs when reactants are exposed to ultraviolet light

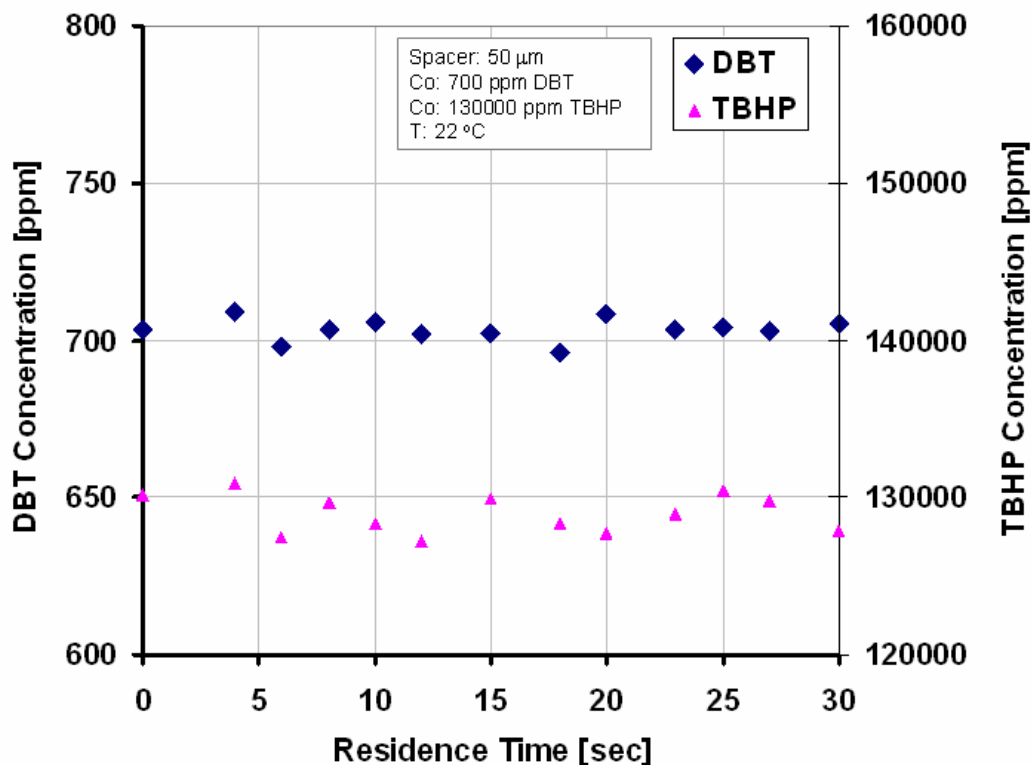


Figure 6.1. DBT and TBHP Concentrations at Multiple Residence Times Without the Presence of UV Light Using a 50 μm Spacer at a System Temperature of 22 $^{\circ}\text{C}$

6.2 Desulfurization with 100 Micron Spacer

Reaction kinetics and performance parameters are desired for the micro-reactor in the oxidation of dibenzothiophene with tert-butyl hydro peroxide in the presence of ultraviolet light. Therefore, experiments were done at multiple residence times for three different temperatures using a spacer of 100 μm . Figure 6.2 shows the normalized concentration of dibenzothiophene as a function of mean residence time for different operating temperatures with dashed trend lines to guide the eye.

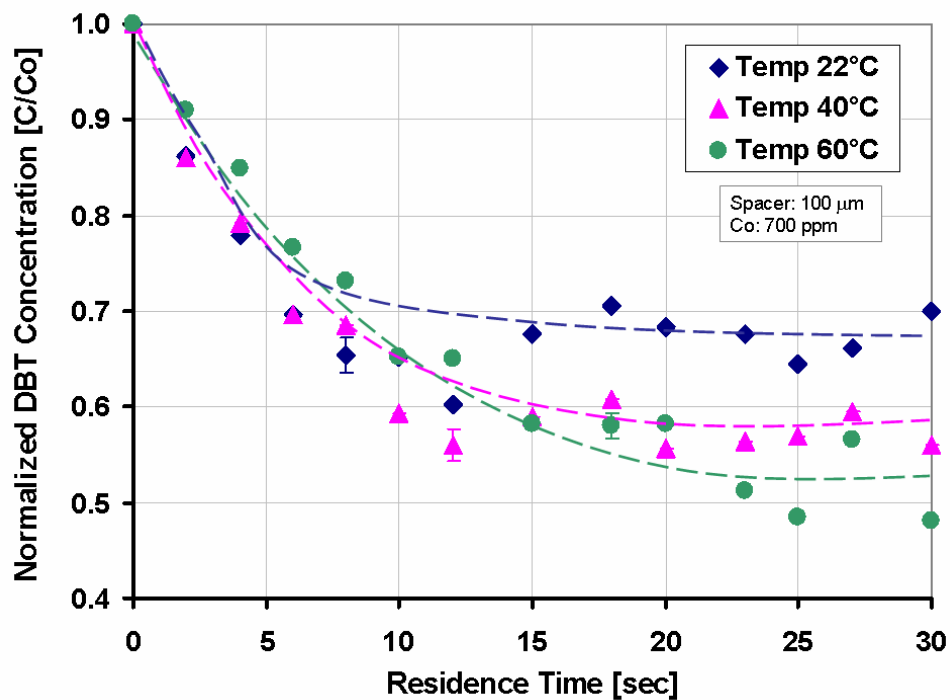


Figure 6.2. Normalized Concentration of DBT at Various Residence Times for Three Temperatures in Micro-Reactor with 100 μm Thick Spacer

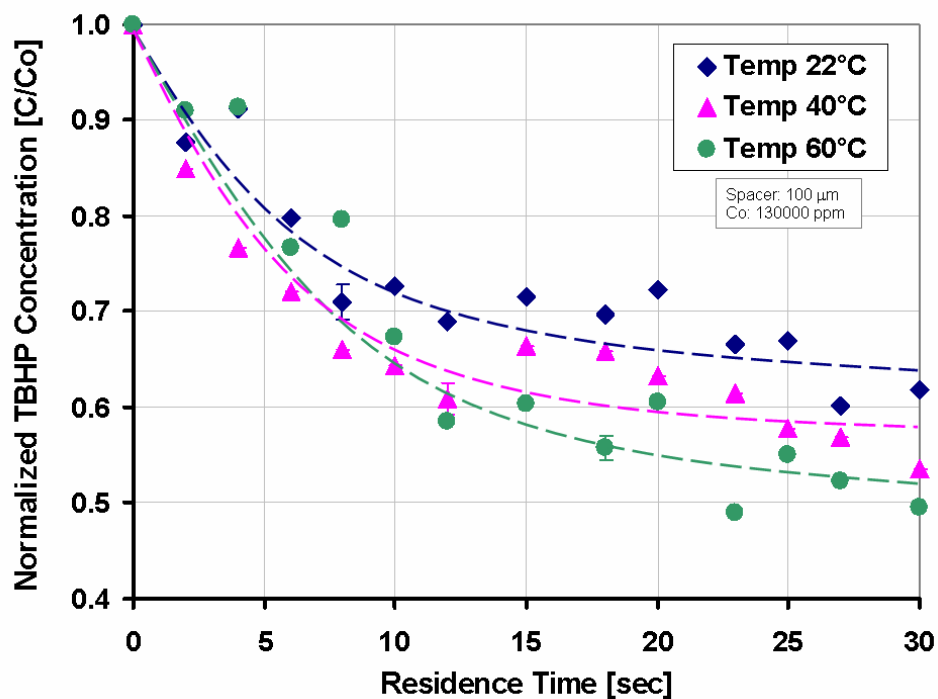


Figure 6.3. Normalized Concentration of TBHP at Various Residence Times for Three Temperatures in Micro-Reactor with 100 μm Thickness

The data set at 22°C shows a dibenzothiophene concentration reduction of about 32% with a final concentration of 491 ppm dibenzothiophene (or 85 ppm sulfur). At a temperature of 40 °C the conversion of dibenzothiophene is 42% with a drop to 394 ppm dibenzothiophene or 69 ppm sulfur. The highest temperature yields a decrease to 362 ppm dibenzothiophene or 63 ppm sulfur for an ultimate desulfurization of 47%.

Tert-butyl hydro peroxide concentrations were also recorded for the 100 µm spacer experiments and are listed in Appendix H. Figure 6.3 and Figure 6.5 show the amount of tert-butyl hydro peroxide present in the micro-reactor outlet changes significantly with residence time. The trend in tert-butyl hydro peroxide concentration mimics that of dibenzothiophene. However, much more tert-butyl hydro peroxide is consumed compared to the stoichiometric amount required on molar basis. The ultimate destination of the tert-butyl hydro peroxide not utilized in the oxidation reaction is not clear, and is absorbed into the previously mentioned k_4 reaction rate constant.

6.3 Desulfurization with 50 Micron Spacer

In order to evaluate the effect of micro-channel thickness on system performance, experiments were done at multiple residence times for two temperatures using the 50 µm spacer in the micro-reactor. Figure 6.4 shows the normalized concentration of dibenzothiophene as a function of mean residence time for different operating temperatures. Dashed lines are meant to guide the eye.

The data set at 22 °C shows a dibenzothiophene concentration reduction of about 63 % with a final concentration of 250 ppm dibenzothiophene (or 43 ppm sulfur). At a temperature of 40 °C the conversion of dibenzothiophene is about 79 % with a drop to 182 ppm dibenzothiophene or 32 ppm sulfur.

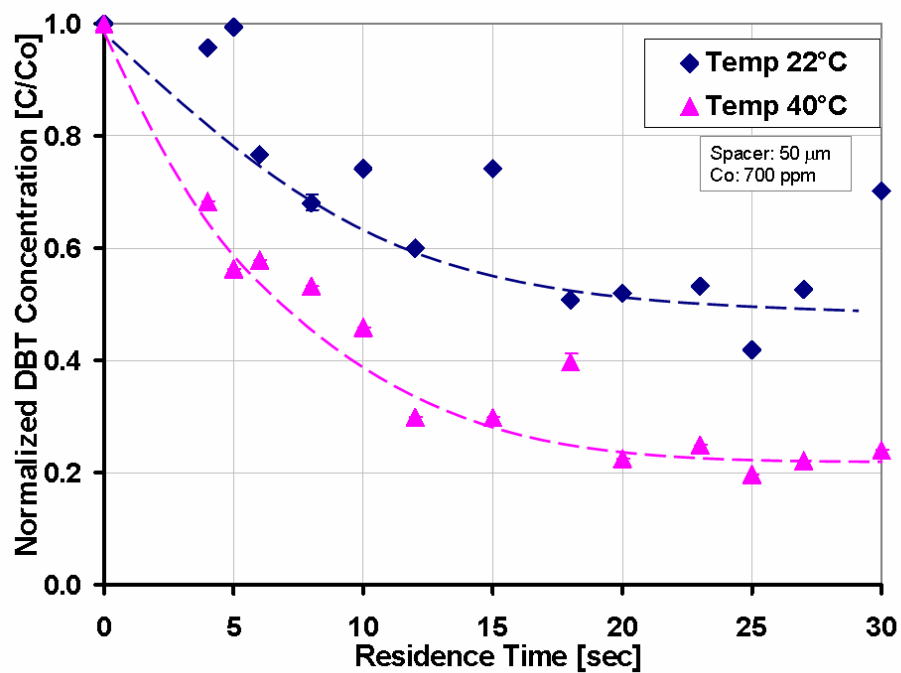


Figure 6.4. Normalized Concentration of DBT at Various Residence Times for Two Temperatures in Micro-Reactor with 50 μm Thick Spacer

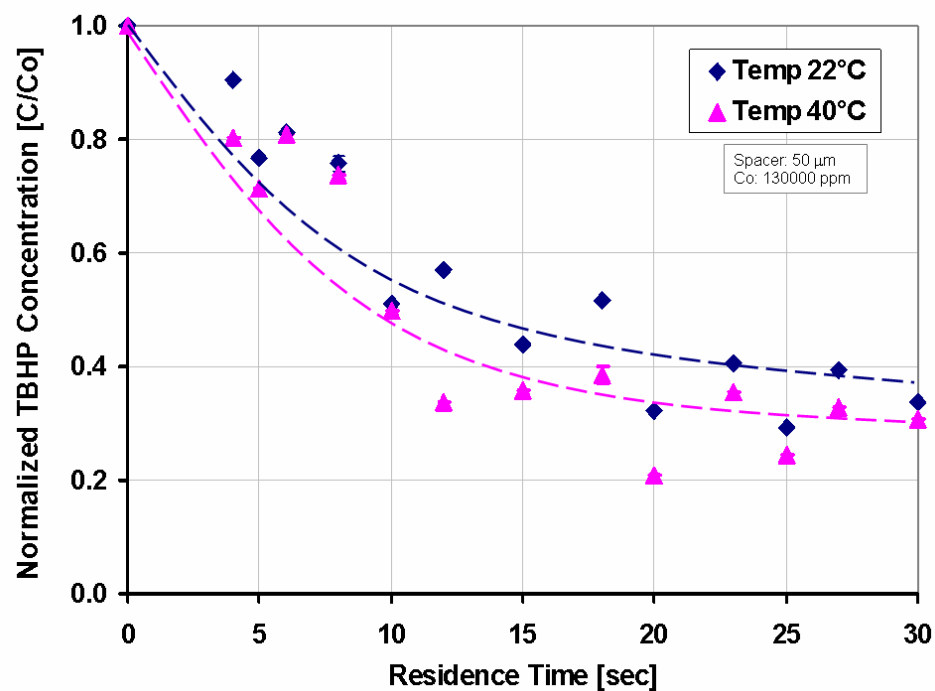


Figure 6.5 Normalized Concentration of TBHP at Various Residence Times for Two Temperatures in Micro-Reactor with 50 μm Thickness

6.4 Material Balance on Sulfur

Material balances account for material entering and leaving a system as matter can not disappear or be created according to the mass conservation principle. All sulfur that enters the micro-reactor must either leave the system or accumulate within the system. In this arrangement, sulfur enters as dibenzothiophene and exits in two forms; unreacted dibenzothiophene and oxidation product sulfone. Therefore, for any given residence time through the reactor the sulfur concentration of the reactor outlet should be the same as the sulfur concentration of the feed.

The micro-reactor product stream is analyzed to yield the concentration of newly created sulfone and remaining dibenzothiophene. Each is converted into sulfur concentrations, added together to give the final sulfur concentration, and compared to the original sulfur concentration.

The material balance information is gathered for one temperature for the 100 μm spacer system and for two temperatures for the 50 μm spacer assembly. The material balance is not explored at every set of operating conditions as the systems listed above are representative of the other arrangements.

6.4.1 100 Micron System

Appendix J contains all of the material balance information from the micro-reactor system with 100 μm spacer and an operating temperature of 22°C. Figure 6.6 shows the downward trend of dibenzothiophene and increase of sulfone in the micro-reactor outlet at various residence times. Dashed lines guide the eye. The final normalized dibenzothiophene concentration, on the left y axis, is about 0.70. In other words, about 70% of the original dibenzothiophene is still present. This is consistent with the results depicted in Figure 6.2 for the same arrangement. The normalized sulfone concentration, the right y axis, documents growth from zero in the feed to about 25% of the total sulfur at the longest residence time.

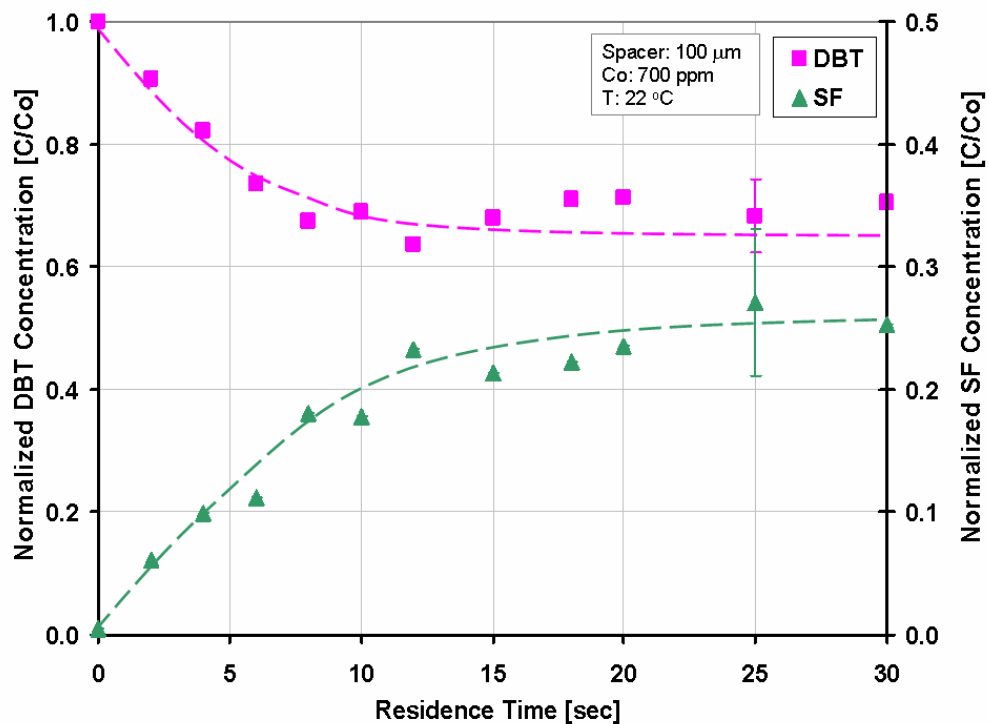


Figure 6.6. Material Balance on Sulfur Containing Species in Micro-Reactor System with 100µm Spacer Operated at 22°C

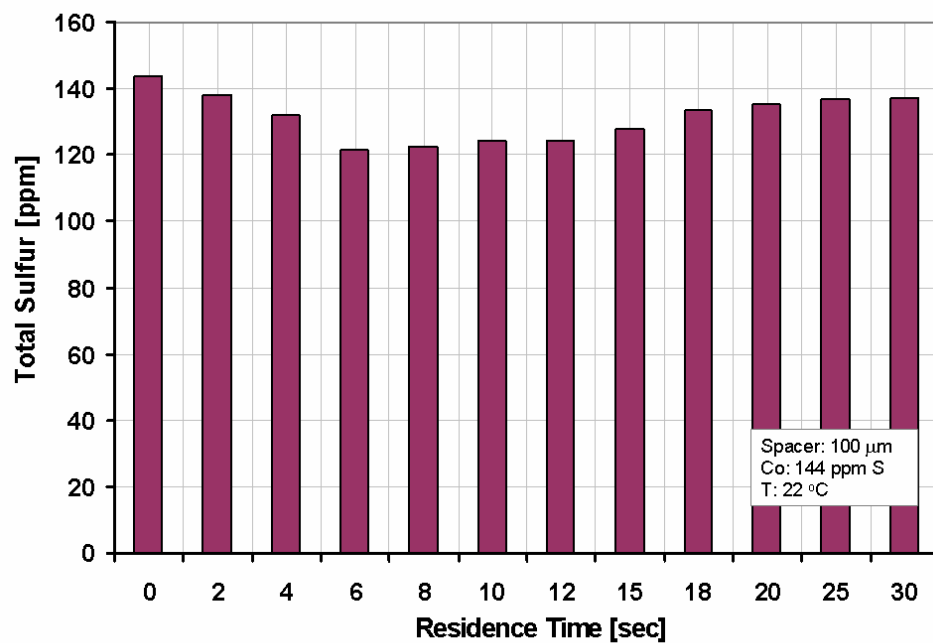


Figure 6.7. Total Sulfur Concentration of Micro-Reactor System Outlet Operated with 100µm Spacer and Temperature of 22°C

As shown in Figure 6.7, the sulfur concentration of the feed or at a residence time of zero seconds is about 145 ppm of sulfur. The total amount of sulfur, present as both dibenzothiophene and sulfone, is given for each residence time. On average, about 13 ppm of sulfur is unaccounted for or “missing” from the original sulfur count. This corresponds to about 9% of the total sulfur in the material balance. This is close to the experimental error observed for the overall system.

6.4.2 50 Micron System

Material balance information from the micro-reactor system with 50 μ m spacer and an operating temperature of 22 $^{\circ}$ C are summarized in Appendix K. Figure 6.8 depicts a decrease in dibenzothiophene and an upward trend for sulfone in the micro-reactor outlet as a function of residence time. About 40% of unreacted dibenzothiophene is present (left axis). These results are similar to the results depicted in Figure 6.4 for the same arrangement. An accumulation of about 70% is shown for sulfone.

In Figure 6.9, the sulfur feed concentration is 125 ppm of sulfur. Only 2 ppm of sulfur is absent from the original sulfur mark. This indicates that only 1.2% of the total sulfur in the material balance is lost. Essentially, all of the reacted dibenzothiophene forms sulfone; implying that the oxidation intermediate molecule is not significantly present.

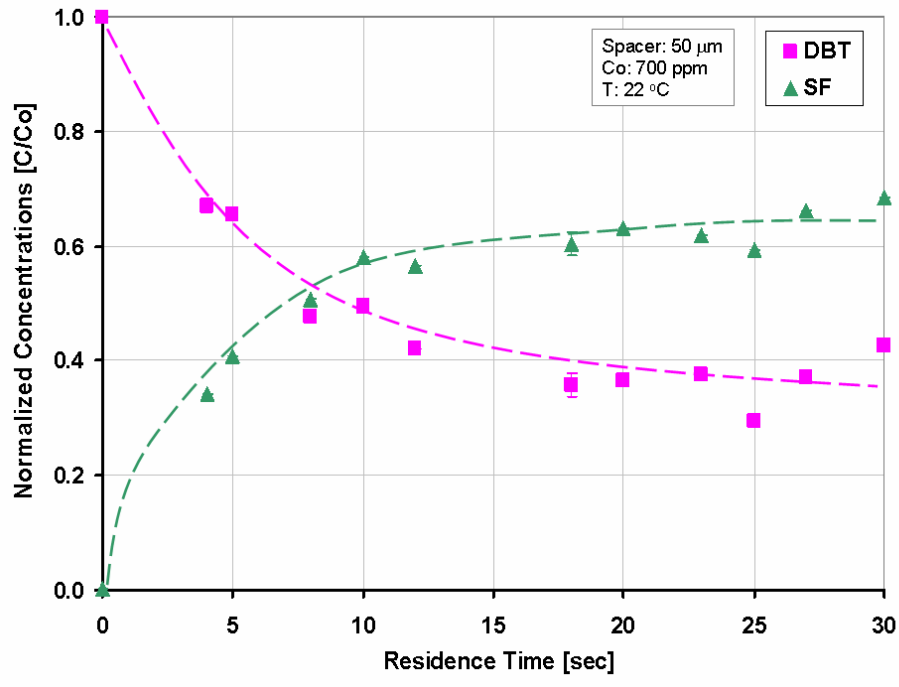


Figure 6.8. Material Balance on Sulfur Containing Species in Micro-Reactor System with 50 μm Spacer Operated at 22 $^{\circ}\text{C}$

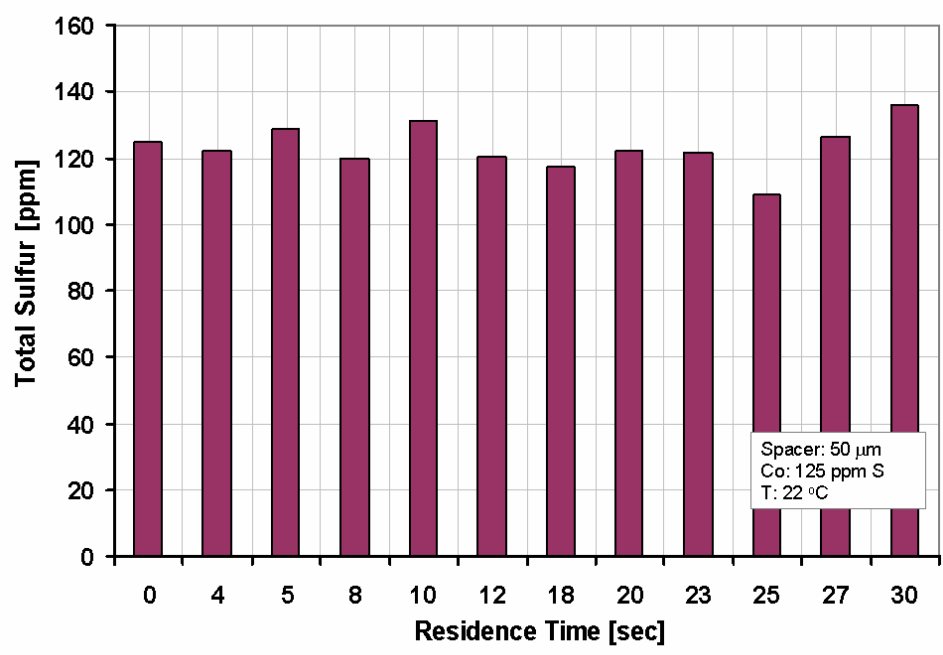


Figure 6.9. Total Sulfur Concentration of Micro-Reactor System Outlet Operated with 50 μm Spacer and Temperature of 22 $^{\circ}\text{C}$

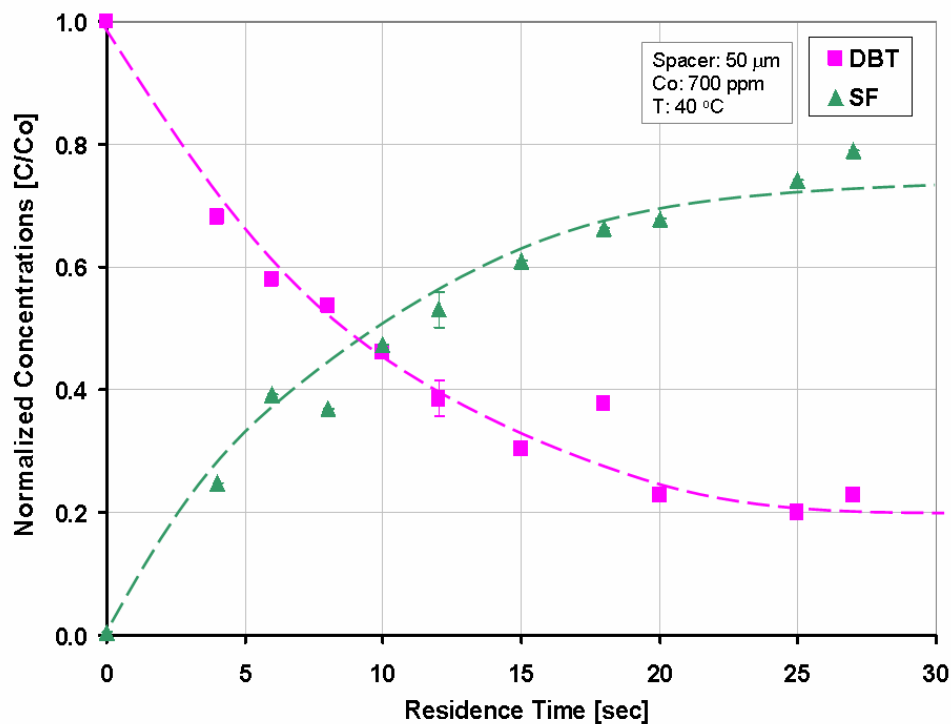


Figure 6.10. Material Balance on Sulfur Containing Species in Micro-Reactor System with 50 μm Spacer Operated at 40 $^{\circ}\text{C}$

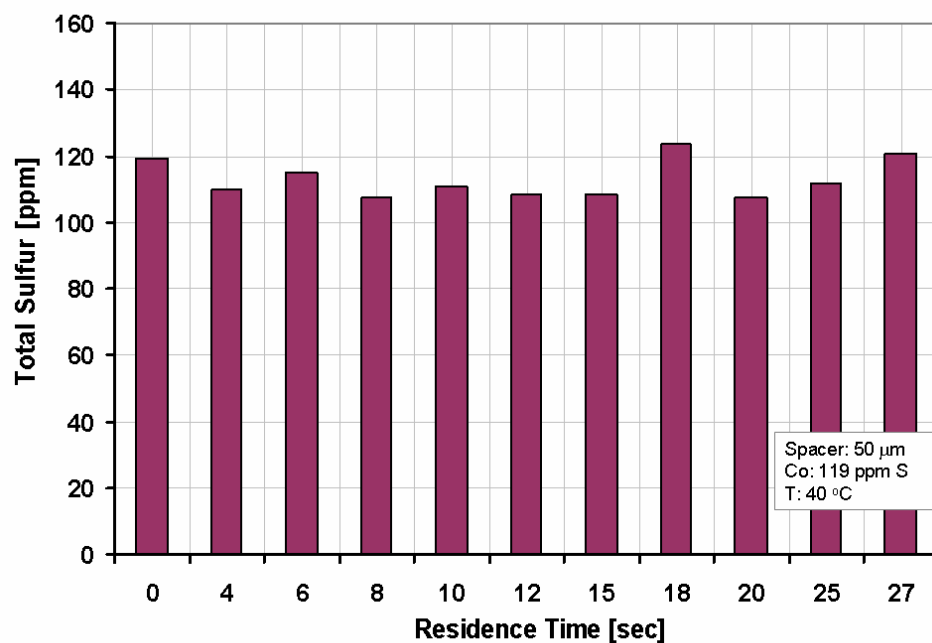


Figure 6.11. Total Sulfur Concentration of Micro-Reactor System Outlet Operated with 50 μm Spacer and Temperature of 40 $^{\circ}\text{C}$

Appendix K contains all of the material balance information from the micro-reactor system with 50 μ m spacer and an operating temperature of 40°C. Figure 6.10 illustrates diminishing dibenzothiophene concentrations and strengthening sulfone concentrations. Dibenzothiophene is reduced to almost 20%. These results are compatible with Figure 6.4. Sulfone concentrations, right axis, approach 80% at longer residence times. Dashed lines guide the eye.

Figure 6.11 shows a sulfur feed concentration of about 120 ppm. The amount of sulfur missing from the original sulfur tally is only 6 ppm. Again, it is suggested that a majority of the reacted dibenzothiophene becomes sulfone as only 5% of the total sulfur in the material balance is not detected, which is within experimental error.

CHAPTER 7

RESULTS AND DISCUSSION

7.1 Effect of Spacer Thickness

Experiments were conducted under similar experimental conditions with different spacer thicknesses. Changing the spacer thickness or reducing the film thickness within the micro-reactor, changes the light intensity in the system. As intensity is a function of reactor thickness, a higher ratio of light is available to activate the oxidation reaction in the 50 micron system.

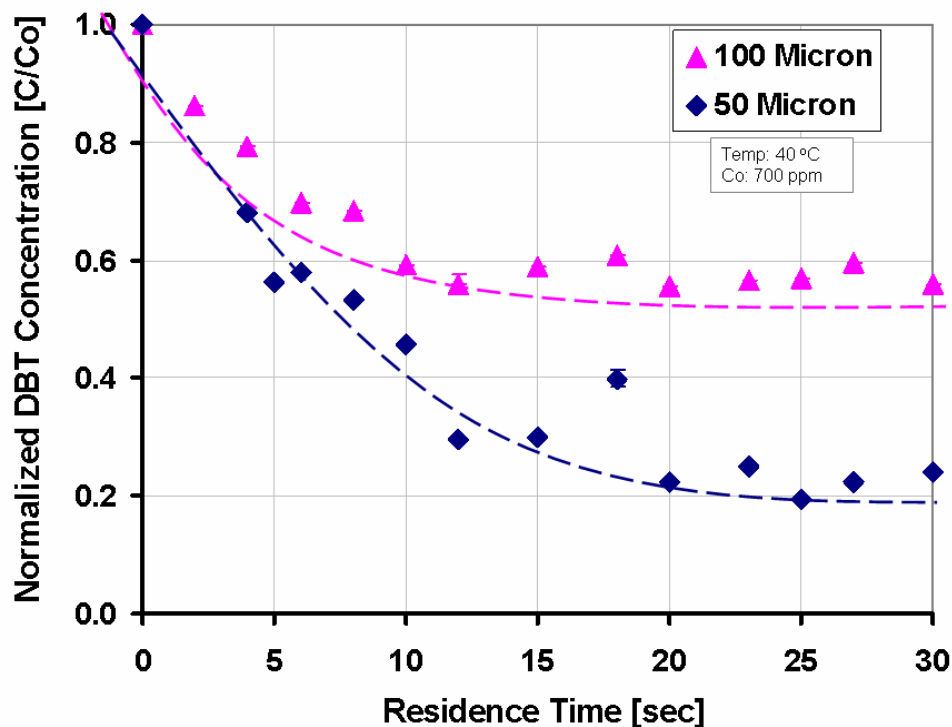


Figure 7.1. Normalized Concentration of DBT at Various Residence Times for Micro-Reactor Spacers of 50 μm and 100 μm at 40 °C Temperature

Figure 7.1 shows that a reduction in spacer thickness yields lower outlet concentrations of dibenzothiophene. With smaller film thicknesses and smaller

reaction volumes come consequently smaller diffusion path lengths, giving faster mixing and higher reactant conversion. Thus, all reactants have a greater chance of reacting. This diminishes diffusion limitations on the process.

7.2 Effect of Temperature

Temperature conditions were varied for experiments with the same micro-reactor spacer thickness. Changing the temperature changes diffusion rates of each species, which influence mixing within the micro-reactor and reaction kinetics.

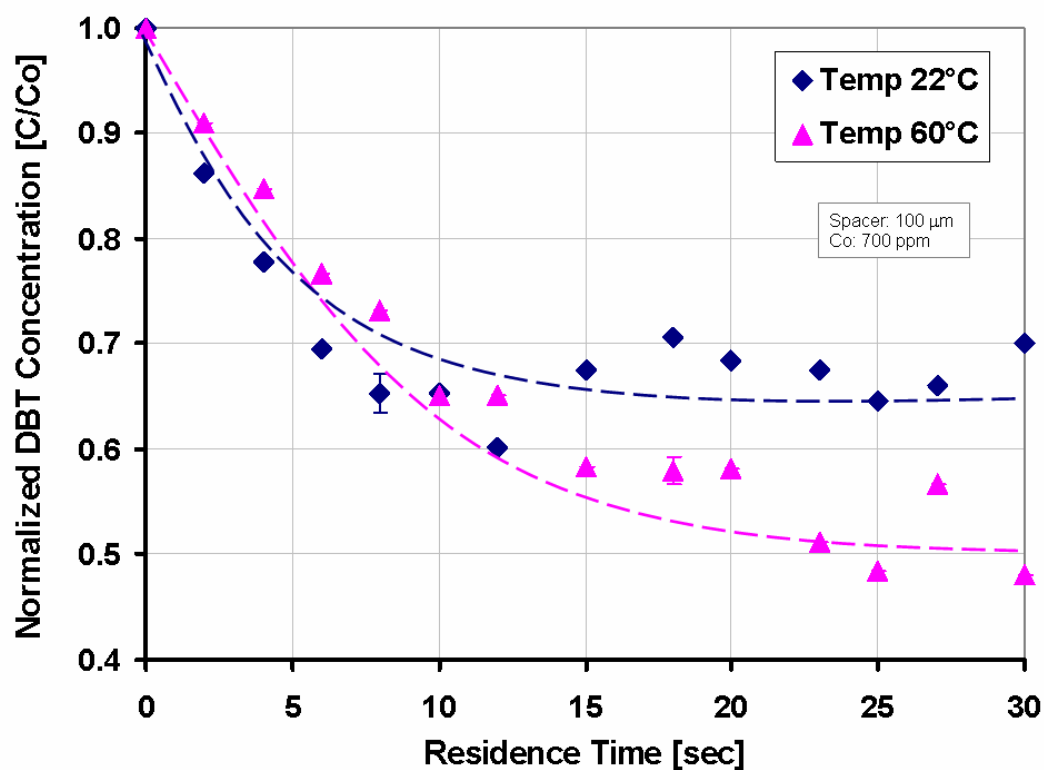


Figure 7.2. Normalized Concentration of DBT at Various Residence Times for Micro-Reactor 100 μm Spacer at Temperatures of 22 $^{\circ}\text{C}$ and 60 $^{\circ}\text{C}$

Figure 7.2 reveals that an increase in system temperature generates lower outlet concentrations and enhanced dibenzothiophene conversion. Higher temperatures will yield faster reactant diffusion and superior reaction rates for a given reaction

volume. Thus, greater dibenzothiophene conversion is achieved at 60 °C compared to 22 °C.

7.3 Mathematical Model

The mathematical model derived in Chapter 4 predicts performance of the micro-reactor process at various experimental conditions. The software package COMSOL Multiphysics is used to solve the model numerically by applying the finite element modeling approach. The search is complete when the objective function, least squares error, has reached a minimum.

$$(7.1) \quad \text{Objective Function} = \sum_{i=1}^n (C_{\text{exp}} - C_{\text{model}})_i^2$$

First, optimization was conducted on COMSOL models in which the reactor thicknesses were both 100 microns and 50 microns and the temperature was 22 °C. The average molar extinction coefficient, ϵ , and reaction rate constant, k , were allowed to float. Four separate initial guesses were used. The surface plot in Figure 7.3 illustrates morphology of the COMSOL solutions in parameter space. The model is relatively insensitive to changes in extinction coefficient, but shows significant response to the reaction rate parameter. Therefore, a reasonable extinction coefficient is selected and focus is on the reaction rate constant.

Figure 7.4 shows the results of a global fit to the objective function for all data points shown in Figure 6.2 and Figure 6.4. There is a clear global minimum when k is approximately $9.5 \cdot 10^{-17} \text{ m}^2/\text{photon}$. Identical results were obtained regardless of which reaction rate seed value was used.

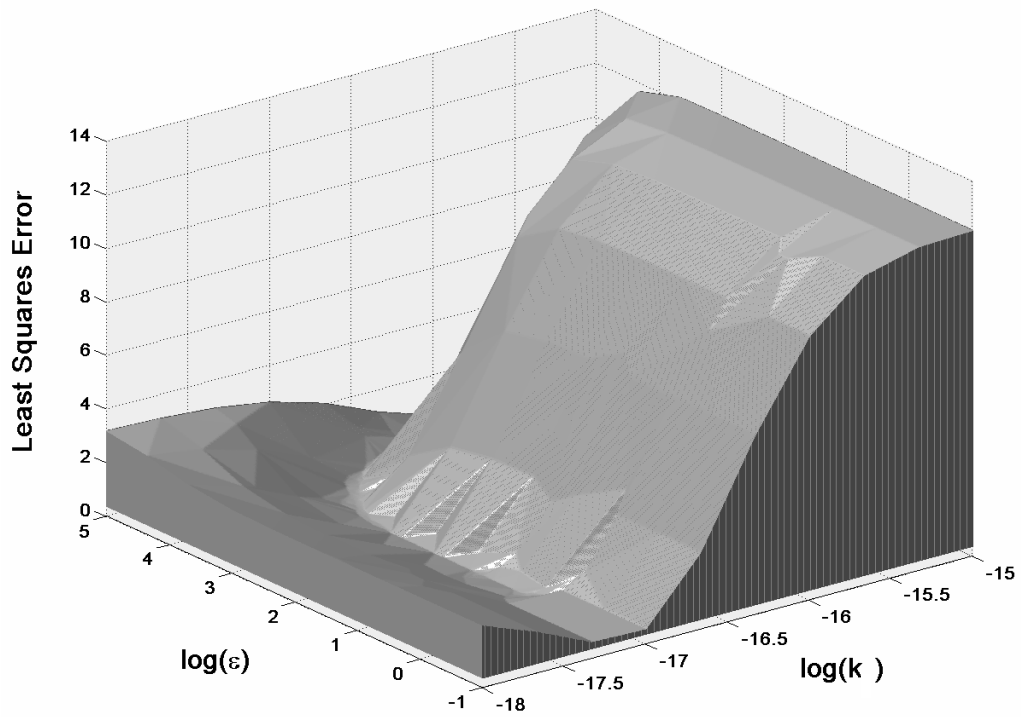


Figure 7.3. Surface Plot of Optimized COMSOL Model with Extinction Coefficient and Reaction Rate Constant as Adjustable Parameters

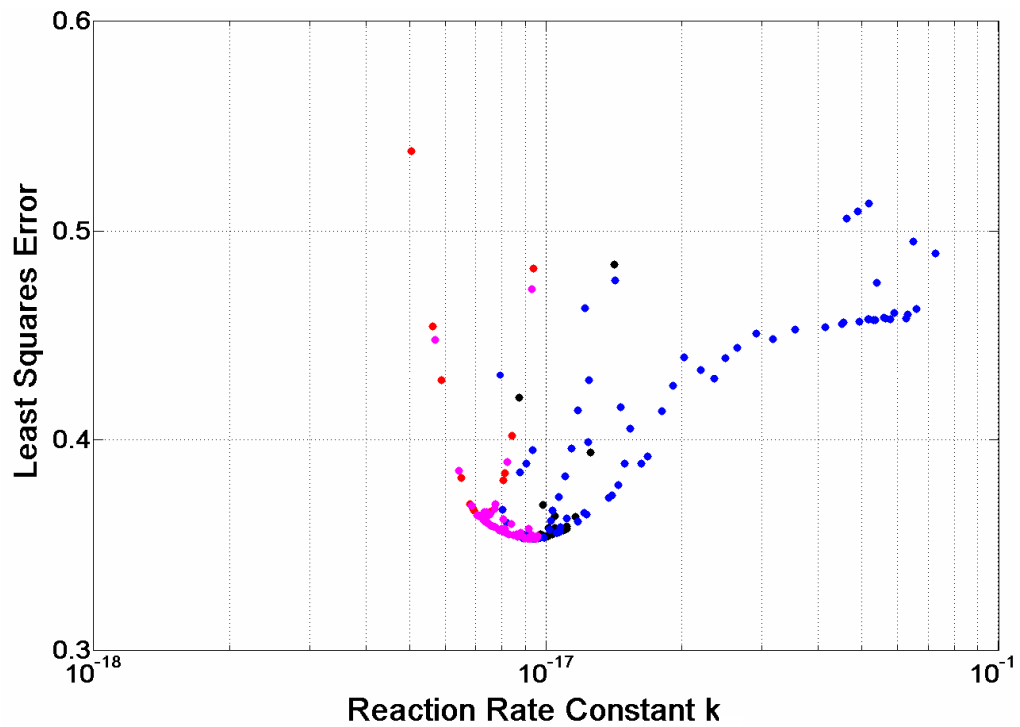


Figure 7.4. COMSOL Model Solutions for Various Initial Rate Constant Values

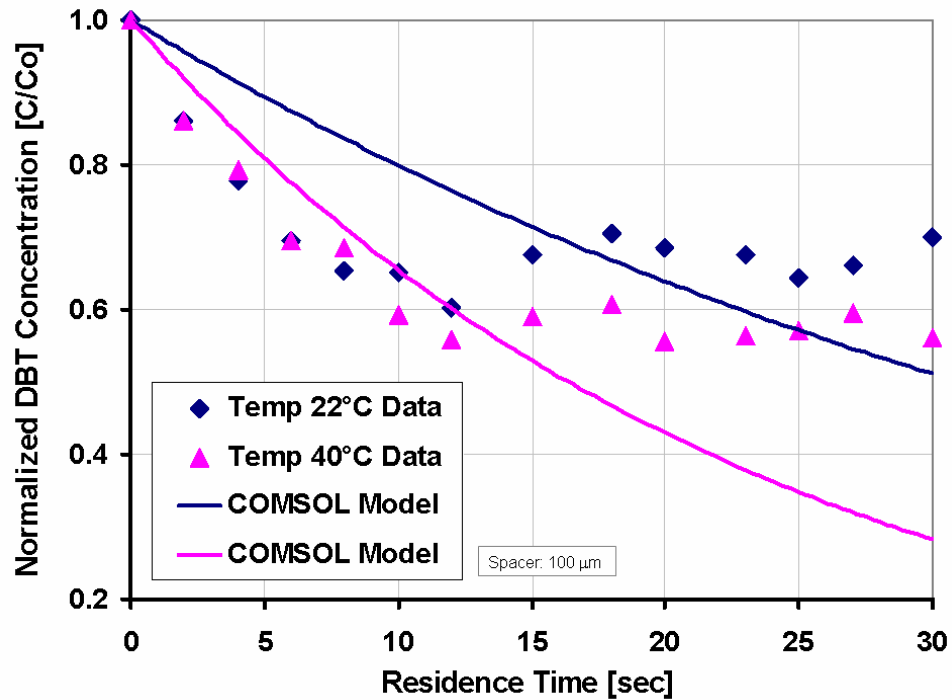


Figure 7.5. 100 Micron Spacer Experimental Data Fitted With Optimized COMSOL Model

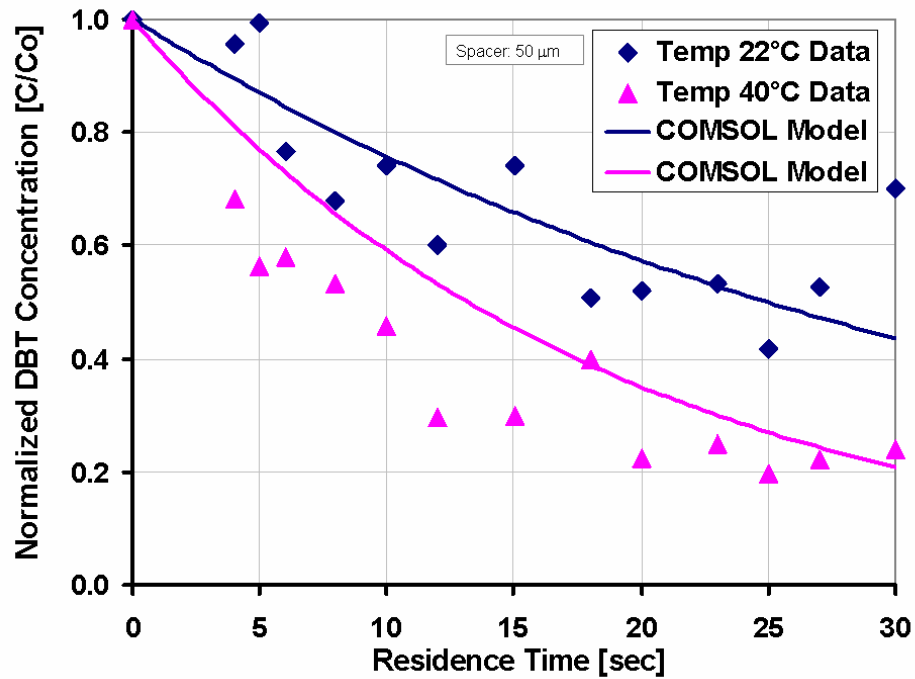


Figure 7.6. 50 Micron Spacer Experimental Data Fitted With Optimized COMSOL Model

The pseudo first order reaction rate constants, k , are determined as $1.02 \cdot 10^{-17}$ m^2/photon and $1.92 \cdot 10^{-17}$ m^2/photon for temperatures of 22 °C and 40 °C, respectively. This corresponds to reaction rate constants, k_1 , of $7.76 \cdot 10^{-4}$ sec^{-1} and $1.47 \cdot 10^{-3}$ sec^{-1} for temperatures of 22 °C and 40 °C, respectively.

Figure 7.5 and Figure 7.6 compares the trend of optimized COMSOL model to experimental data from 100 and 50 micron spacers, respectively. The model has a reasonable fit for each temperature and thickness.

CHAPTER 8 CONCLUSIONS AND RECOMMENDATIONS

8.1 Conclusions from Experimental Data

A model for the oxidative desulfurization of fuels by reaction with organic peroxides was created by studying the oxidation of dibenzothiophene in a light activated micro-reactor. The micro-reactor in the investigation utilized spacers with thicknesses of 50 μ m and 100 μ m yielding characteristic dimensions of the same size. The experiments were conducted at various temperatures ranging from 22°C to 60°C. Different volumetric flow rates of decane containing dibenzothiophene and tert-butyl hydro peroxide corresponding to different micro-reactor residence times were set in the range of 2 to 30 seconds. A constant intensity ultraviolet light source irradiated the reactants within the micro-reactor through a quartz window. Samples were collected and analyzed via HPLC to determine the concentration of unreacted dibenzothiophene.

It was determined that ultraviolet light plays a major role in the desulfurization of dibenzothiophene. Experiments show that the oxidative reaction does not take place in the absence ultraviolet light. This confirms the reaction mechanism indicating that hydroxyl radicals generated from the irradiated hydro peroxide directly oxidize dibenzothiophene.

The dibenzothiophene concentration exiting the micro-reactor decreases as mean residence time increases. The compounds are exposed to favorable reaction conditions longer and therefore dibenzothiophene conversion increases with time.

The experimental results obtained in this study are compared with the work reported by other researchers in this field. It is found that a micro-reaction system is much more efficient than a batch reactor for desulfurization. The micro-scaled process was capable of 79 % dibenzothiophene conversion in less than a minute;

compared to the 240-600 minutes necessary for macroscopic batch reactor operation (Shiraishi, et al., 2002). When further compared to similar photochemical micro-scaled systems, this process is superior. Using a single reaction phase and organic peroxide as an oxidant, extensive conversions are attainable within seconds; compared to the 10 minutes required in two phase systems with hydrogen peroxide (Al-Raie, 2005).

In this research, the effect of micro-reactor film thickness and overall system temperature in the feed were observed.

In this study, a reduction of film thickness within the micro-reactor results in better performance. Decreasing the spacer thickness reduces the diffusion path lengths for all components, yielding better mixing of reactants and accelerating the overall reaction process.

In this research, an increase of overall system temperature results in better performance. Higher temperatures enhance the overall reaction process due to faster reaction rates.

In summary, this research has shown that desulfurization of dibenzothiophene can be achieved in a micro-reactor by combining the dibenzothiophene and tert-butyl hydro peroxide under ultraviolet irradiation.

8.2 Conclusions from Model

A mathematical model was derived from first principles. The mathematical model, with the reaction rate constant as an adjustable system parameter, was used to match experimental data.

A mathematical model is proposed that includes convective mass transfer, axial and radial diffusion, and homogeneous chemical reaction throughout the fluid.

Appropriate boundary conditions are incorporated. A numerical solution using COMSOL Multiphysics is successfully implemented and presented in this work. The simulation results, namely chemical kinetic information for the oxidative desulfurization reaction of dibenzothiophene, are consistent with experimental data. The reaction rate constant k_1 , is determined and found to be of the order of 10^{-3} s^{-1} .

Table 8.1. Comparison of This Study's Conditions and Results to Open Literature

Reference	Oxidant	Catalyst	Reaction Rate Constant	Method
Houalla, et al. 1980	H ₂	CoMo / NiMo	$7.38 \times 10^{-5} \text{ L (g cat)}^{-1}$	HDS
Otsuki, et al. 2000	H ₂ O ₂	Formic Acid	$7.66 \times 10^{-4} \text{ L (mol sec)}^{-1}$	Batch Process
Shiraishi and Hirai, 2002	H ₂ O ₂	UV Light	$2.86 \times 10^{-5} \text{ sec}^{-1}$	Batch Process
Wang, et al., 2003	TBHP	Mo/Al ₂ O ₃	$2.73 \times 10^{-4} \text{ sec}^{-1}$	Batch Process
Al-Raie, 2005	H ₂ O ₂	UV Light	$1.47 \times 10^{-7} \text{ sec}^{-1}$	Micro-Reactor
Stanger and Angelici, 2006	TBHP	Silica	$2.88 \times 10^{-3} \text{ sec}^{-1}$	Batch Process
Stanger, et al., 2006	TBHP	(SiO ₂ -RTA)Re(O)(Me)(PPh ₃)	$8.88 \times 10^{-3} \text{ sec}^{-1}$	Batch Process
This Work	TBHP	UV Light	$1.47 \times 10^{-3} \text{ sec}^{-1}$	Micro-Reactor

The dibenzothiophene reaction rate constant, k_1 , is compared to values reported by other investigators in Table 8.1. Our value is on par with other suggested dibenzothiophene reaction rate constants.

The numerical solutions from the proposed mathematical model were sufficiently accurate to extract a reaction rate constant and predict the concentration profile of dibenzothiophene.

8.3 Recommendations

Diesel hydrodesulfurization is limited by the low reactivity of highly aromatic sulfur containing compounds. Literature shows that the addition of aromatic rings decreases the species reactivity. Hence, reactivity of thiophene is higher than benzo-thiophene which is more reactive than dibenzothiophene. In addition, species reactivity is further lowered when substituents are present in sterically hindering positions. Experimentation using sulfur-model compounds such as 4-

methylthiophene and 4,6-dimethylthiophene would simulate oxidative desulfurization of molecules that are more stable and more difficult to remove from fuels.

The reactivity of alkylated thiophene species is further decreased in the presence of other inhibitors like aromatics and organic nitrogen compounds, which are generally also present in the feed. Authentic fuels, like gasoline and diesel would more accurately portray the reaction environment of actual fuel treatment. Precise analytics are necessary to correctly recognize the many species present in authentic fuels.

An appropriate heat activated catalyst would remove the need for ultraviolet radiation and increase the activity for thiophene oxidation. Two main catalysts are used for selective desulfurization of thiophene derivatives: organic acids and polyoxometalates. Catalysts might be beneficial in micro-reaction systems due to better contacting in lower reaction volumes.

An investigation to fully determine the optimal reactant ratio of tert-butyl hydro peroxide and thiophene in the system is required.

Tert-butyl hydro peroxide is one of many organic peroxides that may be used for oxidative desulfurization. Additional organic peroxides that are soluble in hydrocarbons such as decane and nonane should be investigated as they maintain the benefits of a single phase reaction system and add the potential to improve performance.

For true desulfurization, the present oxidation must be followed by an extraction step, since, though oxidized, sulfur compounds still remain in the fluid. Many extraction solvents can be used in tandem with or following fuel desulfurization. Contact with an extraction solvent would physically remove the reacted sulfur from the stream. Water is an inexpensive polar extraction solvent that is easily

obtained and safe to use. Other extraction solvents including ionic fluids could be used to draw out oxidation products and possibly some of the unreacted reactants. Implementing an extraction step following the desulfurization would yield a cleaner, more polished product.

Bibliography

- Ackerson, M.D. and Byars, M.S., (2005). 'Two-phase hydroprocessing with an eliminated hydrogen recirculation'. Application: US US: (Process Dynamics, Inc., USA). 14 pp , Cont -in-part of U S Ser No 162,310.
- Adiwidjaja, G., Sawluk, A., Volz, W. and Voss, J., (1993). 'New results on the preparation and reactivity of benzo[c]thiophenes'. *Phosphorus, Sulfur and Silicon and the Related Elements*, 74 (1-4):451-452.
- Al-Raie, A., (2005). 'Desulfurization of Thiophene and Dibenzothiophene with Hydrogen Peroxide in a Photochemical Micro-Reactor'. *Chemical Engineering*. Corvallis: Oregon State University, 142.
- Ania, C.O. and Bandosz, T.J., (2006). 'Sodium on the Surface of Activated Carbons as a Factor Enhancing Reactive Adsorption of Dibenzothiophene'. *Energy & Fuels*, 20 (3):1076-1080.
- Atlas, R.M., Boron, D.J., Deever, W.R., Johnson, A.R., McFarland, B.L. and Meyer, J.A., (2000). 'Biodesulfurization of gasoline: An assessment of technical and economic feasibility and outline of R&D roadmap toward commercialization'. *Book of Abstracts, 219th ACS National Meeting, San Francisco, CA, March 26-30, 2000*:IEC-269.
- Ayakawa, Y. and Ono, M., (2002). 'High-energy beam irradiating desulfurization device'. Application: EP: (Rigaku Industrial Corporation, Japan). 12 pp.
- Bej, S.K., Maity, S.K. and Turaga, U.T., (2004). 'Search for an Efficient 4,6-DMDBT Hydrodesulfurization Catalyst: A Review of Recent Studies'. 1227-1237.
- Brown, K.N. and Espenson, J.H., (1996). 'Stepwise Oxidation of Thiophene and Its Derivatives by Hydrogen Peroxide Catalyzed by Methyltrioxorhenium(VII)'. 7211-7216.
- Campos-Martin, J.M., Capel-Sanchez, M.C. and Fierro, J.L.G., (2004). 'Highly efficient deep desulfurization of fuels by chemical oxidation'. *Green Chemistry*, 6 (11):557-562.
- Collins, F.M., Lucy, A.R. and Sharp, C., (1997). 'Oxidative desulphurisation of oils via hydrogen peroxide and heteropolyanion catalysis'. *Journal of Molecular Catalysis A: Chemical*, 117 (1-3):397-403.
- Corma Canos, A., Domine Marcelo, E. and Martinez Sanchez, C., (2002). 'Process and catalysts for eliminating sulfur compounds from the gasoline fraction'. Application: WO: (Consejo Superior De Investigaciones Cientificas, Spain; Universidad Politecnica De Valencia). 44 pp.

Fletcher, S., (2007). 'US diesel use rising in ultralow-sulfur era'. *Oil & Gas Journal*.

Han, Y.-Z. and Leyshon, D.W., (2005). 'Desulfurization process'. Application: US US: (Lyondell Chemical Technology, L.P., USA). 6 pp.

Houalla, M., Broderick, D.H., Sapre, A.V., Nag, N.K., De Beer, V.H.J., Gates, B.C. and Kwart, H., (1980). 'Hydrodesulfurization of methyl-substituted dibenzothiophenes catalyzed by sulfided cobalt-molybdenum/g-alumina'. *Journal of Catalysis*, 61 (2):523-527.

Hulea, V., Fajula, F. and Bousquet, J., (2001). 'Mild Oxidation with H₂O₂ over Ti-Containing Molecular Sieves--A very Efficient Method for Removing Aromatic Sulfur Compounds from Fuels'. *Journal of Catalysis*, 198 (2):179-186.

Hulea, V., Maciucă, A.-L., Fajula, F. and Dumitriu, E., (2006). 'Catalytic oxidation of thiophenes and thioethers with hydrogen peroxide in the presence of W-containing layered double hydroxides'. *Applied Catalysis, A: General*, 313 (2):200-207.

Ito, E. and van Veen, J.A.R., (2006). 'On novel processes for removing sulphur from refinery streams'. *Catalysis Today*, 116 (4):446-460.

Jackson, P.M. and Moody, C.J., (1990). 'Preparation and Diels-Alder reactivity of benzothieno[2,3-c]- and benzothieno[3,2-c]pyran-3-ones, benzothiophene-2,3-quinodimethane analogs. Synthesis of dibenzothiophenes'. *Journal of the Chemical Society, Perkin Transactions 1: Organic and Bio-Organic Chemistry (1972-1999)* (3):681-687.

Kim, J.H., Ma, X., Song, C., Lee, Y.K. and Oyama, S.T., (2005). 'Kinetics of Two Pathways for 4,6-Dimethyldibenzothiophene Hydrodesulfurization over NiMo, CoMo Sulfide, and Nickel Phosphide Catalysts'. 353-364.

Kleemann, A., (2002). 'Microreaction technology, innovation in chemical synthesis'. *Chemie Ingenieur Technik*, 74 (5):557.

Kleinjan, W.E., de Keizer, A. and Janssen, A.J.H., (2003). 'Biologically produced sulfur'. *Topics in Current Chemistry*, 230 (Elemental Sulfur and Sulfur-Rich Compounds I):167-188.

Luo Mingfang, G.Z.X.J.L.H.C.J., (2003). 'Microbial desulfurization of model and straight-run diesel oils'. 873-876.

Mei, H., Mei, B.W. and Yen, T.F., (2003). 'A new method for obtaining ultra-low sulfur diesel fuel via ultrasound assisted oxidative desulfurization*'. *Fuel*, 82 (4):405-414.

- Mochida, I. and Choi, K.-H., (2004). 'An overview of hydrodesulfurization and hydrodenitrogenation'. *Journal of the Japan Petroleum Institute*, 47 (3):145-163.
- Murata, S., Murata, K., Kidena, K. and Nomura, M., (2004). 'A Novel Oxidative Desulfurization System for Diesel Fuels with Molecular Oxygen in the Presence of Cobalt Catalysts and Aldehydes'. 116-121.
- Nag, N.K., Sapre, A.V., Broderick, D.H. and Gates, B.C., (1979). 'Hydrodesulfurization of polycyclic aromatics catalyzed by sulfided cobalt(II) oxide-molybdenum(VI) oxide/g-alumina: the relative reactivities'. *Journal of Catalysis*, 57 (3):509-512.
- Otsuki, S., Nonaka, T., Takashima, N., Qian, W., Ishihara, A., Imai, T. and Kabe, T., (2000). 'Oxidative Desulfurization of Light Gas Oil and Vacuum Gas Oil by Oxidation and Solvent Extraction'. 1232-1239.
- Palomeque, J., Clacens, J.-M. and Figueras, F., (2002). 'Oxidation of Dibenzothiophene by Hydrogen Peroxide Catalyzed by Solid Bases'. *Journal of Catalysis*, 211 (1):103-108.
- Pedro Arrais, C.N.S., (2006). 'Diesel fuel's sulphur content cut by 97 per cent'. *The Vancouver Sun* British Columbia.
- Purta, D.A., Portnoff, M.A., Pourarian, F., Nasta, M.A. and Zhang, J., (2004). 'Petroleum refining by hydroconversion using interstitial metal hydride catalysts'. Application: US
US: (Carnegie Mellon University, USA). 30 pp.
- Qu, Z., Yan, N., Zhao, Y., Jia, J. and Wu, D., (2006). 'Removal of Dibenzothiophene from the Simulated Petroleum by γ -Irradiation Induced Reaction'. *Energy & Fuels*, 20 (1):142-147.
- Report, (2007). 'Environment: Commission Thinks Up Fuel Quality Standards'. European Report.
- Robertson, J. and Bandosz, T.J., (2006). 'Photooxidation of dibenzothiophene on TiO₂/hectorite thin films layered catalyst'. *Journal of Colloid and Interface Science*, 299 (1):125-135.
- Rossi, L.I. and de Rossi, R.H., (2004). 'FeBr₃-cyclodextrin complexes as efficient and chemoselective catalysts for sulfoxidation reactions'. *Applied Catalysis A: General*, 267 (1-2):267-272.
- Shiraishi, Y., Hirai, T. and Komasa, I., (2000). 'Photochemical Denitrogenation Processes for Light Oils Effected by a Combination of UV Irradiation and Liquid-Liquid Extraction'. 2826-2836.

Shiraishi, Y., Tachibana, K., Hirai, T. and Komasaawa, I., (2002). 'Desulfurization and Denitrogenation Process for Light Oils Based on Chemical Oxidation followed by Liquid-Liquid Extraction'. *Industrial & Engineering Chemistry Research*, 41 (17):4362-4375.

Shiraishi, Y., Taki, Y., Hirai, T. and Komasaawa, I., (1999). 'Visible Light-Induced Deep Desulfurization Process for Light Oils by Photochemical Electron-Transfer Oxidation in an Organic Two-Phase Extraction System'. *Industrial & Engineering Chemistry Research*, 38 (9):3310-3318.

Song, C., (2003). 'An overview of new approaches to deep desulfurization for ultra-clean gasoline, diesel fuel and jet fuel'. *Catalysis Today*, 86 (1-4):211-263.

Stanger, K.J., Wiench, J.W., Pruski, M., Espenson, J.H., Kraus, G.A. and Angelici, R.J., (2006). 'Catalytic oxidation of a thioether and dibenzothiophenes using an oxorhenium(V) dithiolate complex tethered on silica'. *Journal of Molecular Catalysis A: Chemical*, 243 (2):158-169.

Sugimoto, Y., Aihara, Y., Matsuura, A., Ohi, A., Sato, S., Saito, I. and Yui, S., (2006). 'Processing of Middle East crude with Canadian oil sands bitumen-derived synthetic crude oil'. *Journal of the Japan Petroleum Institute*, 49 (1):1-12.

Tam, P.S., Kittrell, J.R. and Eldridge, J.W., (1990). 'Desulfurization of fuel oil by oxidation and extraction. 1. Enhancement of extraction oil yield'. *Industrial & Engineering Chemistry Research*, 29 (3):321-324.

Thirugnanasampanthar, J., Xu, R. and Dautzenberg, F.M., (2005). 'Novel process for removing sulfur from automobile fuels to reduce exhaust emission'. Application: WO: (Agency for Science, Technology and Research, Singapore). 47 pp.

UPI, (2007). 'Abu Dhabi Progresses toward Introduction of Green Diesel as Fuel Abu Dhabi'. *ARABIA 2000*: Emirates News Agency.

Wang, G., Zhao, Y. and Zhu, J., (2005). 'Remarks on diesel oil oxidation desulfurization technique at abroad'. *Huagong Shikan*, 19 (10):49-52.

Yu, G., Lu, S., Chen, H. and Zhu, Z., (2005). 'Oxidative Desulfurization of Diesel Fuels with Hydrogen Peroxide in the Presence of Activated Carbon and Formic Acid'. *Energy & Fuels*, 19 (2):447-452.

Zanibelli, L., Bellussi, G., Corma Canos, A., Domine, M.E. and Gagliardi, M.F., (2004). 'Process and catalysts for deep desulphurization of fuels'. Application: EP EP: (ENI S.p.A., Italy; Enitecnologie S.p.A.). 17 pp.

Zhan, F., Lv, Z., Xu, Y. and Zhang, X., (2005). 'Study on diesel fuel desulfurization with photosensitized oxidation'. *Lianyou Jishu Yu Gongcheng*, 35 (4):40-43.

Zhang, S., Zhang, Q. and Zhang, Z.C., (2004). 'Extractive Desulfurization and Denitrogenation of Fuels Using Ionic Liquids'. *Industrial & Engineering Chemistry Research*, 43 (2):614-622.

APPENDICIES

Appendix A Literature Review Summary

The following tables present the information available in literature regarding liquid oxidative desulfurization systems:

Table A.1. Summary of Two Phase Liquid Systems Using H₂O₂ Oxidation

Reference	Sulfur Compounds	Additional Oxidant	Catalyst	Extraction Solvent
Lu, et al., 2007	T, BT, DBT	1-methyl-1H-imidazolium Monotetrafluoroborate Ionic Liquid	--	--
Shiraishi and Hirai, 2004	BT, DBT	Acetic Acid	--	Acetonitrile
Komintarachat and Trakarnpruk, 2006	BT, DBT, 4,6-DMDBT	Acetic Acid	Tetrabutylammonium Salts, Polyoxometalates	Acetonitrile, DMF
Otsuki, et al. 2000	T, BT, 2-MT, 2,5-DMT, DBT, 4-MDBT, 4,6-DMDBT	Formic Acid	--	Acetonitrile, Methanol, DMF
Yu, et al. 2005	DBT	Formic Acid	Activated Carbon	--
Huang, et al., 2006	DBT	Phosphotungstic Acids	Octadecyltrimethylammonium Bromide	2-Methylnaphthalene
Mei, et al. 2003	DBT	Phosphotungstic Acids, Heteropolyacids	--	--
Collins, et al. 1997	DBT	Phosphotungstic Acids, Tetraoctylammonium Bromide	Silica Gel	Toluene, Water
Ania and Bandosz, 2006	DBT	--	Activated Carbon, Sodium	--
Campos-Martin, et al. 2004	BT, DBT, 4-E,6M-DBT	--	Biperoxotungstate	Acetonitrile
Palomeque, et al. 2002	DBT	--	Hydrotalcite and MgLa Mixed Oxide	Acetonitrile, Methanol, 3-Methoxypropionitrile, Benzonitrile
Hulea, et al. 2001	T, 2,5-DMT, DBT	--	Titanium Silicalite, Titanium Silica	Acetonitrile, Methanol, Ethanol, Tert-butanol

Table A.2. Summary of Single Phase Liquid Oxidation Systems

Reference	Sulfur Compounds	Oxidant	Catalyst
Stanger, et al., 2006	4,6-DMDBT	Tert-butyl Hydro Peroxide	Oxorhenium(V) Dithiolate
Corma Canos, et al., 2002	--	Tert-butyl Hydro Peroxide	Titanium Silica
Chica, et al., 2006	T, BT, 2-MT, 2-BMT, DBT, 4-MDBT, 4,6-DMDBT	Tert-butyl Hydro Peroxide	Ti-MCM-41, MoOx/Al ₂ O ₃
Wang, et al., 2003	BT, DBT, 4-MDBT, 4,6-DMDBT	Tert-butyl Hydro Peroxide	Mo/Al ₂ O ₃
Stanger and Angelici, 2006	DBT, 4,6-DMDBT	Tert-butyl Hydro Peroxide	Silica
Zhou, et al., 2007	DBT	Cyclohexanone Peroxide	MoO ₃

Appendix B
Micro-Reactor Flow Rates and Velocities

Volumetric flow rates and fluid velocities are determined by the following:

$$Q = \frac{V}{t} \quad v = \frac{Q}{A}$$

Where...

Q = Volumetric Flow Rate V = Reactor Internal Volume v = Fluid Velocity
t = Residence Time A = Reactor Cross-sectional Area

Table B.1. Volumetric Flow Rates and Fluid Velocities for Given Residence Times in Micro-Reactor with a Spacer Thickness of 100 Microns

Residence Time [sec]	Volumetric Flow Rate [μ l/min]	Fluid Velocity [m/sec]
2	660	0.0110
4	330	0.0055
6	220	0.0037
8	165	0.0028
10	132	0.0022
12	110	0.0018
15	88	0.0015
18	73	0.0012
20	66	0.0011
23	57	0.0010
25	53	0.0009
27	49	0.0008
30	44	0.0007

Table B.2. Volumetric Flow Rates and Fluid Velocities for Given Residence Times in Micro-Reactor with a Spacer Thickness of 50 Microns

Residence Time [sec]	Volumetric Flow Rate [μ l/min]	Fluid Velocity [m/sec]
4	165	0.0055
5	132	0.0044
6	110	0.0037
8	83	0.0028
10	66	0.0022
12	55	0.0018
15	44	0.0015
18	37	0.0012
20	33	0.0011
23	29	0.0010
25	26	0.0009
27	24	0.0008
30	22	0.0007

Appendix C Diffusion Coefficient Calculations

An estimation of diffusivities of non-electrolytes in liquids at low concentration is given by Wilke and Chang, 1955:

$$D_{12} = \frac{T}{\mu_2} \cdot \frac{7.4 \times 10^{-8} [\phi \cdot M_2]^{1/2}}{V_1^{0.6}} \quad V_1 = 0.285V_c^{1.048}$$

Where...

D_{12} = Diffusivity of solute at infinite dilution (cm²/sec)

Φ = Association parameter (dimensionless)

M_2 = Solvent molecular weight (g/mol)

T = Absolute temperature (K)

μ_2 = Solution viscosity (centipoises)

V_1 = Molar volume of solute at normal boiling point (cm³/mol)

V_c = Critical volume of solute (cm³/mol)

All of the relevant physical parameters are specified in the following tables:

Compound	M [g/gmol]	μ [cp]	ϕ []
Decane	142.3	0.92	1

Compound	V_c [m ³ /Kmole]*
Dibenzothiophene	0.547
Hydroxyl Radicals	0.056
Tert-Butyl Hydro Peroxide	0.297

* Note: Calculated from R. F. Fedors critical volume correlation, 1979.

The final calculated diffusion coefficients are outlined in Table C.1.

Table C.1. Diffusion Coefficients at Various Temperatures

Diffusion Coefficient (m ² /sec)	22°C	40°C	60°C
Dibenzothiophene in decane	1.14*10 ⁻⁹	1.21*10 ⁻⁹	1.29*10 ⁻⁹
Hydroxyl Radicals in decane	4.78*10 ⁻⁹	5.07*10 ⁻⁹	5.40*10 ⁻⁹
Tert-Butyl Hydro Peroxide in decane	1.68*10 ⁻⁹	1.78*10 ⁻⁹	1.89*10 ⁻⁹

Appendix D Dibenzothiophene Calibration Curves

The following figures graphically display the relation between five averaged HPLC peak areas and dibenzothiophene or elemental sulfur concentrations:

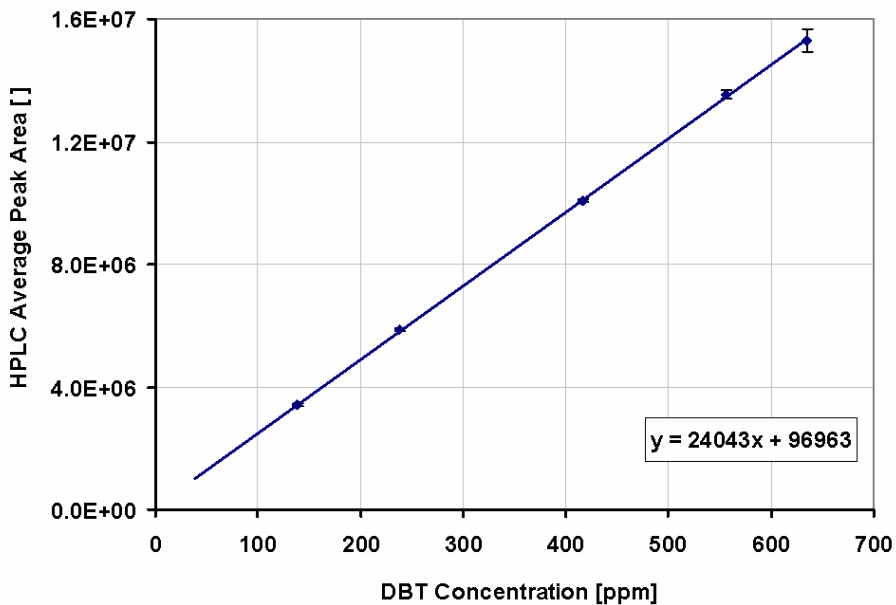


Figure D.1. Dibenzothiophene Calibration Curve

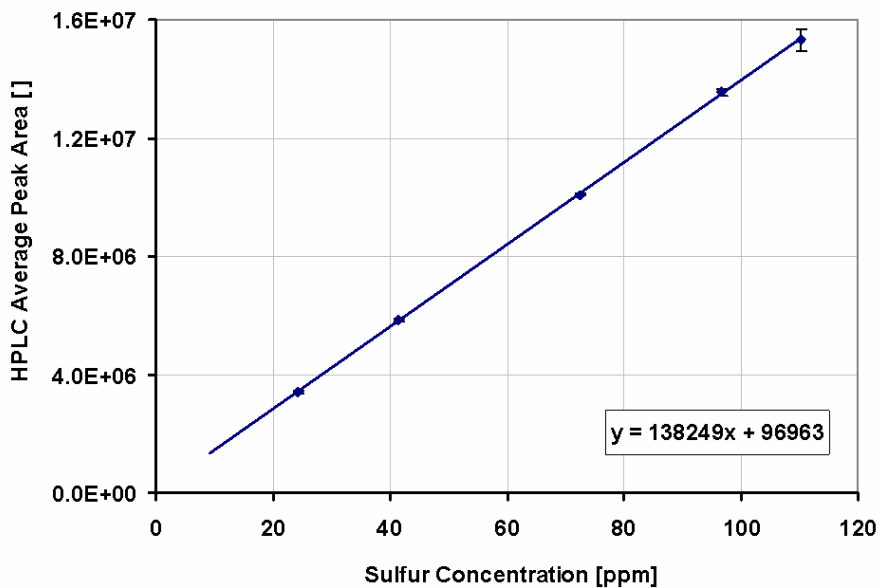


Figure D.2. Sulfur Calibration Curve for Dibenzothiophene

Appendix E Sulfone Calibration Curves

The following figures graphically display the relation between five averaged HPLC peak areas and sulfone or elemental sulfur concentrations:

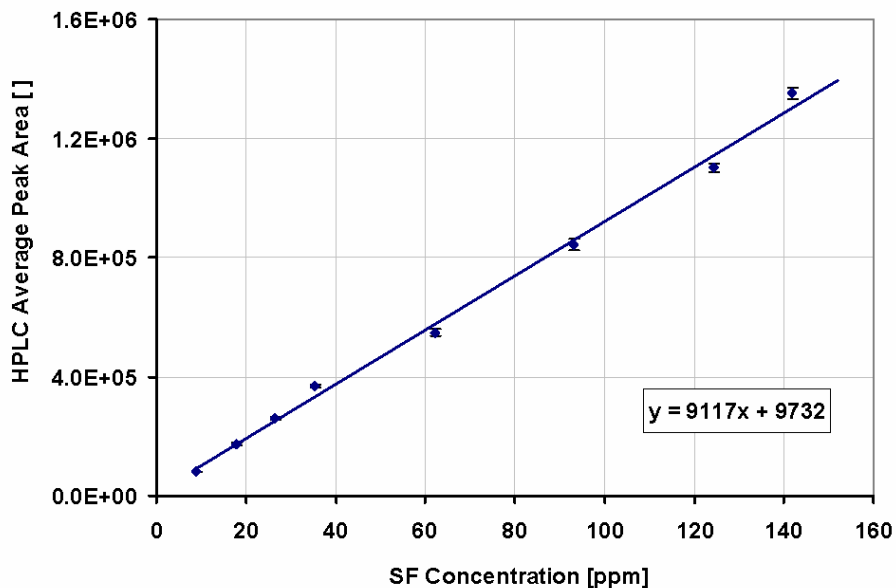


Figure E.1. Sulfone Calibration Curve

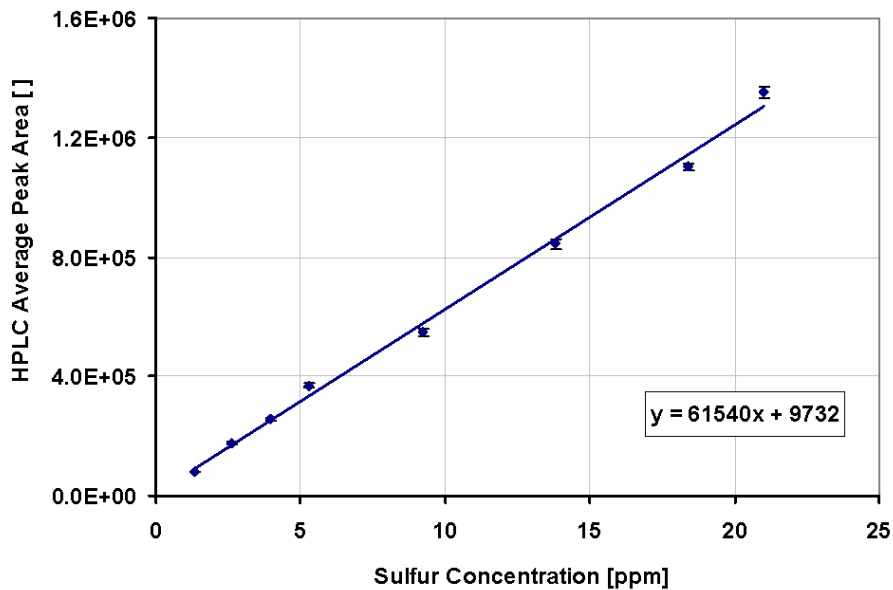


Figure E.2. Sulfur Calibration Curve for Sulfone

Appendix F
Tert-Butyl Hydro Peroxide Calibration Curve

The following figures graphically display the relation between five averaged HPLC peak areas and tert-butyl hydro peroxide concentrations:

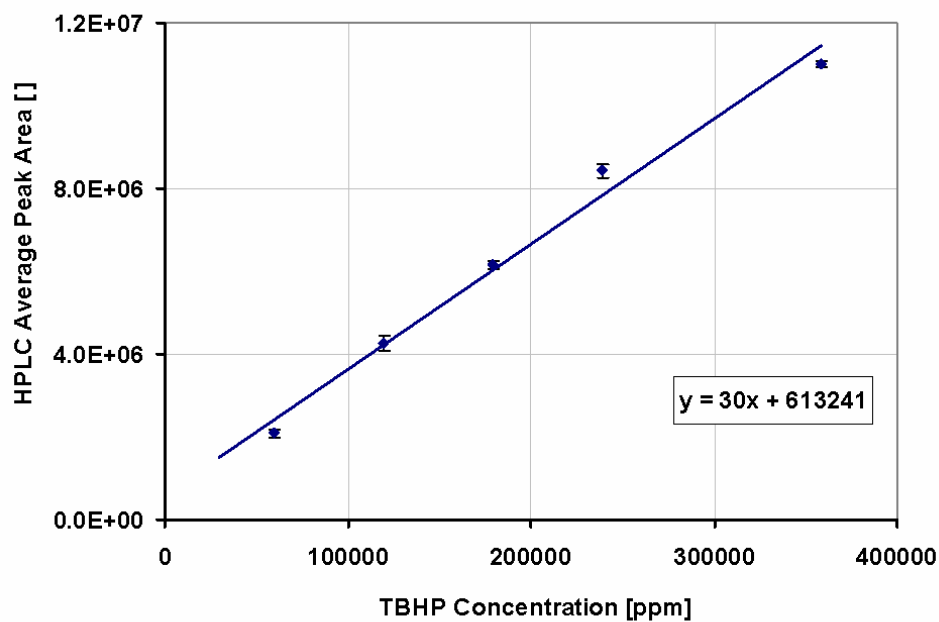


Figure F.1. Tert-Butyl Hydro Peroxide Calibration Curve

Appendix G
 HPCL Measurements for NO LIGHT Experiments

All data for experiments without UV light are tabulated in the following Table:

Table G.1. HPLC Measurements of Tert-Butyl Hydro Peroxide and
 Dibenzothiophene for Experiments Conducted Without Ultraviolet Light at 22 °C
 and 50 Micron Spacer

Mean Res Time [sec]	TBHP		DBT		
	TBHP Peak Area []	TBHP Concentration [ppm]	DBT Peak Area []	DBT Concentration [ppm]	Sulfur Concentration [ppm]
0	476300	130174	17002828	703	122
4	479087	130948	17137822	709	123
6	466644	127491	16875680	698	121
8	474652	129716	17009178	703	122
10	469615	128317	17069150	706	123
12	465512	127177	16980074	702	122
15	475176	129861	16985516	702	122
18	469485	128281	16825382	696	121
20	467551	127743	17121900	708	123
23	471654	128883	17009216	703	122
25	476942	130352	17025212	704	122
27	474718	129734	17000036	703	122
30	468055	127883	17059168	705	123

Appendix H
 HPCL Measurements for 100 Micron Experiments

All experimental data using the 100 μm spacer are tabulated in Tables H.1 – H.3:

Table H.1. HPLC Measurements of Tert-Butyl Hydro Peroxide and Dibenzothiophene for Experiments Conducted at 22 °C and 100 Micron Spacer

Mean Res Time [sec]	TBHP		DBT		
	TBHP Peak Area []	TBHP Concentration [ppm]	DBT Peak Area []	DBT Concentration [ppm]	Sulfur Concentration [ppm]
0	407544	111075	17501796	724	126
2	357298	97118	15091946	624	108
4	371318	101012	13652747	564	98
6	325327	88237	12213102	504	88
8	289325	78236	11173019	461	80
10	296259	80162	11450385	472	82
12	281278	76001	10051138	414	72
15	291591	78866	11263661	464	81
18	284032	76766	11761284	485	84
20	294978	79806	11799144	487	85
23	271665	73331	11266627	465	81
25	273097	73728	11323910	467	81
27	245448	66048	11017942	454	79
30	251918	67845	11676726	482	84

Table H.2. HPLC Measurements of Tert-Butyl Hydro Peroxide and Dibenzothiophene for Experiments Conducted at 40 °C and 100 Micron Spacer

Mean Res Time [sec]	TBHP		DBT		
	TBHP Peak Area []	TBHP Concentration [ppm]	DBT Peak Area []	DBT Concentration [ppm]	Sulfur Concentration [ppm]
0	476926	130348	16559921	685	119
2	405402	110480	14247285	589	102
4	365960	99524	13123602	542	94
6	343906	93398	11524512	475	83
8	315099	85396	11357590	468	81
10	307165	83192	9832114	405	70
12	290854	78661	9265782	381	66
15	317039	85934	9758298	402	70
18	314044	85103	10070983	415	72
20	301560	81635	9220846	379	66
23	293125	79292	9344610	385	67
25	275515	74400	9441488	389	68
27	271536	73295	9845018	405	71
30	255444	68825	9286254	382	66

Table H.3. HPLC Measurements of Tert-Butyl Hydro Peroxide and Dibenzothiophene for Experiments Conducted at 60 °C and 100 Micron Spacer

Mean Res Time [sec]	TBHP		DBT		
	TBHP Peak Area []	TBHP Concentration [ppm]	DBT Peak Area []	DBT Concentration [ppm]	Sulfur Concentration [ppm]
0	459879	125612	16424250	679	118
2	418347	114076	14940972	617	107
4	420088	114559	13931714	575	100
6	352305	95731	12582305	519	90
8	366576	99695	12020563	496	86
10	309543	83852	10697960	441	77
12	269237	72656	10687023	440	77
15	277992	75088	9571129	394	69
18	256606	69148	9521629	392	68
20	278598	75256	9557083	393	68
23	225201	60424	8400043	345	60
25	252817	68095	7957733	327	57
27	240480	64668	9302848	383	67
30	227912	61177	7889730	324	56

Appendix I
 HPCL Measurements for 50 Micron Experiments

All experimental data using the 50 μm spacer are tabulated in Tables I.1 – I.2:

Table I.1. HPLC Measurements of Tert-Butyl Hydro Peroxide and Dibenzothiophene for Experiments Conducted at 22 °C and 50 Micron Spacer

Mean Res Time [sec]	TBHP		DBT		
	TBHP Peak Area []	TBHP Concentration [ppm]	DBT Peak Area []	DBT Concentration [ppm]	Sulfur Concentration [ppm]
0	487326	133236	16559921	685	119
4	440684	120280	15828421	654	114
5	374105	101786	16464279	681	118
6	395333	107683	12721608	525	91
8	369042	100380	11298115	466	81
10	248767	66970	12289568	507	70
12	277694	75005	9972546	411	71
15	214473	57444	12328741	509	88
18	251003	67591	8462577	348	61
20	156463	41330	8662120	356	62
23	198512	53010	8882923	365	64
25	142239	37379	6985592	287	50
27	191655	51106	8782705	361	63
30	163707	43342	11634622	480	83

Table I.2. HPLC Measurements of Tert-Butyl Hydro Peroxide and Dibenzothiophene for Experiments Conducted at 40 °C and 50 Micron Spacer

Mean Res Time [sec]	TBHP		DBT		
	TBHP Peak Area []	TBHP Concentration [ppm]	DBT Peak Area []	DBT Concentration [ppm]	Sulfur Concentration [ppm]
0	487547	133298	16809296	695	119
4	392027	106764	11491702	474	114
5	348454	94661	9520181	392	118
6	394062	107330	9775336	403	91
8	358805	97536	9012811	371	81
10	242675	65278	7747756	318	70
12	164998	43701	5063253	207	71
15	174679	46390	5092854	208	88
18	188187	50142	6754257	277	61
20	102386	26309	3856037	156	62
23	172473	45777	4254581	173	64
25	118660	30829	3366565	136	50
27	159693	42227	3817875	155	63
30	149907	39509	4131413	168	83

Appendix J
Material Balance for 100 Micron Experiments

A material balance on sulfur is performed based on experimental data collected from experiments conducted with the 100 micron spacer at a temperature of 22 °C. The results are tabulated in Tables J.1 – J.2 on the following pages:

Table J.1. HPLC Measurements of Tert-Butyl Hydro Peroxide, Sulfone, and Dibenzothiophene for Experiments Conducted at 22 °C and Micro-Reactor Spacer of 100 Micron Thickness

Mean Residence Time [sec]	TBHP			SF				DBT			
	TBHP Peak Area []	TBHP Concentration [ppm]	Normalized TBHP Concentration []	SF Peak Area []	SF Concentration [ppm]	Normalized SF Concentration []	Sulfur Concentration [ppm]	DBT Peak Area []	DBT Concentration [ppm]	Normalized DBT Concentration []	Sulfur Concentration [ppm]
0	3981056	112261	1.00	49500	4	0.00	1	19905280	824	1.00	143
2	3502067	96294	0.88	551484	59	0.06	9	18010335	745	0.90	130
4	3376659	92114	0.85	892384	97	0.10	14	16383296	677	0.82	118
6	3178144	85497	0.80	1001296	109	0.11	16	14655722	606	0.74	105
8	2581524	65609	0.65	1615055	176	0.18	26	13407622	554	0.67	96
10	2648092	67828	0.67	1591547	174	0.18	26	13740461	567	0.69	99
12	2432273	60634	0.61	2072841	226	0.23	34	12661365	523	0.64	91
15	2503278	63001	0.63	1897445	207	0.21	31	13516393	558	0.68	97
18	2922708	76982	0.73	1984030	217	0.22	32	14113540	583	0.71	101
20	2631794	67285	0.66	2090607	228	0.23	34	14158972	585	0.71	102
25	2577738	65483	0.65	2406686	263	0.27	39	13588692	561	0.68	98
30	2492414	62639	0.63	2257832	247	0.25	37	14012071	579	0.70	101

Table J.2. Sulfur Material Balance on Sulfone and Dibenzothiophene for 100 Micron and 22 °C Experiment. Lists Amount of Sulfur Present and Absent at Various Residence Times.

Res Time (sec)	SF	DBT	Total ppm S	S Unaccounted	% Unaccounted
	ppm S	ppm S		Feed - After [ppm]	(Feed-After) / Feed
0	0.6	143.3	143.9	0.0	0.0%
2	8.8	129.6	138.4	5.5	3.9%
4	14.3	117.8	132.1	11.8	8.2%
6	16.1	105.3	121.4	22.5	15.6%
8	26.1	96.3	122.4	21.6	15.0%
10	25.7	98.7	124.4	19.5	13.6%
12	33.5	90.9	124.4	19.5	13.6%
15	30.7	97.1	127.7	16.2	11.2%
18	32.1	101.4	133.5	10.5	7.3%
20	33.8	101.7	135.5	8.4	5.8%
25	38.9	97.6	136.5	7.4	5.1%
30	36.5	100.7	137.2	6.7	4.7%

Appendix K
Material Balance for 50 Micron Experiments

Two material balances on sulfur are performed based on experimental data collected from experiments conducted with the 50 micron spacer at temperatures of 22 °C and 40 °C. The results are tabulated in Tables K.1 – K.4 on the following pages:

Table K.1. HPLC Measurements of Tert-Butyl Hydro Peroxide, Sulfone, and Dibenzothiophene for Experiments Conducted at 22 °C and Micro-Reactor Spacer of 50 Micron Thickness

Mean Residence Time [sec]	TBHP			SF				DBT			
	TBHP Peak Area []	TBHP Concentration [ppm]	Normalized TBHP Concentration []	SF Peak Area []	SF Concentration [ppm]	Normalized SF Concentration []	Sulfur Concentration [ppm]	DBT Peak Area []	DBT Concentration [ppm]	Normalized DBT Concentration []	Sulfur Concentration [ppm]
0	4571178	131931	1.00	28339	2	0.00	0	16559921	685	1.00	119
4	2891571	75944	0.63	2639856	288	0.34	43	11079894	457	0.67	79
5	2972708	78649	0.65	3147854	344	0.41	51	10824995	446	0.65	78
8	2335343	57403	0.51	3905108	427	0.51	63	7908680	325	0.48	57
10	2114728	50050	0.46	4475148	490	0.58	73	8202697	337	0.50	59
12	1784811	39052	0.39	4357421	477	0.57	71	6980782	286	0.42	50
18	1699426	36206	0.37	4645896	509	0.60	75	5923803	242	0.36	42
20	1937140	44130	0.42	4865159	533	0.63	79	6063484	248	0.37	43
23	1778872	38854	0.39	4774123	523	0.62	77	6218045	255	0.38	44
25	1620276	33568	0.35	4578411	501	0.59	74	4889914	199	0.30	35
27	1559931	31556	0.34	5095178	558	0.66	83	6147893	252	0.37	44
30	1801943	39623	0.39	5268749	577	0.68	85	7044235	289	0.43	50

Table K.2. Sulfur Material Balance on Sulfone and Dibenzothiophene for 50 Micron and 22 °C Experiment. Lists Amount of Sulfur Present and Absent at Various Residence Times

Res Time (sec)	SF	DBT	Total ppm S	S Unaccounted	% Unaccounted
	ppm S	ppm S		Feed - After [ppm]	(Feed-After) / Feed
0	0.3	124.5	124.8	0.0	0.0%
4	42.7	79.4	122.2	2.6	2.1%
5	51.0	77.6	128.6	-3.8	-3.0%
8	63.3	56.5	119.8	5.0	4.0%
10	72.6	58.6	131.2	-6.4	-5.1%
12	70.6	49.8	120.4	4.4	3.5%
18	75.3	42.1	117.5	7.3	5.9%
20	78.9	43.2	122.1	2.7	2.2%
23	77.4	44.3	121.7	3.1	2.5%
25	74.2	34.7	108.9	15.9	12.7%
27	82.6	43.8	126.4	-1.6	-1.3%
30	85.5	50.3	135.7	-10.9	-8.7%

Table K.3. HPLC Measurements of Tert-Butyl Hydro Peroxide, Sulfone, and Dibenzothiophene for Experiments Conducted at 40 °C and Micro-Reactor Spacer of 50 Micron Thickness

Mean Residence Time [sec]	TBHP			SF				DBT			
	TBHP Peak Area []	TBHP Concentration [ppm]	Normalized TBHP Concentration []	SF Peak Area []	SF Concentration [ppm]	Normalized SF Concentration []	Sulfur Concentration [ppm]	DBT Peak Area []	DBT Concentration [ppm]	Normalized DBT Concentration []	Sulfur Concentration [ppm]
0	4908379	143171	1.00	41035	3	0.00	1	16494598	682	1.00	119
4	3064897	81722	0.62	1819369	198	0.25	29	11216326	462	0.68	80
6	2670059	68561	0.54	2880875	315	0.39	47	9566866	394	0.58	68
8	2852331	74636	0.58	2720169	297	0.37	44	8841104	364	0.54	63
10	2086151	49097	0.43	3486425	381	0.47	56	7620504	313	0.46	54
12	2109428	49873	0.43	3898145	427	0.53	63	6364760	261	0.39	45
15	1809358	39871	0.37	4486266	491	0.61	73	4997862	204	0.30	35
18	1669248	35200	0.34	4880573	534	0.66	79	6230828	255	0.38	44
20	933178	10665	0.19	4986184	546	0.68	81	3777262	153	0.23	27
25	1409675	26548	0.29	5445359	596	0.74	88	3298919	133	0.20	23
27	1223281	20335	0.25	5802343	635	0.79	94	3744273	152	0.23	26

Table K.4. Sulfur Material Balance on Sulfone and Dibenzothiophene for 50 Micron and 40 °C Experiment. Lists Amount of Sulfur Present and Absent at Various Residence Times

Res Time (sec)	SF	DBT	Total ppm S	S Unaccounted	% Unaccounted
	ppm S	ppm S		Feed - After [ppm]	(Feed-After) / Feed
0	0.5	118.6	119.1	0.0	0.0%
4	29.4	80.4	109.8	9.3	7.8%
6	46.7	68.5	115.2	4.0	3.3%
8	44.0	63.3	107.3	11.8	9.9%
10	56.5	54.4	110.9	8.2	6.9%
12	63.2	45.3	108.5	10.6	8.9%
15	72.7	35.5	108.2	10.9	9.2%
18	79.1	44.4	123.5	-4.4	-3.7%
20	80.9	26.6	107.5	11.6	9.8%
25	88.3	23.2	111.5	7.6	6.4%
27	94.1	26.4	120.5	-1.4	-1.2%

Appendix L Paired T-Test Statistics

The paired t -test statistic for the mean difference of the experimental data obtained for dibenzothiophene will determine if two sets of data are statistically different. A modification to the paired t -test statistic allows for weighing the data's significance. Data points at shorter residence times are more likely to be less significant than data at longer residence times. The following equations are used:

$$t - test = \frac{\bar{D} - \mu_D}{s_D / \sqrt{n}}$$

$$\bar{D} = \frac{\sum_{i=1}^n D_i}{n}$$

$$s_D = \sqrt{\frac{\sum_{i=1}^n (t_i/t)(D_i - \bar{D})^2}{n-1}}$$

Where,

D_i = Difference in data points at i^{th} residence time

D = Average difference

n = Number of data points

t = Longest residence time

t_i = i^{th} residence time

s_D = Standard deviation

μ_D = Population mean difference

For a specified significance level, α , null hypothesis (H_0) is rejected if the calculated t -test statistic surpasses the upper-tailed critical value t_{n-1} or falls short of the lower-tailed critical value $-t_{n-1}$ of the t distribution. The evaluation rule of thumb is:

Reject H_0 if $t > t_{n-1}$
or if $t < -t_{n-1}$
Otherwise do not reject H_0 .

The null hypothesis in question is that there is no difference between the two sets of paired data. Table L.1 presents the output of each *t*-test analysis conducted for each pair of dibenzothiophene experimental data conducted at 100 microns. While Tables L.2 presents the output of the *t*-test analysis conducted for the pair of dibenzothiophene experimental data conducted at 50 microns. For α value of 0.02, the limits are (+2.681) and (-2.681). Since each *t*-test result of is greater than 2.681 or less than -2.681, the three sets of experimental data are statistically different.

Table L.1. *T*-Test Results from Three Dibenzothiophene Data Pairs from Experiments Conducted with 100 μm Thick Spacer

Set 1	Set 2	Paired t-test
22°C	40°C	5.542
22°C	60°C	2.773
40°C	60°C	-2.937

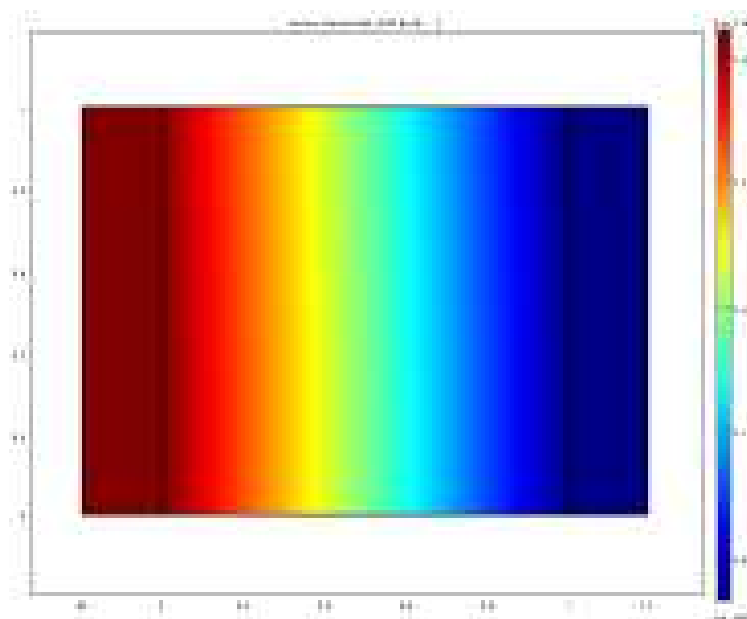
Table L.2. *T*-Test Results from Dibenzothiophene Data Pair from Experiment Conducted with 50 μm Thick Spacer

Set 1	Set 2	Paired t-test
22°C	40°C	4.212

Appendix M COMSOL Model Report

The following pages are a detailed report of the COMSOL Multiphysics model. This summary recreates the model for a micro-reaction system with a 100 micron spacer, diffusion coefficient for 40 °C, volumetric flow rate corresponding to a 2 second residence time, and a k_1 reaction rate constant of $1.8 \cdot 10^{-17} \text{ sec}^{-1}$.

COMSOL Model Report



1. Table of Contents

- Title - COMSOL Model Report
- Table of Contents
- Model Properties
- Constants
- Geometry
- Geom1
- Solver Settings
- Postprocessing
- Variables

2. Model Properties

Property	Value
Model name	
Author	
Company	
Department	
Reference	
URL	
Saved date	Aug 10, 2007 1:55:07 PM
Creation date	Jun 29, 2007 1:38:59 PM
COMSOL version	COMSOL 3.3.0.511

File name: Z:\Research\pseudo 1st order.mph

Application modes and modules used in this model:

- Geom1 (2D)
 - Convection and Diffusion (Chemical Engineering Module)

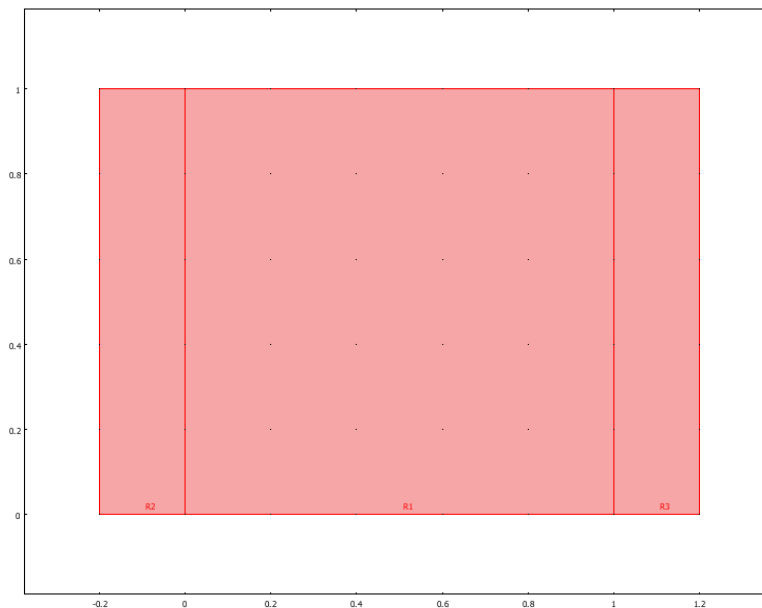
3. Constants

Name	Expression	Value	Description
Ddbx	$1.21e-9/l^2$	2.5e-6	
Ddby	$1.21e-9/H^2$	0.121	
I0	7.644e13	7.644e13	
eta	4282	4282	
k1	$1.38e-3/l0$	1.805338e-17	
cDBT0	3.26	3.26	
H	10e-5	1e-4	
F	1.1e-8	1.1e-8	
W	.01	0.01	
l	.022	0.022	

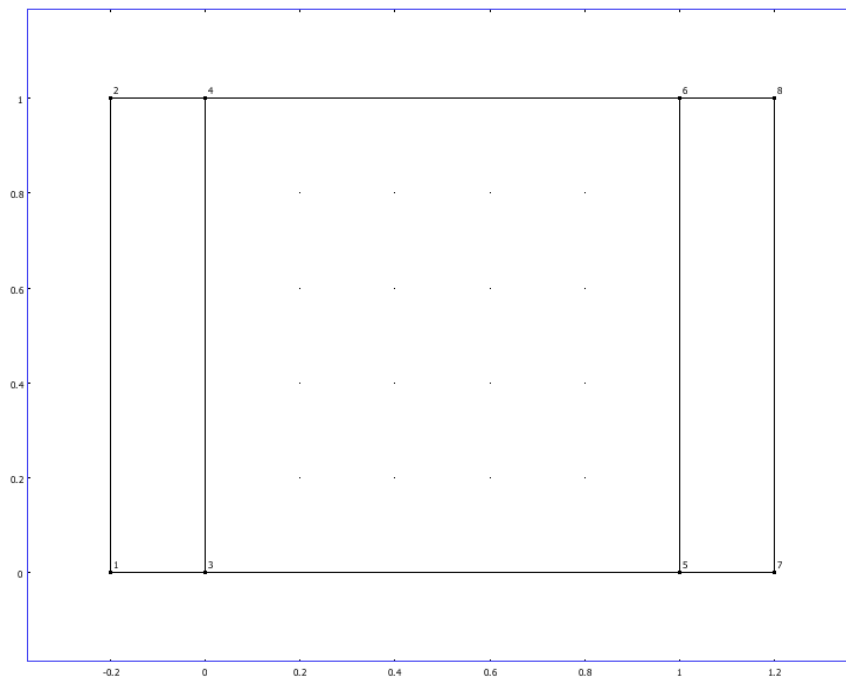
4. Geometry

Number of geometries: 1

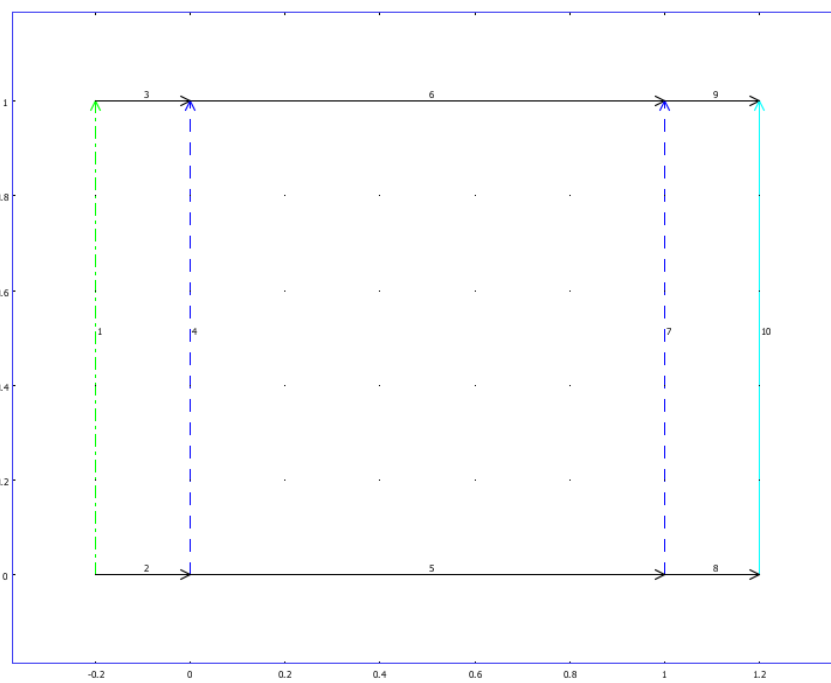
4.1. Geom1



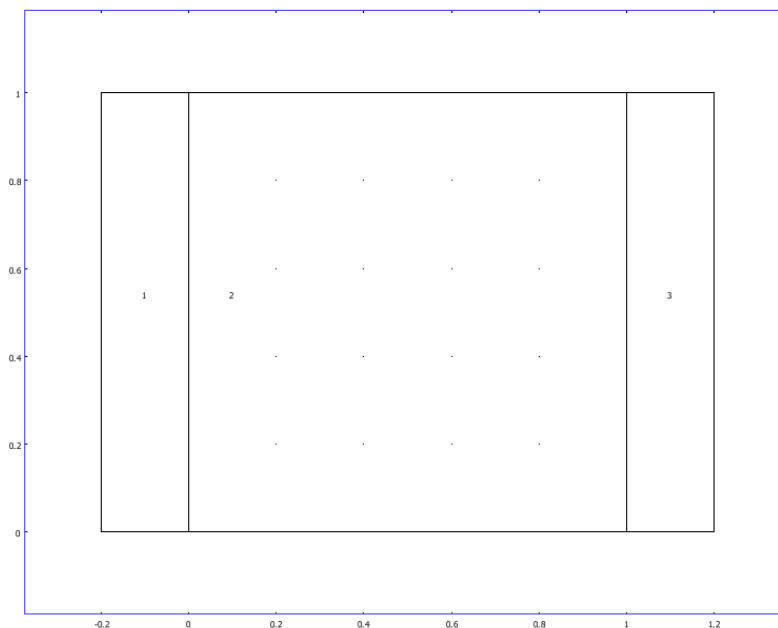
4.1.1. Point mode



4.1.2. Boundary mode



4.1.3. Subdomain mode



5. Geom1

Space dimensions: 2D

Independent variables: x, y, z

5.1. Scalar Expressions

Name	Expression
ux	$6 \cdot F / H / W \cdot y \cdot (1 - y)$
Rdb	$-k_1 \cdot c \cdot DBT \cdot I$
Intensity	$I_0 \cdot 10^{-(\eta \cdot (1 - y) \cdot H)}$

5.2. Expressions

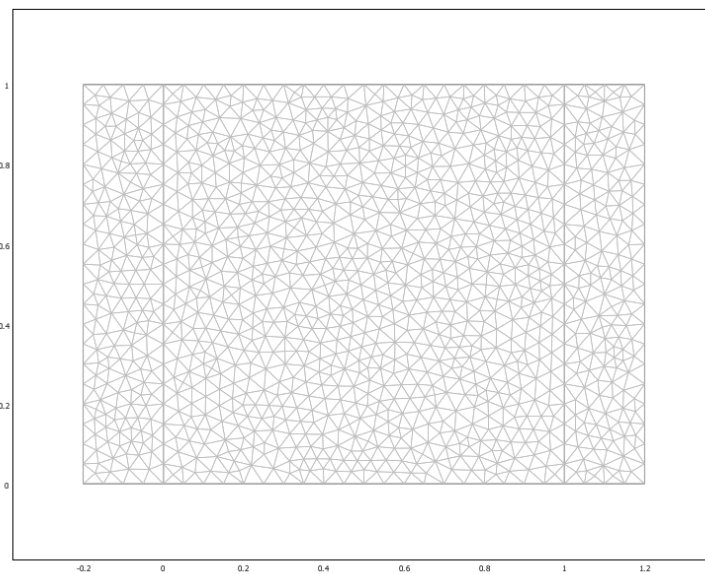
5.2.1. Subdomain Expressions

Subdomain	1, 3	2
I	0	Intensity

5.3. Mesh

5.3.1. Mesh Statistics

Number of degrees of freedom	4665
Number of mesh points	1191
Number of elements	2284
Triangular	2284
Quadrilateral	0
Number of boundary elements	136
Number of vertex elements	8
Minimum element quality	0.721
Element area ratio	0.217



5.4. Application Mode: Convection and Diffusion (chcd)

Application mode type: Convection and Diffusion (Chemical Engineering Module)

Application mode name: chcd

5.4.1. Application Mode Properties

Property	Value
Default element type	Lagrange - Quadratic
Analysis type	Stationary
Equation form	Non-conservative
Equilibrium assumption	Off
Frame	Frame (xy)
Weak constraints	Off

5.4.2. Variables

Dependent variables: cDBT

Shape functions: shlag(2,'cDBT')

Interior boundaries not active

5.4.3. Boundary Settings

Boundary		1	2-3, 5-6, 8-9
Type		Concentration	Insulation/Symmetry
Concentration (c0)	mol/m ³	cDBT0	0

Boundary	10
Type	Convective flux
Concentration (c0)	0

5.4.4. Subdomain Settings

Subdomain		1-3
Diffusion coefficient (dtensor)	m ² /s	{{Ddbx,0;0,Ddby}}
dtype		aniso
Reaction rate (R)	mol/(m ³ ·s)	Rdb
x-velocity (u)	m/s	ux

6. Solver Settings

Analysis type	Stationary
Auto select solver	On
Solver	Stationary
Solution form	Automatic
Symmetric	Off
Adaption	Off

6.1. Direct (UMFPACK)

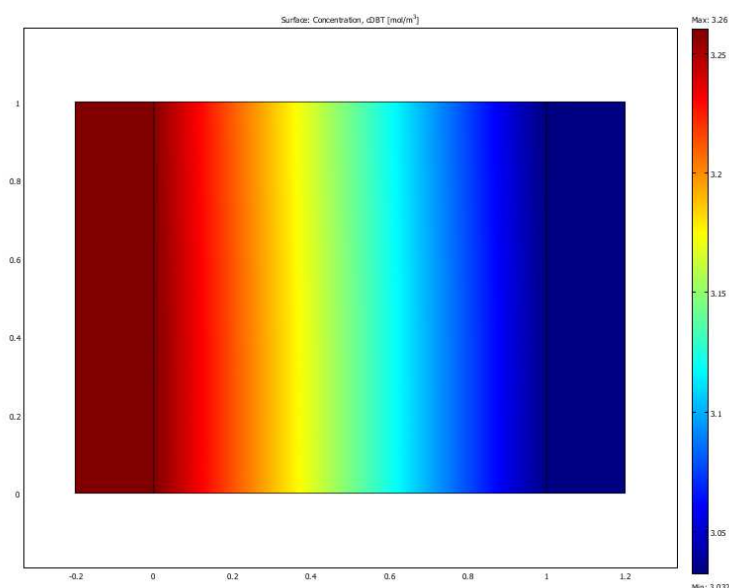
Solver type: Linear system solver

Parameter	Value
Pivot threshold	0.1
Memory allocation factor	0.7

6.2. Advanced

Parameter	Value
Constraint handling method	Elimination
Null-space function	Automatic
Assembly block size	5000
Use Hermitian transpose of constraint matrix and in symmetry detection	Off
Use complex functions with real input	Off
Stop if error due to undefined operation	On
Type of scaling	Automatic
Manual scaling	
Row equilibration	On
Manual control of reassembly	Off
Load constant	On
Constraint constant	On
Mass constant	On
Damping (mass) constant	On
Jacobian constant	On
Constraint Jacobian constant	On

7. Postprocessing



8. Variables

8.1. Boundary

Name	Description	Expression
ndflux_cDBT_chcd	Normal diffusive flux, cDBT	$nx_chcd * dflux_cDBT_x_chcd + ny_chcd * dflux_cDBT_y_chcd$
ncflux_cDBT_chcd	Normal convective flux, cDBT	$nx_chcd * cflux_cDBT_x_chcd + ny_chcd * cflux_cDBT_y_chcd$
ntflux_cDBT_chcd	Normal total flux, cDBT	$nx_chcd * tflux_cDBT_x_chcd + ny_chcd * tflux_cDBT_y_chcd$

8.2. Subdomain

Name	Description	Expression
grad_cDBT_x_chcd	Concentration gradient, cDBT, x component	cDBTx
dflux_cDBT_x_chcd	Diffusive flux, cDBT, x component	$-Dxx_cDBT_chcd * cDBTx - Dxy_cDBT_chcd * cDBTy$

cflux_cDBT_x_chcd	Convective flux, cDBT, x component	$cDBT * u_cDBT_chcd$
tflux_cDBT_x_chcd	Total flux, cDBT, x component	$dflux_cDBT_x_chcd+cflux_cDBT_x_chcd$
grad_cDBT_y_chcd	Concentration gradient, cDBT, y component	$cDBTy$
dflux_cDBT_y_chcd	Diffusive flux, cDBT, y component	$-Dyx_cDBT_chcd * cDBTx-Dyy_cDBT_chcd * cDBTy$
cflux_cDBT_y_chcd	Convective flux, cDBT, y component	$cDBT * v_cDBT_chcd$
tflux_cDBT_y_chcd	Total flux, cDBT, y component	$dflux_cDBT_y_chcd+cflux_cDBT_y_chcd$
beta_cDBT_x_chcd	Convective field, cDBT, x component	u_cDBT_chcd
beta_cDBT_y_chcd	Convective field, cDBT, y component	v_cDBT_chcd
grad_cDBT_chcd	Concentration gradient, cDBT	$\sqrt{grad_cDBT_x_chcd^2+grad_cDBT_y_chcd^2}$
dflux_cDBT_chcd	Diffusive flux, cDBT	$\sqrt{dflux_cDBT_x_chcd^2+dflux_cDBT_y_chcd^2}$
cflux_cDBT_chcd	Convective flux, cDBT	$\sqrt{cflux_cDBT_x_chcd^2+cflux_cDBT_y_chcd^2}$
tflux_cDBT_chcd	Total flux, cDBT	$\sqrt{tflux_cDBT_x_chcd^2+tflux_cDBT_y_chcd^2}$
cellPe_cDBT_chcd	Cell Peclet number, cDBT	$h * \sqrt{beta_cDBT_x_chcd^2+beta_cDBT_y_chcd^2} / Dm_cDBT_chcd$
Dm_cDBT_chcd	Mean diffusion coefficient, cDBT	$(Dxx_cDBT_chcd * u_cDBT_chcd^2+Dxy_cDBT_chcd * u_cDBT_chcd * v_cDBT_chcd+Dyx_cDBT_chcd * v_cDBT_chcd * u_cDBT_chcd+Dyy_cDBT_chcd * v_cDBT_chcd^2)/(u_cDBT_chcd^2+v_cDBT_chcd^2+eps)$
res_cDBT_chcd	Equation residual for cDBT	$-Dxx_cDBT_chcd * cDBTxx-Dxy_cDBT_chcd * cDBTxy+cDBTx * u_cDBT_chcd-Dyx_cDBT_chcd * cDBTyx-Dyy_cDBT_chcd * cDBTyy+cDBTy * v_cDBT_chcd-R_cDBT_chcd$
res_sc_cDBT_chcd	Shock capturing residual for cDBT	$cDBTx * u_cDBT_chcd+cDBTy * v_cDBT_chcd-R_cDBT_chcd$
da_cDBT_chcd	Total time scale factor, cDBT	Dts_cDBT_chcd

